No. 41027

Ecole doctorale sciences pour l'Ingénieur

L'Université des sciences et technologiques de Lille

Development of multi self-cleaning PET fabric by growth of ZnO nanorods

Dissertation

Presented in Partial Fulfillment of the Requirements for the Degree Doctor of Philosophy in the University of Lille 1

In the Field of: **Mechanic, Energy and Materials**

By

Munir ASHRAF

Defended on 20 December 2012 in front of jury;

Prof. Claire Peyratout	Université de Limoges	President of jury
Prof. Frédéric Guittard	Université de Nice	Reviewer
Prof. Stephan Brossillon	Université Montpellier 2	Reviewer
Prof. Niaz Ahmed	NTU, Faisalabad, Pakistan	Examiner
Prof. Anne Perwuelz	Ensait Roubaix	Director of thesis
Prof. Anne Leriche,	Université de Valenciennes	Co-director of thesis
Dr. Philippe Champagne	Université de Valenciennes	Co-director of thesis
Prof. Christine Campagne	Ensait Roubaix	Co-director of thesis

I dedicate this work to

My parents, Brother Javed ASHRAF and his Wife Nargis NAZ

Acknowledgement

Foremost, I would like to express my sincere gratitude to Prof. Anne PERWUELZ, Prof. Anne LERICHE, Dr Philippe CHAMPAGNE and Prof. Christine CAMPAGNE for their continuous support of my Ph.D study and research, for their patience, motivation, enthusiasm, and immense knowledge. Their guidance helped me throughout my research work and writing of this thesis. I could not have imagined having a better advisors and mentors for my Ph.D study.

This dissertation would have not been possible unless the support of Mr. Christian COURTOIS and Mr. Frédéric DUMONT. I am thankful to Director of PROBIOGEM and Mr. Nour-Eddine CHIHIB for letting us carry out antibacterial test.

My sincere thanks also go to Mr. Gerard MOUREAU for carrying out various tests to characterize functionalized samples. I owe sincere and earnest thankfulness to Mr. Christian CATEL for his tireless support and help throughout my thesis work and Mr. François DASSONVILLE for carrying out AFM analysis. I would like to show my gratitude to Mr. Jaoid KARAOUZENE for carrying out atomic absorption spectroscopy. I thank my fellow labmates at GEMTEX-ENSAIT Roubaix and LMPA Maubeuge for their help.

I am also very grateful to higher education commission of Pakistan for offering me scholarship for master and Ph.D.

Last but not the least; I would like to thank my family: my parents, brothers and sisters for supporting me spiritually throughout my life.

Munir ASHRAF

List of Abbreviations

A	Antibacterial activity
AAS	Atomic absorption spectroscopy
AFM	Atomic force microscopy
CVD	Chemical vapor deposition
CFU	Colony-Forming Units
DBD	Dielectric Barrier Discharge
DNA	Deoxyribonucleic acid
HMT	Hexamethylenetetramine
IBTMOS	Isobutyl(trimethoxy)silane
mM/l	milimole per litre
MTMS	Methyltrimethoxysilane
ODS	Octadecyltrimethoxysilane
PCL	Poly (caprolactone)
PEG	Poly(ethylene)glycol
PEI	Polyethylenimine
PET	Poly (ethyleneterephtalate)
PPFEMA	Polymerized perfluoroalkyl ethyl methacrylate
QACs	Quaternary ammonium compounds
RNA	Ribonucleic acid
ROS	Reactive oxygen species
SAED	Selected area electron diffraction
SAM	Self assembly monolayer
SEM	Scanning electron microscope
SM	Semiconductor
TEM	Transmission electron microscopy
UV	Ultraviolet
WCA	Water contact angle
XRD	X-ray diffraction spectroscopy
XPS	X-ray photoelectron spectroscopy

General Introduction

The cleaning of textiles has always been a problem but it was enhanced with the usage of fabric for automotive and upholstery due its difficulty to remove for washing purpose after every few days or weeks. This process was not only cumbersome but also very energy consuming. To overcome this problem, Du pont introduced its fluorochemical based product for treating fabrics in 1963 which it called Zepel fabric fluoridizer. After treatment, the fabric showed water - and oil – repellency, therefore, it became resistant to oil – and water – borne stains. The launch of this product followed by several other similar chemicals and research works to improve the durability as well as the repellency characteristics. The main focus of this research work was to find ways to make the surfaces hydrophobic by changing their chemistry.

In 1997, Wilhelm Barthlott studied the self-cleaning of plant leaves, and lotus leaf was the first, he analyzed. It was found that plant leaves had this unique characteristic due to the presence of hierarchical roughness structure. Since then, this cleaning of plant leaves is called lotus effect. This work opened the new horizons for researchers and the focus of research activity was changed from changing surface chemistry to modifying its structure to mimic lotus leaf. This effect has been mimicked on different surfaces including textiles.

Another aspect of self-cleaning which came in limelight during late 1990s, is the photocatalytic degradation of stains deposited on a surface. The research work was focused to degrade the color stains deposited on a surface which was not repellent to water and oil. In 2001, Pilkington Glass announced the development of the first self-cleaning windows with name of Pilkington Activ ^{TM} which was followed by self-cleaning glass by Saint Gobain. A very thin transparent layer of TiO_2 was deposited on glass surface which during sunlight irradiation, chemically degraded the organic species deposited on surface. During last decade, the photocatalytic self-cleaning has been developed on textile surfaces as well. For this, the textile surface was functionalized with TiO_2 to degrade the stains of red wine and discoloration of dye solution.

The last type of self-cleaning is the inhibition of bacterial growth. Silver is one of the oldest antibacterial agents which have been used for prevention of bacterial growth and their killings. Many other species have also been used for antibacterial purposes during the recent years. It includes quaternary ammonium compounds, N-hexyl,methyl-polyethylenimine and different derivatives of chitosan.

The functionalization of textiles with nanostructures for antibacterial activity was started during the last decade. The nanostructuration increases the antibacterial activity as well as it has minimum effect on hand feel of the fabric.

There has been lot of work to develop each type of self-cleaning textiles particularly cotton but the development of self-cleaning polyester fabric is yet to be explored. Also, a little work has been done to integrate more than one self-cleaning. Therefore, we decided to focus on polyester fabric for multi self-cleaning characteristics. The idea was to functionalize polyester fabric with ZnO to integrate all three self-cleanings. The ZnO is an excellent photocatalyst as well as antibacterial agent. It is also human friendly.

This project was realized at Laboratoire de GEnie de Matériaux TExtiles (GEMTEX), Roubaix in collaboration with Laboratoire de Matériaux céramiques et Procédés Associés (LMPA), Maubeuge.

The first step was to optimize the process conditions for the growth of ZnO nanorods to develop nanoroughness on fiber surface. After the growth of nanorods, the next step was to characterize the functional properties of treated textile. This dissertation is divided into three chapters;

First chapter is bibliography which describes the;

- Pre-requisites to obtain the physical self-cleaning
- Photocatalysis and its application for chemical self-cleaning
- Antibacterial activity and antibacterial surfaces
- Surface functionalization methods with oxides
- Characteristics of ZnO
- Growth of ZnO nanostructures

Second chapter is about the growth of nanorods. This chapter covers the materials, processes and characterization techniques for nanorods. It also covers;

- Optimization of process conditions
- Characterization of nano nanorods

- Effect of seed concentration on nano-roughness

Third chapter is about the characterization and study of functional properties;

- Superhydrophilicity
- Physical self-cleaning (lotus effect)
- Chemical self-cleaning (degradation of colors)
- Biological self-cleaning (antibacterial activity)

The work will be followed by a conclusion, perspectives and annexes.

CHAPTER 1

Bibliography

I Self-cleaning textile

Self-cleaning is the term which has attracted lot of attention in the recent years. When we think of any surface, three kinds of self-cleanings come to our mind; physical, chemical and biological self-cleanings. The physical self-cleaning means physically removal of dust and dirt particles present on any surface. These surfaces are available in nature like lotus leaves, rice leaves [1] and duck feathers [3]. The chemical self-cleaning refers to chemically degradation of stains present on the surface, and the biological self-cleaning means killing of bacteria if they attach on the surface and prevention of their growth [4].

I.1 Physical self-cleaning (lotus effect)

Lotus effect refers to cleaning of lotus leaves by rain water. When droplets of rain fall on these leaves, rather than sliding, they start rolling like tennis ball rolls on the ground and take away all the dust and dirt present on them rendering the leaves very neat and clean.

I.1.1 Characteristics of lotus effect

The surface with physical self-cleaning has two indispensible properties; superhydrophobicity and low water roll off angle [5].

I.1.1.1 Superhydrophobicity

Hydrophobicity comes from the Greek hydro, meaning *water*, and phobos, meaning *fear*. Therefore, a hydrophobic surface is one which repels the water while hydrophilicity is the direct opposite of it. Before going into details of superhydrophobicity, it is better to understand wetting phenomenon.

According to the affinity with gas and solid, the liquid spread over the surface as shown in Figure1-1. Therefore, there are three types of wetting; total, partial and nonwetting. In order to determine if droplet spreads over the surface or not, we take into consideration the parameter of spreading "S" which depends on the surface energy of solid and liquid.

$$S = \gamma_{SG} - (\gamma_{SL} + \gamma_{LG})$$

Where, γ_{SG} , γ_{SL} and γ_{LG} are the interfacial tensions between solid and gas, solid and liquid, and liquid and gas respectively. If "S" is positive, the liquid spreads over the completely. If "S" is negative, the liquid does not

spread and forms a droplet with a contact angle θ on the solid surface. The line at the interface of three phases, liquid, gas and solid is called triple line.

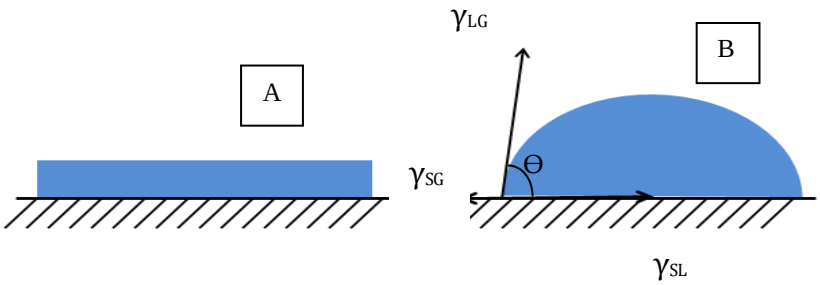

Figure 1-1: A. complete wetting; the liquid spreads over the surface. B. Partial wetting; the liquid forms a droplet with an angle θ with surface

I.1.1.1.1 Fundamental laws

a. Young's law

In 1805, Thomas Young proposed an equation to determine the contact angle of the liquid on a homogeneous and perfectly smooth surface. According to his law, the droplet can only be in equilibrium if the forces acting on the triple are equal (Figure 1-1b)

$$\gamma_{LG}\cos\theta = \gamma_{SG} - \gamma_{SL}$$

Now, if S<0 the parameter of spreading can be written

$$S = \gamma_{LG}(\cos\theta - 1)$$

The contact angle depends on the difference of interfacial tension between solid, gas and solid, liquid. If we take the example water, the contact angle will depend on the chemistry of the solid surface. The highest water contact angle that can be obtained is 120° on PTFE (polytetrafluoroethylene) surface

b. Wenzel model

There is not a single surface in nature which is completely homogeneous and perfectly smooth. There is always more or less roughness present on the surface. Therefore, the Young's law does not give the exact value of contact angle. In order to calculate the contact angle on rough surface, Wenzel put forward the following equation.

$$\cos\theta_w = r\cos\theta$$

where " θ_w", is the contact angle on a surface with roughness, "θ" is that of on an ideal surface and "r" is roughness fraction which is defined as the ratio between contact area to projected area of the surface. The "r" is either equal to 1 or more than 1. If it is equal to 1 that means the surface is 100% homogeneous and smooth which is not possible. If the surface is already hydrophilic (water contact angle<90º), the introduction of roughness will increase its hydrophilicity. If the contact angle is less than 10°, the surface will be superhydrophilic. Similarly, if the surface is already hydrophobic, the roughness will increase the hydrophobicity and the surface will become superhydrophobic, if the contact angle is greater than 150° [6]. This equation is valid only when the water droplet penetrates into the asperities of roughness as shown in Figure 1-2.

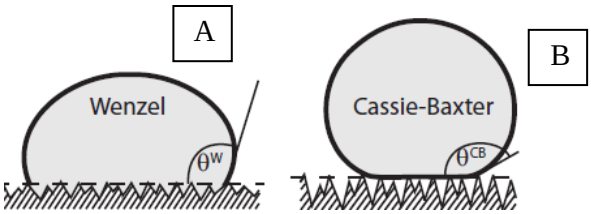

Figure 1-2: A. Wenzel droplet. B. Cassie-Baxter droplet

c. Cassie-Baxter model

If the interface is heterogeneous i.e. the air is trapped between water and the solid surface (Figure 1-2) then a composite interface is formed between water-air and water-solid due to the air trapped in asperities. The Cassie-Baxter equation defines this state.

$$\mathrm{Cos}\theta_{CB} = f_1 \cos\theta_1 + f_2 \cos\theta_2$$

On applying this equation to air/solid composite interface, the equation becomes

$$\mathrm{Cos}\theta_{CB} = f(\cos\theta + 1) - 1$$

Where, θ_{CB} and θ are the composite contact angle and the angle on surface without roughness, respectively. *f* is the surface fraction of solid in contact the droplet. This equation explains the superhydrophobicity due to roughness (*f*), when roughness increase, the value of *f* decreases and the contact angle also increases.

As the droplet do not penetrate between the asperities of roughness, therefore, the surface non-sticky and the droplet will roll over it.

I.1.1.1.2 Hierarchical versus unitary roughness for superhydrophobicity

As we have seen, the roughness of the surface plays a vital role for hydrophobicity. This roughness can be divided into two types; unitary roughness which can be micro or nano-roughness and hierarchical roughness which is the micro-roughness covered by nano-roughness as shown in Figure 1-3. The stability of the interface of the water on any surface depends on the type of the roughness. If the surface has only unitary roughness, then the stability of the composite interface between water, solid and air will be fragile. M. Nosonovsky and B. Bhushan [7] studied the factors affecting the stability of composite interface which can be summarized as follow; due to an external perturbation, a standing capillary wave can be formed at the liquid–air interface. If amplitude of the capillary wave is greater than the height of the asperity, the liquid can touch the valley between the asperities which leads to collapse of interface. The nanodroplets may condensate and accumulate in the valleys between asperities and eventually destroy the composite interface. The third factor which can affect the interface is the inhomogeneity of the surface (presence of hydrophilic spots). In order to overcome these problems and to obtain permanent composite interface, the presence of hierarchical roughness is obligatory. Because the microstructure resists capillary waves present at the liquid-air interface while nano-roughness prevents nanodroplets from filling the valleys between asperities and pin the droplet [8].

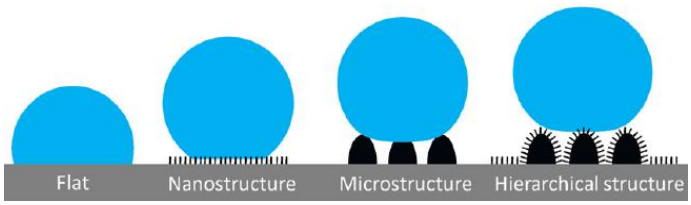

Figure 1-3: Water droplets on flat, nano, micro and hierarchical structures

I.1.1.2 Roll off angle

Roll off angle is the angle at which when hydrophobic surface is tilted, the falling droplet starts rolling. The roll off angle is directly link with superhydrophobicity and contact angle hysteresis. It has been reported that a surperhydrophic surface has low contact angle hysteresis and low roll off angle because they offer very low friction to rolling water droplet [9]. Bhushan et al. studied the effect of unitary and hierarchical structures on roll off angles and self-cleaning of surfaces. They found that not only the roll off angle was minimum but also the most of the dust and dirt particles placed on a surface with hierarchical structure, were removed [10].

A superhydrophobic surface with roll off angle less than 10º is called self-cleaning. Because the rolling water droplet takes away all the dust and dirt particles with it and leaves the surface very clean. These self-cleaning

surfaces have numerous applications in diverse fields like windshields, exterior paints for buildings and navigation ships, utensils, roof tiles, textiles, solar panels, and applications requiring anti-fouling and a reduction of drag in fluid flow, e.g., in micro/nanochannels [11].

I.1.2 Physical self-cleaning in nature

At the beginning of 90s decade, the scientists started exploring the superhydrophobic and self-cleaning natural surfaces. These include the leaves of lotus plant, rice and Colocasia esculenta. The surface structure analysis of these plants shows that they have hierarchical structures. For instance, lotus leaf contains 3-10µm hills and valley which are covered with nanocrystals of wax of size 70-100nm (Figure 1-4) [1]. Self-cleaning is the intrinsic property of hierarchical structure [12]. This particular structure increases the superhydrophobicity and reduces the contact between the surface and water droplet. Hierarchical structure provides air pocket formation, leading to the lowest contact area of an applied water droplet resulting in the reduction of contact angle hysteresis, tilt angle, and adhesive force [9, 13] The water contact angle on lotus leaf is 164º and contact angle hysteresis is 3º. Due to this structure, the falling droplet rolls over these leaves and make them clean.

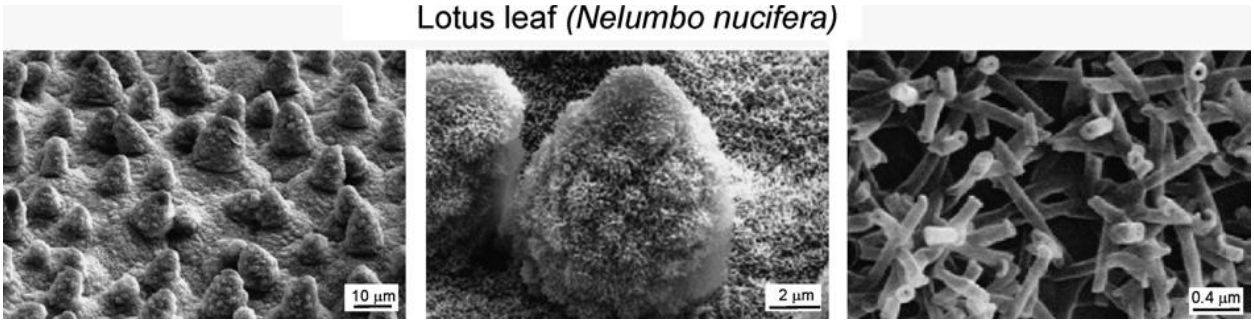

Figure 1-4: SEM micrographs (shown in three magnifications) of the Lotus (Nelumbo nucifera) leaf surface, which consists of a microstructure formed bypapillose epidermal cells covered with epicuticular wax tubules on surface, which create a nanostructure [14].

Another example of natural self-cleaning surface is floating water ferns of genus Salvinia (Figure 1-5). They never get wet even under several meters of water. Investigations have shown that the hierarchical nature of the S. molesta leaf is predominantly composed of tiny eggbeater-shaped hairs, which are almost completely hydrophobic due to a coating of nanoscopic wax crystals except for the terminal cells of each hair which lack the crystals thus making them hydrophilic. These hydrophilic patches are located at the top of each hair where the individual follicles forming the egg beater shape join together. Due to the hydrophilic patches at the tip of each hair, S. molesta exhibits a pinning effect of water against the top of the hairs which enables the formation of air pockets between each hair. The combination of hydrophilic patches coupled with an inner hydrophobic

coating of the S. molesta hairs, and the subsequent ability of S. molesta to pin water and retain air when submerged underwater is referred to as ‘‘Salvinia Effect’’ [15, 16].

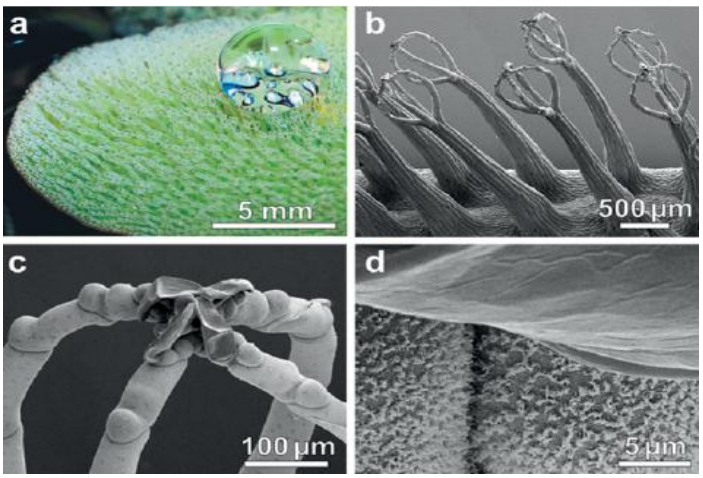

Figure 1-5: a.Upper side of the leaf surface densely covered with hairs. The spherical shape of the water drop on the leaf indicates the superhydrophobic character of the surface. b–d) SEM images of the complex hair structures. b) Four multicellular hairs grouped [15]

I.1.3 Mimicking the nature; Development of lotus effect

With the advent of modifying and synthesizing the surfaces at nanoscales, lot of work has been done to mimic hierarchical structures as different natural species have. Whatever the substrate have been used, the basic theme of all the work was either to develop hierarchical structure like lotus leaf or to generate just nano-roughness with different materials and by different processes which was subsequently modified with some hydrophobic chemical to obtain Cassie-Baxter type surface (superhydrophobic) with very high contact angle and low adhesion.

The first reported work focused to develop superhydrophobicity with water contact angle 174° and low adhesion surface was done by Japanese in 1990 [17, 18]. Approximately all the commonly used surfaces have been modified to develop lotus effect. This includes silicon wafers on which roughness was generated by etching [19, 20] or by immersion [21], glass surface by using nanoparticles and pillar like patterns to develop hierarchical structure [22-24], and by growth of ZnO nanorods subsequently modifying with octadecanethiol solution [25]. The cactus-like structure of TiO_2 was prepared on glass surface to develop hierarchical roughness for lotus effect [26]. A versatile method to produce superhydrophobic fabrics by combining electrospinning and initiated chemical vapor deposition (iCVD) has been reported. In this technique, poly(caprolactone) (PCL) was first electrospun and then coated with a thin layer of hydrophobic polymerized perfluoroalkyl ethyl methacrylate (PPFEMA) by iCVD. The hierarchical surface roughness inherent in the PCL electrospun mats and the

extremely low surface free energy of the coating layer obtained by iCVD yields stable superhydrophobicity with a contact angle of 175° and a threshold roll off angle less than 2.5° for a 20 mg droplet [27]. The binary structure was developed on copper foil by galvanic cell corrosion method to develop lotus effect [28].

One of the most important surfaces which has been the subject of lot research work to develop lotus effect is textile. This includes both cotton and polyester fabrics. A complex layer of SiO_2 was prepared on cotton fabric by using two different methods which was subsequently modified with hydrophobic chemicals to develop lotus effect and a very high contact angle around 170º was developed [29, 30]. A comb-like polymer comprising acrylate and organic siloxane was prepared on wool fabric. The combination of acrylate and organic siloxane resulted in unique characteristics and the fabric exhibits excellent superhydrophobicity [31]. The polymethylsilsesquioxane nanofilaments were grown as layers by gas phase coating on individual fibers of eleven different fabrics [32]. In another approach, ZnO nanorods have been grown to develop lotus effect on cotton fabric. In this method, in the first step nanorods were grown by seeding method as an array of forest on individual fibers which were subsequently modified with n-Dodecyltrimethoxysilane to make it superhydrophobic. This fabric shows self-cleaning characteristics like lotus leaf with contact angle of 161° and water roll off angle of 9°.

I.2 Chemical self-cleaning

Chemical self-cleaning refers to the degradation of stains at solid surface. It also concerns the degradation of chemical species contained in solution with which the solid surface comes in contact for longer period. Normally, this self-cleaning effect takes place under the effect of UV light. The UV light activates the photocatalyst deposited on surface which produces active species capable of degrading organic chemicals [33].

I.2.1 Photocatalysis process

This term is basically combination of two words “photo” and “catalysis”. Photo means light and catalysis means acceleration of chemical reaction in the presence of catalyst. Therefore, photocatalytic effect refers to the acceleration of a chemical reaction under the effect of light [34]. This term "photocatalysis" is still the subject of some debate. For example, it is argued that the idea of a photocatalysed reaction is fundamentally incorrect, since it implies that, in the reaction, light is acting as a catalyst, whereas it always acts as a reactant which is consumed in the chemical process. Therefore, it should be called "acceleration of a photoreaction by the presence of a catalyst" [34]. All the photocatalysis based reactions produce hydroxyl radicals which are the basic

ingredients of advanced oxidation processes. These processes have emerged as a promising water and wastewater treatment technology for the degradation or mineralization of a wide range of organic contaminants [35].

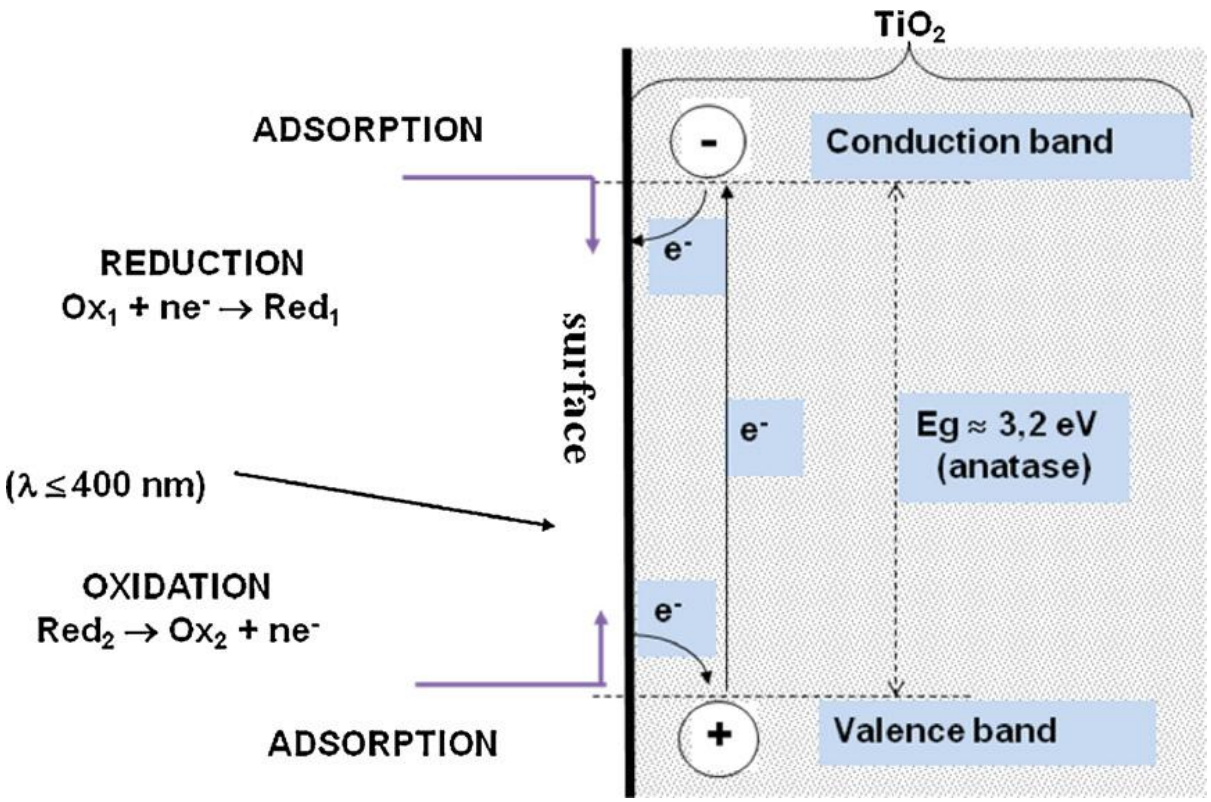

Figure 1-6: Mechanism of photocatalyst excitation of anatse TiO_2 by UV [36]

When UV falls on these semiconductors, the electron present in the valence band jumps to the conduction band, as result of it, a positive hole is generated (Figure 1-6). The recombination of the electron and the hole must be prevented as much as possible if a photocatalyzed reaction is to be favored. The ultimate goal of the process is to have a reaction between the activated electrons with an oxidant to produce a reduced product, and also a reaction between the generated holes with a reductant to produce an oxidized product.

Due to the generation of positive holes and electrons, oxidation-reduction reactions take place at the surface of semiconductors. In the oxidative reaction, the positive holes react with the moisture present on the surface and produce hydroxyl radical.

Oxidative reactions due to photocatalytic effect(semiconductor SM)[37]

$$UV + SM \rightarrow SM\,(h^+ + e^-) \qquad \text{eq.1}$$

Here SM stands for semiconductor, h^+ is the positive hole generated and e^- is electron

$$h^+ + H_2O \rightarrow H^+ + \bullet OH \qquad \text{eq.2}$$

$$2h^+ + 2H_2O \rightarrow 2H^+ + H_2O_2 \qquad \text{eq.3}$$

$$H_2O_2 \rightarrow HO\bullet + \bullet OH \qquad \text{eq.4}$$

The reductive reaction due to photocatalytic effect

$$e^- + O_2 \rightarrow \bullet O_2 \qquad \text{eq.5}$$

$$\bullet O2^- + HO\bullet_2 + H^+ \rightarrow H_2O_2 + O_2 \qquad \text{eq.6}$$

$$HOOH \rightarrow HO\bullet + \bullet OH \qquad \text{eq.7}$$

Ultimately, the hydroxyl radicals are generated in both the reactions. These hydroxyl radicals are very oxidative in nature and non selective with redox potential of (E^0=+3.06V) [38]. They behave like the radicals generated during hydrogen peroxide bleaching of textiles [39] and have the ability not only to prevent the growth but also to kill bacteria [40-44] and to degrade organic compounds [45-47].

I.2.2 Photocatalysis for chemical self-cleaning

During the recent years, various attempts have been made to functionalize textiles with photocatalysts to obtain self-cleaning effect by degrading organic and red wine stains. The nanoparticles of TiO_2 were attached on textiles like on cotton by different techniques like with the help of dicarboxylic acid spacer [48], by generating polar groups on poly (ethyleneterephtalate) (PET) fabric with the help of plasma treatment [49], by treating it with caustic soda [50]. The polar groups generated by different methods are used to attach photocatalysts nanoparticles on textiles.

These treated textiles have ability to degrade color stains of red wine and coffee under the effect of UV. For instance, Meilert, K.T., D. Laub, and J. Kiwi studied the degradation of red wine by TiO_2 under the effect of UV light and in 24 hours, the stain was degraded completely [48]. In another study, the polyester fabric was treated with TiO_2 nanoparticles which has ability to decolorize the solution of methyl orange [50]

I.3 Biological self-cleaning (Antibacterial activity)

A biological self-cleaning refers to a surface which has ability to kill the bacteria if they attach on it, hence prevent their further growth and formation of biofilm. During the recent years, a lot of work has been done to develop antibacterial surfaces. For this purpose, various organic and inorganic substances were used to functionalize them. In order to understand the mechanism of antibacterial activity of different substances, it is imperative to understand the anatomy, types and cell wall structure of bacteria.

I.3.1 Bacteria

Bacteria are single-celled microorganisms that can exist either as independent (free-living) organisms or as parasites. Their size ranges from some nano meters to hundreds micrometers. The most basic method used for identifying bacteria is based on the bacterium's shape and cell arrangement. The common shapes are following [51, 52];

- *Cocci* are round cells, sometimes slightly flattened when they are adjacent to one another
- *Bacilli* are rod-shaped bacteria
- *Spirilla* are curved bacteria which can range from a gently curved shape to a corkscrew-like spiral

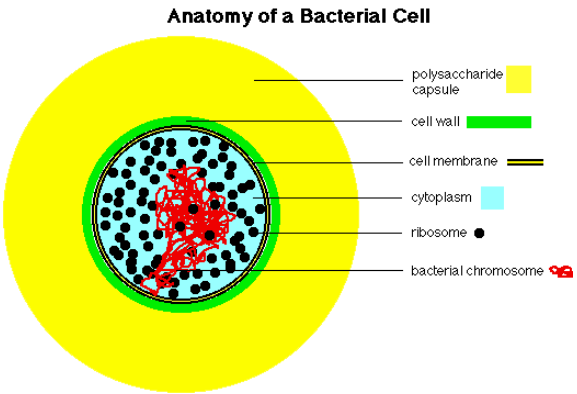

Figure 1-7: Anatomy of a bacterial cell

I.3.1.1 Anatomy of bacteria

The major anatomical structures found in most bacterial cells (Figure 1-7)are following [53];

1. Capsule: slimy layer, consisting of polysaccharide and water surrounding many cells. Also called slime coat, extracellular layer, etc.

2. Cell wall: rigid layer surrounding the bacterial cell. Made of peptidoglyan in bacteria, other materials in *archaea*(single cell organisms). It is porous and allows the movement of small molecules.

3. Cell membrane: flexible, semi-permeable barrier with lipid center that controls diffusion in and out of cell.

4. Cytoplasm: the fluid-filled space inside the cell. Contains hundreds of different enzymes, along with ribosomes, DNA (deoxyribonucleic acid), RNA (ribonucleic acid), and a "pool" of millions of small molecules and ions.

5. Ribosomes: particles made of protein and RNA, sites of protein assembly. Ribosomes may occupy 25% of the volume of a typical bacterial cell.

6. Cell Chromosome: the DNA of a cell, normally a single circular molecule that is tightly supercoiled and packed inside the cell. Actively dividing cells may contain 2 or even 4 copies of this chromosome, replicated and ready for dividing up among future daughter cells.

I.3.1.2 Classification of bacteria

The bacteria can be broadly divided into main categories on the basis of their cell wall structures. This classification was done by a Danish scientist Cristian Gram in 1884 by using Gram staining test.

In this test, bacteria are first stained with crystal violet, and then treated with a mordant - a solution that fixes the stain inside the cell. The bacteria are then washed with a decolorizing agent, such as alcohol, and counterstained with safranin, a light red dye. The walls of Gram-positive bacteria (e.g. *Staphylococcus aureus*) have more peptidoglycans (the large molecular network of repeating disaccharides attached to chains of four or five amino acids) than Gram-negative bacteria. Thus, Gram-positive bacteria retain the original violet dye and cannot be counterstained (Figure 1-8).

Gram-negative bacteria (e.g. *Escherichia coli*) have thinner walls, containing an outer layer of lipopolysaccharide, which is disrupted by the alcohol wash. This permits the original dye to escape, allowing the cell to take up the second dye, or counter stain. Thus, Gram-positive bacteria stain violet, and Gram-negative bacteria stain pink [54]

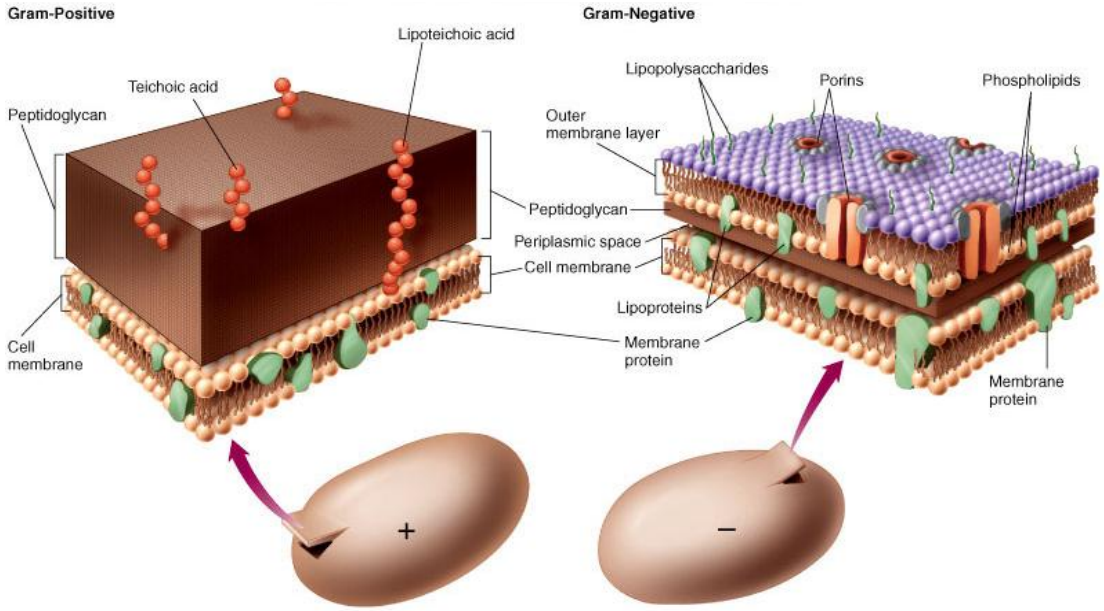

Figure 1-8: Cell walls of gram positive and gram negative bacteria [55]

I.3.1.3 Pathogenicity of Bacteria

A pathogen is a microorganism that is able to cause disease in a plant, animal or insect while a non pathogen does not cause any disease. Pathogenicity is the ability to produce disease in a host organism. Microbes express their pathogenicity by means of their virulence, a term which refers to the degree of pathogenicity of the microbe. Hence, the determinants of virulence of a pathogen are any of its genetic or biochemical or structural features that enable it to produce disease in a host [56]. Some of the pathogen gram positive and gram negative bacteria and the diseases which they cause are presented in the Table 1 [57]

Table 1. Some Gram + and Gram – bacteria and the diseases they cause

Gram positive bacteria	Disease	Gram negative bacteria	Disease
Actinomyces	Respiratory Diseases, cavities	*Escherichia coli* O157:H7 strain	Hemolytic-uremic syndrome (HUS
Bacillus anthracis	anthrax, food poisoning	*Pseudomonas aeruginosa*	Inflammation, sepsis
Clostridium	Tetanus, food poison	*Klebsiella*	Hemorrhagic pneumoniae
Corynebacterium	Diphtheriae	*Salmonella*	Food poisoning
Lactobacillus	Vaginal Flora	*Vibrio*	Cholera
Staphylococcus aureus	Boils, impetigo	*Yersinia*	Plague
Nocardia	Respiratory Diseases	*Serratia*	Respiratory Infections

I.3.1.4 Formation of biofilm

Biofilms are defined as matrix-enclosed bacterial populations' adherent to each other and/or to surfaces or interfaces. This definition includes microbial aggregates and floccules and also adherent populations within the pore spaces of porous media [58]. A common model for the formation of a differentiated and mature bacterial biofilm has been proposed and generally proceeds via at least five developmental stages [59] as shown in Figure 1-9.

i. An initial reversible attachment of planktonic bacteria that approach the solid surface by fluid stream or through motility, and that have overcome the repulsive forces between the cell and the surface. The solid surface generally is a conditioned surface, meaning that the surface is modified by adsorption of various solutes and has altered properties compared to the unconditioned surface.
ii. Transition from reversible to irreversible attachment by production of extracellular polymers by the bacteria and/or by specific adhesions located on pili and fimbriae, which interact with the surface.
iii. Early development of biofilm architecture.
iv. Development of microcolonies into a mature biofilm. Also during this stage, extracellular polymeric substances that serve as an adhesive matrix and trap nutrients from the environment continue to be produced. Complex architectures with pedestal-like structures, water channels and pores are formed, in which bacteria develop specific patterns of growth and a different physiology and metabolism from planktonic cells.
v. Dispersion of cells from the biofilm into the surrounding environment and return to the planktonic state.

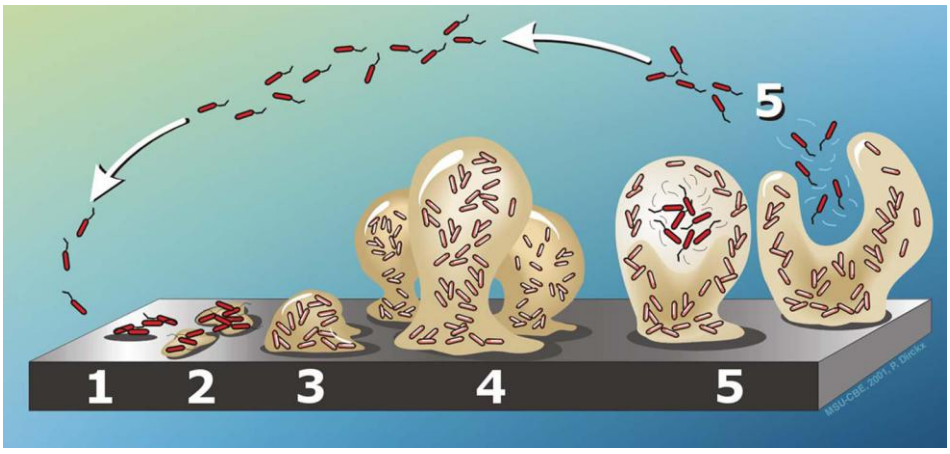

Figure 1-9: Schematic diagram of biofilm formation on a surface [60]

I.3.2 Antimicrobial Surfaces

Biofilms on materials are extremely hard to remove and show great resistance to all kinds of biocides. Thus, the prevention of biofilm formation by antimicrobial surfaces is the best way to avoid spreading of diseases and material deterioration [61]. On the basis of antibacterial mechanism, the surfaces can be divided into two categories; Antifouling surfaces and biocidal surfaces

I.3.2.1 Antifouling surface

The antifouling surfaces are the ones which the bacteria find difficult to attach to [61]. Different techniques have been used to develop these surfaces. One of the method is attachment of poly(ethylene)glycol (PEG) on a surface. The PEG polymeric surfaces are antifouling because of firstly the hydrophilic interaction with the otherwise hydrophobic microbial cell envelope, which does not favor microbial attachment to the surface. The second reason for the antifouling properties lies in the dynamic movement (also known as exclusion steric repulsion) of the PEG chains tethered to the surface, coupled with their lack of binding sites—these factors make it more difficult for a microbe to become attached to the surface modified with PEG [62] (Figure 1-10). Here, it is worth mentioning that the attachment of all the bacteria cannot be prevented by this mean.

The prevention of bacterial adhesion can also be done by either making the surfaces superhydrophobic like lotus leaf or by developing surface which has lot of negative charge (Figure 1-10). The bacteria also carry negative charge on its membrane. Therefore, the surface repels the attachment of bacteria. Nature uses roughness induced superhydrophobicity for self-cleaning surfaces like lotus leaves. Barthlott, W. and C. Neinhuis showed that the attachment of bacteria on lotus leaves is minimum. If they attach on such kind of surfaces, the possibility of their growth is also minimum because of the absence of water required for their germination [63].

J.Genzer and K.Efinmenko, in their review summarized the recent works by different researchers on repelling of bacteria. According to their conclusion, there is a window of surface energy (20 – 30 mJm^{-2}) within which the attachment of bacteria was minimum [64].

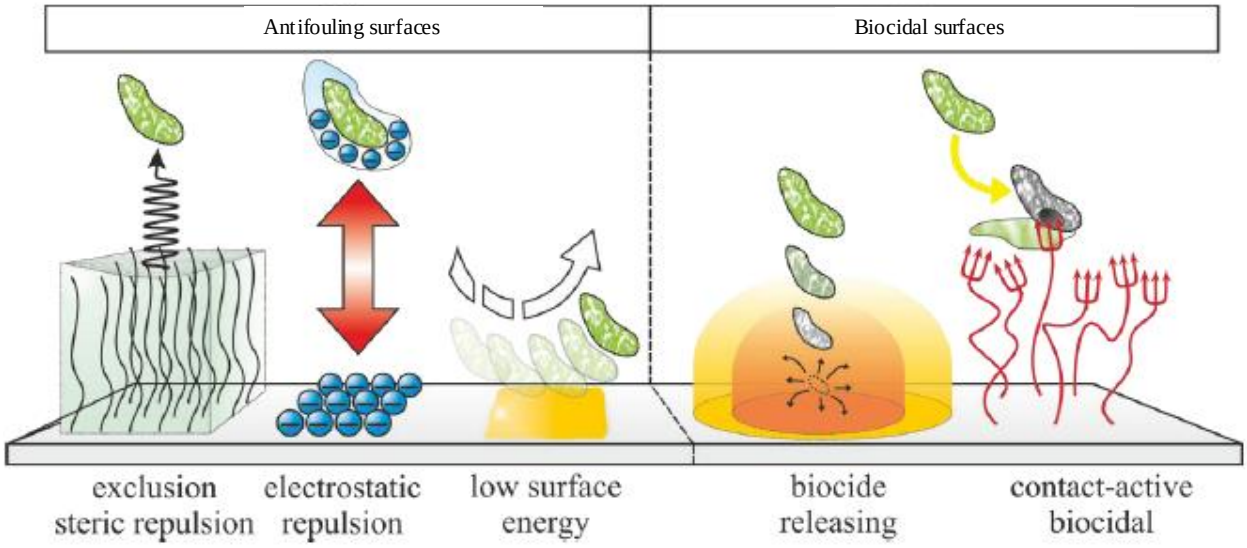

Figure 1-10: General principles of antimicrobial surface [77].

I.3.2.2 Biocidal surfaces

Biocidal surface is the one which kills the bacteria if it attaches on it or comes in its vicinity. On the basis of killing mechanisms, the biocidal surfaces can be divided into two classes; contact active biocidal and biocide releasing

I.3.2.2.1 Contact active biocidal

These surfaces have abilities to prevent the formation of biofilm by killing the bacteria at the very early stage of its adhesion on the surface if they try to attach on it (Figure 1-10). These surfaces are functionalized with immobilized antibacterial chemicals like; quaternary ammonium compounds (QACs), N-hexyl,methyl-polyethylenimine (PEI) and different derivatives of chitosan. The model is based on the idea that a surface-grafted membrane-active biocide on a polymeric spacer might be capable of penetrating the bacterial cell wall of an adhered bacteria, thus reaching its cell membrane and killing the microorganism [65]. J.C. Tiller *et al* functionalized the glass surface with poly (4-vinyl-*N*-hexylpyridinium bromide) and studied its antibacterial activity on Gram positive bacteria (*S. epidermidis*) and Gram negative bacteria (*E.coli*). They found that it worked very well on both bacteria [66]. In another study, Milović, N.M., *et al* found the same results on Gram positive bacteria (*S. aureus*) and Gram negative bacteria (*E.coli*) [67]. Lin, J., *et al* functionalized the textiles (cotton, polyester and nylon) with *N*-hexylated + methylted high molecular-weight polyethylenimine (PEI) and *N*-alkylated PEIs of low molecular weight. They found that high molecular weight compounds have much better antibacterial activity as compared to low ones [68].

The mode of action of all the amine based antibacterial agents is the same. G. Mcdonell and A.D.Russell in their review summarized the bactericidal mechanism of QACs which was presented by Salton;

i. Electrostatic attraction due to positive charge on QACs and negative charge on bacteria
ii. Adsorption and penetration of the agent into the cell wall
iii. Reaction with the cytoplasmic membrane (lipid or protein) followed by membrane disorganization
iv. Leakage of intracellular low-molecular-weight material
v. Degradation of proteins and nucleic acids
vi. Wall lysis caused by autolytic enzymes.

There is thus a loss of structural organization and integrity of the cytoplasmic membrane in bacteria, together with other damaging effects to the bacterial cell [69]

Chitosan is the deacetylated derivative of chitin, which is the main component of the shells of crustaceans such as shrimps, crabs and lobsters. The antimicrobial mechanism is not clear but is generally accepted that the primary amine groups provide positive charges which interact with negatively charged residues on the surface of microbes (same like QACs). Such interaction causes extensive changes in the cell surface and cell permeability, leading to leakage of intracellular substances [70].

I.3.2.2.2 Biocide releasing surfaces

These surfaces release active species which have ability to kill bacteria. These surfaces are unique in nature because they function even under those conditions in which other surfaces like antifouling and contact active do not work. In an environment, where huge amounts of bacteria deposit on the surface and block the active sites, only biocide releasing surfaces are suitable. The biocide releasing surfaces can be divided on the basis of the rate of release of active species [65];

i. Controlled release surfaces: these surfaces release active species progressively with the passage of time. The examples of controlled surfaces are the ones which release silver or zinc ions. This is one of the oldest techniques which are also used nowadays with slight variations.
ii. Catalytic formation of biocides and their release: the above mentioned types of antibacterial surface exhaust sooner or later. Therefore, they lose their antibacterial activity. During the recent years, semiconductors (ZnO, TiO_2, SnO_2 etc) have been used to functionalize surfaces for antibacterial

activity [43, 71, 72]. They release reactive oxygen species (ROS) which degrade the bacteria not only on the surface but also nearby surroundings.

I.3.3 Biological self-cleaning textiles

Various attempts have been made to develop biologically self-cleaning textiles by using some of above mentioned techniques for bacterial growth prevention. For example, in order to develop contact active biocidal effect, the cotton fabric was functionalized with reactive siloxane sulfopropybetaine (SSPB). The SSPB molecules convalently bound onto the cotton fabric and does not leach into the environment. The functionalized fabric prevented the growth of *E. coli*, *S. aureus* and fungi *Candida albicans* on its surface [73]. Similarly, biocide releasing textiles have been developed by functionalizing them with silver, ZnO and TiO_2 [74-76].

I.4 Multi self-cleaning of textiles

During the recent years, some attempts have been made to integrate different self-cleaning into one fabric. The first reported attempt towards integration of more than one functional property into one fabric was carried out by functionalizing cotton fabric with silver particles which was subsequently modified with octyltriethoxysilane to make it hydrophobic. This fabric showed superhydrophobicity with 151° water contact angle with 10µl. the functionalized fabric exhibited the antibacterial activity (biological self-cleaning) against Gram-negative as well as Gram-positive bacteria [77]. Although more than one functional characteristic were integrated into cotton fabric but the fabric was sticky because the droplet could not roll over the surface. Therefore, it did not have physical self-cleaning. Also the impact of superhydrophobicity on antibacterial activity of fabric was not studied.

In another attempt, the polyester fabric was treated with TiO_2 and Ag nanoparticles which were attached on fabric surface by using polysiloxane. The functionalized fabric showed chemical self-cleaning by degrading dye stains and antibacterial activity [78]. In a very recent study, ZnO nanoparticles were attached on cotton fabric by using polystyrene-block-poly(acrylic acid) copolymer development biological self-cleaning against *E. coli* and *S. aureus*, and chemical self-cleaning by discoloration of methylene blue solution [79].

As we have seen that in the recent work, chemical and biological self-cleanings have been developed on cotton fabric but none of study presented the all three self-cleanings into one fabric.

II Functionalization of surfaces with oxides

Various methods have been used to functionalize different surfaces by the deposition of semiconductor nanoparticles and nanorods. The basic purposes of these functionalizations were to develop superhydrophilic, superhydrophobic, antibacterial, self-cleaning and conducting textiles. The most commonly used methods of functionalization are following.

II.1 Sol-gel method

The sol-gel process is a wet-chemical technique widely employed recently in the fields of materials science and ceramic engineering. Such methods are utilized primarily for the fabrication of materials (typically a metal oxide) starting from a chemical solution which acts as the precursor for an integrated network (or gel) of either discrete particles or network polymers.

Typical precursors are metal alkoxides and metal chlorides, which undergo hydrolysis. A general mechanism of sol-gel process is described below[80]

$$Si(OR)_4 + H_2O \rightarrow HO\text{-}Si(OR)_3 + R\text{-}OH \qquad \text{eq.8}$$

Depending on the amount of water and catalyst present, hydrolysis may proceed to completion, so that all of the OR groups are replaced by OH groups as follows:

$$Si(OR)_4 + 4H_2O \rightarrow Si(OH)_4 + 4R\text{-}OH \qquad \text{eq.9}$$

Any intermediate species ($(OR)_2$–Si-$(OH)_2$) or ($(OR)_3$–Si-(OH)) would be considered the result of partial hydrolysis. In addition, two partially hydrolyzed molecules can link together in a condensation reaction to form a siloxane [Si–O–Si] bond:

$$(OR)_3\text{–Si-OH} + \text{HO–Si-}(OR)_3 \rightarrow [(OR)_3\text{Si–O–Si}(OR)_3] + \text{H-O-H} \qquad \text{eq.10}$$

or

$$(OR)_3\text{–Si-OR} + \text{HO–Si-}(OR)_3 \rightarrow [(OR)_3\text{Si–O–Si}(OR)_3] + \text{R-OH} \qquad \text{eq.11}$$

The precursor sol can be either deposited on a substrate to form a film (e.g., by dip coating or spin coating), casted into a suitable container with the desired shape (e.g., to obtain monolithic ceramics, glasses, fibers, membranes, and aerogels), or used to synthesize powders (e.g., microspheres, nanospheres). The sol-gel approach is a cheap and low-temperature technique which finely controls the product's chemical composition [81].

This technique has been used to functionalize silicon wafer, ceramic glass plate with thin film of SnO_2 [82], with WO_3 and TiO_2. The textiles have also been functionalized by using sol-gel method to develop

superhydrophobicity by deposition of SnO_2 [22, 29, 83], and to develop self-cleaning textiles by deposition of TiO_2 [33, 48].

In context with textile, this process poses unavoidable problem. It makes the textiles very stiff due cross linking of gel which leads to loss of softness of fabric.

II.2 Electro-deposition

Electro-deposition is commonly employed to produce a coating [84]. By this technique, approximately all the semiconductors and many other materials have been deposited at nano scale on different substrates. ZnO nano porous structures have been prepared on fluorine-doped SnO_2-coated glass slides for dye sensitized cells [85], TiO_2 was deposited on multi-walled carbon nano tubes for hydrogen peroxide sensing [86]. Superhydrophobic glass was developed by electro-deposition of ZnO nanoparticles and subsequently modification with hydrophobic chemical [87]. The technique to functionalize textiles is very difficult because they are non-conducting and it needs pretreatment to make them conductor. For instance, textile based photovoltaic cell was prepared by electro-deposition of ZnO on textiles [88].

II.3 Hydrothermal process

The term 'hydrothermal' is purely of geological origin. It was first used by the British geologist, Sir Roderick Murchison (1792-1871) to describe the action of water at elevated temperature and pressure, in bringing about changes in the earth's crust leading to the formation of various rocks and minerals. Hydrothermal processing can be defined as any heterogeneous reaction in the presence of aqueous solvents or mineralizers under high pressure and temperature conditions to dissolve and re-crystallize (recover) materials that are relatively insoluble under ordinary conditions. Definition for the word hydrothermal has undergone several changes from the original Greek meaning of the words 'hydros' meaning water and 'thermos' meaning heat. Recently, Byrappa and Yoshimura define hydrothermal as any heterogeneous chemical reaction in the presence of a solvent (whether aqueous or non-aqueous) above the room temperature and at pressure greater than 1 atm in a closed system [89].

The low temperature and low pressure synthesis of nano-materials by hydrothermal process has also been reported several times. The thin film of TiO_2 nanoparticles and nanorods are deposited on glass for dye sensitized cells by low temperature and low pressure hydrothermal process [90, 91]. Photovoltaic devices based on TiO_2 are prepared by hydrothermal deposition of nanostructures on substrate [92]. Hierarchical nanostructures of TiO_2 are prepared for the photocatalytic dye degradation [93]. Similarly, other photocatalysts

have been deposited on different substrates by low temperature hydrothermal process. Nanorods of zinc oxide are prepared to functionalize glass [94, 95]. The textiles have also been functionalized by low temperature hydrothermal deposition of nanostructure of ZnO [96-98], nanorods [99, 100]. The application of hydrothermal process in the field of textiles is quite new. Only a little work has been done to functionalize textile surfaces by using this method.

II.4 Solvothermal Method

The solvothermal method is almost identical to the hydrothermal method except that the solvent used here is nonaqueous. It can be described as a reaction or a transformation of precursor(s) in presence of a solvent in a close system and at a temperature higher than the boiling temperature of the solvent. Solvothermal reactions are governed by different factors [101]:

1. The nature of the precursors, in particular their physico-chemical properties (solubility, thermal stability…),

2. The nature of the solvent (chemical composition, physico-chemical properties) solvatation, polarity, viscosity, ability to stabilize some complexes as "intermediate". The nanoparticles of ZnO and TiO_2 were prepared by solvothermal method [102, 103].

III ZnO as functionalizing agent

There is a range of semiconductor photocatalyts which are being used for different purposes but some of them are more commonly used like ZnO, TiO_2, WO_3, VO_4, SnO_2, ZnS and CdSe. The band gap energies of these semiconductors and some others are presented in Table 2.

The choice of ZnO to functionalize textile is due to its large exciton binding energy of 60 meV and direct band gap energy of 3.37 eV at room temperature. It has similar photocatalytic properties as TiO_2 and appears to be alternative to it [104-106,129]. The biggest advantage of ZnO in comparison with TiO_2 is that it absorbs over a larger fraction of UV spectrum and the corresponding threshold of ZnO is 425 nm [107].

For the photocatalytic effect, the semiconductor should have band gap energy more than 1.21eV. The ZnO functionalized surfaces produce hydroxyl free radicals which has the ability to degrade various types of organic and living species like bacteria. It kills the bacteria not only when they attach on the surface but also in the proximity of the surface and to degrade organic species [37]. It has recently been shown that ZnO is toxic for bacteria but it has not significant effect on human cells [109]. Therefore, it has been used as a food additive and it is the most commonly used zinc source in the fortification of cereal-based foods. Because of its antimicrobial

properties, ZnO has been incorporated into the linings of food cans in packages for meat, fish, corn, and peas to preserve colors and to prevent spoilage [110].

Table 2. Band gap energies of different semiconductors [35, 108]

Semiconductors	Bandgap energy (eV)	Semiconductors	Bandgap energy (eV)
Diamond	5.4	TiO_2	3.03
CdS	2.42	WO_3	2.76
ZnS	3.6	Si	1.17
ZnO	3.37	Ge	0.744
CdSe	1.7	Fe_2O_3	2.3

ZnO thin films can be prepared with sol-gel, hydrothermal, sonochemical and microwave processes at low temperature [128]. Various types of nanostructure have been manufactured e.g. nano films [111], nano flower like structures [112-115], nano dumbbell shaped structures [97], nano belts [116], nano cages [117] and nanorods [100, 118-127] and these structures have been used for different functional properties.

III.1 Crystal structure

The crystal structures shared by ZnO are wurtzite (B4), zinc blende (B3), and rocksalt (or Rochelle salt) (B1) as schematically shown in (Figure 1-11). Under ambient conditions, the thermodynamically stable phase is that of wurtzite symmetry. The zinc blende ZnO structure can be stabilized only by growth on cubic substrates, and the rocksalt or Rochelle salt (NaCl) structure may be obtained at relatively high pressures, as in the case of GaN [2].

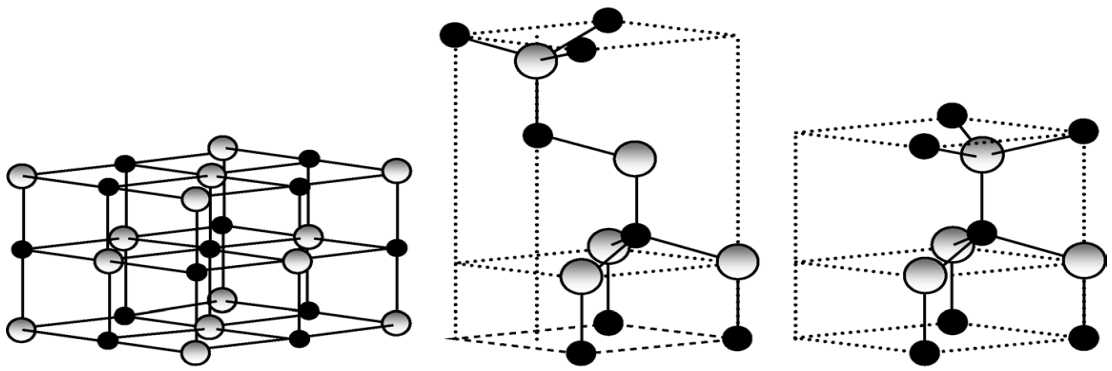

Rocksalt(B1) Zinc blende(B3) Wurtzite(B4)

Figure 1-11: Stick-and-ball representation of ZnO crystal structures:B1 = cubic rocksalt ,B3 = cubic zinc blende, and B4 = hexagonal wurtzite, Shaded gray and black spheres denote Zn and O atoms, respectively [2]

Like other II-VI semiconductors, wurtzite ZnO can be transformed to the rocksalt NaCl structure at relatively modest external hydrostatic pressures. The reason for this is the reduction of the lattice dimensions which causes inter ionic Coulomb interaction to favor the ionicity more over the covalent nature. The wurtzite structure consists of triangularly arranged alternating biatomic close-packed (0001) planes, for example, Zn and O pairs, thus the stacking sequence of the (0001) plane is *AaBbAaBb*…. in the (0001) direction. Another important characteristic of ZnO is polar surfaces. The most common polar surface is the basal plane (0001). One end of the basal polar plane terminates with partially positive Zn lattice sites and the other end terminates in partially negative oxygen lattice sites. The oppositely charged ions produce positively charged Zn-(0001) and negatively charged O-$(000\bar{1})$ surfaces, resulting in a normal dipole moment and spontaneous polarization along the *c*-axis as well as a variance in surface energy [130].

III.2 Growth of ZnO nanostructures

Structurally, ZnO has three fast growth directions of [0001], [0110] and [21 10] which facilitate anisotropic growth of ZnO wurtzite nanocrystals. It can be grown in different shapes like one-dimensional (1D) structures including c-axis oriented nano wires and a-axis oriented nano belts. The surface to volume ratio increases significantly with size reduction of ZnO structures at the nanometer scale. Thus, the effect of the surface, especially the surface polarity, plays an important role in determining the structures as well as the chemical and physical properties of the ZnO nanostructures [131].

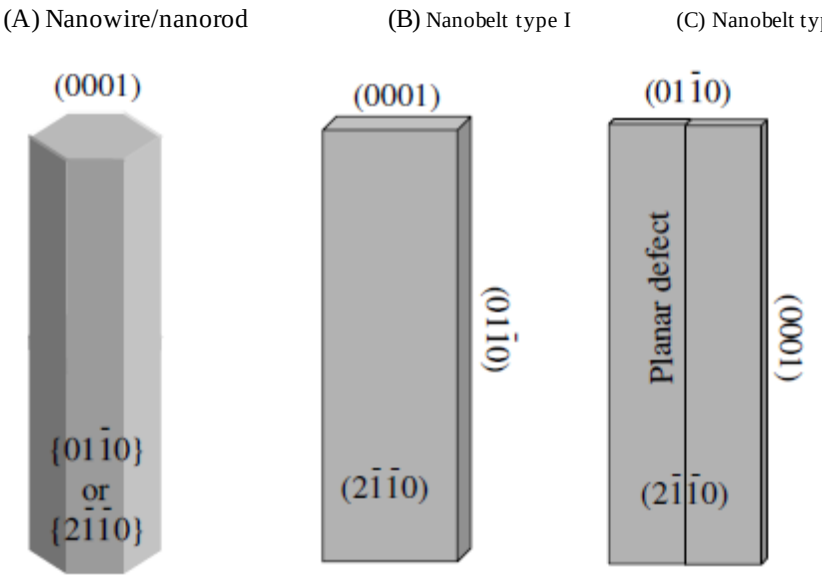

Figure 1-12: Typical growth morphologies of one-dimensional ZnO nanostructures and the corresponding facets.

ZnO exhibits a wide range of novel structures that can be grown by tuning the growth rates along growth directions. Macroscopically, a crystal has different kinetic parameters for different crystal planes. Thus, after an initial period of nucleation and incubation, a crystallite will commonly develop into a three-dimensional object with well-defined faces. The Figure 1-12 (A-C) shows a few typical growth morphologies of 1D nanostructures for ZnO. These structures tend to maximize the areas of the $[2\bar{1}\bar{1}0]$ and $[01\bar{1}0]$ facets because of the lower energy [132]. The ZnO nanostructures have been grown by different ways, like chemical vapor deposition [133, 134], electrodeposition [125, 135], sol-gel method [136] and hydrothermal method [137]. The hydrothermal method of growing ZnO nanostructures is very well known and extensively used because of low temperature, for its simplicity and environment friendly conditions.

III.3 ZnO nanostructures growth mechanism

ZnO is an amphoteric oxide with an isoelectric point value of about 9.5 [138]. ZnO is expected to crystallize by the hydrolysis of Zn salts in a basic solution that can be formed using strong or weak alkalis. Zn^{2+} is known to coordinate in tetrahedral complexes. Due to the $3d^{10}$ electron configuration, it is colorless [139]. The pH of the solution greatly influences the growth of ZnO nanostructures. The morphologies of these structures vary with the change in pH [140]. The most commonly used Zn salts for growth of nanostructures are zinc acetate dihydrate, zinc nitrate hexahydrate and zinc chloride. The alkalis used to maintain pH can be either weak like ammonia liquor and different amines or strong ones like KOH and NaOH.

The basic chemical reactions involved in the growth of nanostructures with strong alkalis are represented in the following equations

$$Zn^{2+} + 2OH^{-} \leftrightarrow Zn(OH)_2 \qquad \text{eq.12}$$

$$Zn(OH)_2 + 2OH^{-} \leftrightarrow [Zn(OH)_4]^{2-} \qquad \text{eq.13}$$

$$[Zn(OH)_4]^{2-} \leftrightarrow ZnO_2^{2-} + 2H_2O \qquad \text{eq.14}$$

$$ZnO_2^{2-} + H_2O \leftrightarrow ZnO + 2OH^{-} \qquad \text{eq.15}$$

ZnO crystal is a polar crystal whose positive polar plane is rich in Zn^{2+} and negative polar plane is rich in O^{2-}. In concentrated alkaline hydrothermal solutions, ZnO is transported from the nutrient to the growth surface mainly as $[Zn(OH)4]^{2-}$ [141]. The negative nature of the growth unit $[Zn(OH)4]^{2-}$ will lead to the different growth rates of planes, that is, $V(0001) > V(1\bar{0}1\bar{1}) > V(\bar{1}010) > V(\bar{1}011) > V(000\bar{1})$ [113].

The amine based basic reagents particularly hexamethylenetetramine also produces hydroxyl ions under hydrothermal conditions. The reactions involved in the growth process are represented here

$$(CH_2)_6N_4 + 6H_2O \rightarrow 6HCHO + 4NH_3 \quad \text{eq.16}$$

$$NH_3 + H_2O \rightarrow NH_4^+ + {}^-OH \quad \text{eq.17}$$

$$Zn^{2+} + NH_3 \rightarrow Zn(NH_3)_4^{2+} \quad \text{eq.18}$$

$$H_2O \rightarrow H^+ + {}^-OH \quad \text{eq.19}$$

$$Zn(NH_3)_4^{2+} + 2{}^-OH \rightarrow ZnO + 4NH_3 + H_2O \quad \text{eq.20}$$

When the concentrations of Zn^{2+} and OH^- ions exceed the critical value, the precipitation of ZnO nuclei starts. One can call this process as the initial nucleation process for the formation of ZnO [142]. The further growth is similar to any alkali assisted growth process.

The nanostructures ZnO can be grown on any substrate. This growth can be of two types, seedless growth and seeded growth.

III.3.1 Seedless growth of nanostructures

The seedless growth refers to the direct nucleation of ZnO on external substrate functionalized with self assembled monolayers (SAMs) which favors the heterogeneous nucleation from supersaturated solutions. The SAMs used for this purpose contain invert methyl groups which have very low nucleation energy barrier. Therefore, these methyl groups favor the growth of nanostructures [143]. Keeping in view said mechanism of seedless growth, various attempts have been made to grow nanorods on different substrates. Morin; *et al* grew the ZnO nanorods on flexible polyester filament. They exposed certain parts of their samples to UV light for generation of hydroxyl groups by oxidation. During the growth process, they observed that nanorods had grown on only unoxidized parts [99]. In another study, Hsu, J.W.P., *et al* prepared the pattern of SAM-COOH on silver treated Silicon wafer. The nanorods grew only bare silver substrate because carboxyl acid group get deprotonated to give $-COO^-$ which inhibits the nucleation [144]. This method of nanostructures growth is very sensitive to surface treatment and the process conditions. A slight change in process condition interrupts the growth process.

III.3.2 Seeded growth of nanostructures

In this method, a layer of ZnO nanoparticles (nano seeds) is deposited on substrate which provides the site for growth of nanorods. As the energy barrier for heterogeneous nucleation on substrate is less than that of homogeneous nucleation in solution [145], the seeding of the surface further reduces it because the interfacial tension between solution species and a crystal nucleation site depends on the degree of structural fit, the same

crystal type having the best fit and lowest energy barrier. Another important thing which favor the seeded growth is the presence of -OH groups on seeds which are similar to those present on (0001) face of ZnO crystals [146, 147]. The Figure 1-13 shows the steps of seeded growth process.

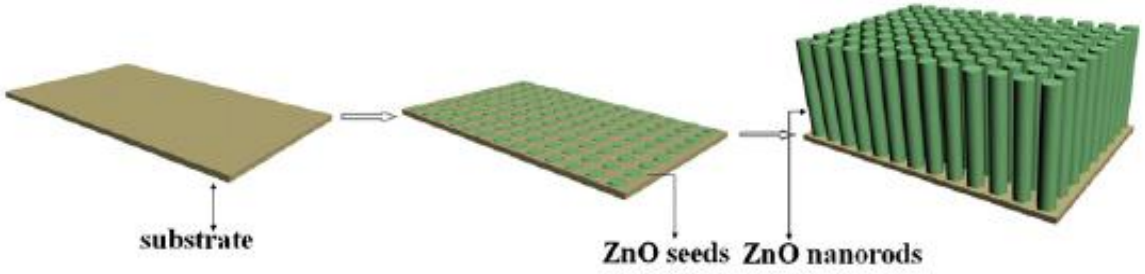

Figure 1-13: Seeded growth of ZnO nanorods on a surface [148]

The nano seeds can be deposited on surface different methods. The methods used for this purpose are atomic layer deposition [118], radio frequency magnetron sputtering deposition system [123, 124], pulse laser deposition [149] and the most commonly used sol-gel method [150]. In this method, zinc acetate dihydrate and sodium hydroxide are used as precursors. Their solutions are prepared in methanol separately, then mixed and refluxed at 60°C. These prepared seeds are applied by spin-coating on substrate [25, 150] or applied on textiles by padding [119].

III.3.3 Growth of nanostructures with different morphologies

The growth of ZnO nanostructures depends on conditions particularly the temperature and pH. The changes in pH and temperature lead to growth of different morphologies. Some of the important and commonly found in literature morphologies are discussed below.

III.3.3.1 Flower like nanostructures

The flowers, composed of either hexagonal nanorods or nano sheets of ZnO, are synthesized at a temperature of 90°C using zinc acetate dihydrate/zinc nitrate hexahydrate and sodium hydroxide in aqueous solutions [151, 152]. Two different mechanisms of flower like structures growth are found in literature. According to first mechanism, at pH>9, the nucleation rate is low and the crystal growth is relatively fast. Owing to the fewer nuclei and much more growth units, the complex $[Zn(OH)_4]^{2-}$ is easy to be connected with the surface at different sites of a single ZnO nucleus. In a short time, every site may act as new nucleation center for growth of the branching structure. Thus the growth units $[Zn(OH)_4]^{2-}$ begin to incorporate into ZnO along *c*-axis at different sites. As a result, flower-like ZnO rod aggregates are formed [153]. The 2nd theory talks about the aggregation of nuclei. At pH>9, nuclei of ZnO starts to aggregate and the interface of two aggregated nuclei

provide site for further nucleation which leads to formation of flower like structures (Figure 1-14)

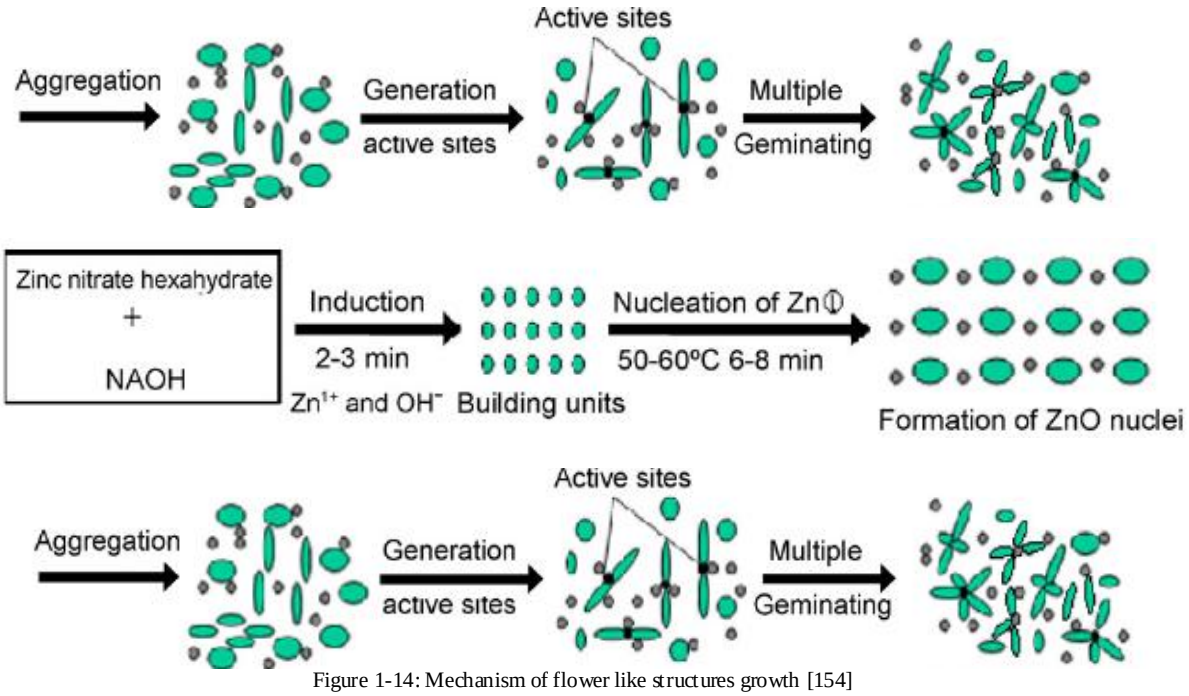

Figure 1-14: Mechanism of flower like structures growth [154]

The hierarchical flower like structures have been grown to functionalize indium doped tin oxide (ITO) glass for self degradation of dyes due to photocatalytic effect of ZnO [155]. Sun, Y., *et al* prepared the hierarchical flower like structures on conductive glass by hydrothermal process which has strong room temperature photoluminescence emission peak at 435 nm. This structure on deposition of hydrophobic chemical becomes a superhydrophobic adhesive surface with a water contact angle of 154°and a high contact angle hysteresis [156]. In another study, the flower like structures grown on Zn foil exhibits superhydrophobicity with water contact angle of 161° when modified with stearic acid [157]. Sivakumar, P.M., *et al* prepared the flower like nanostructures of ZnO by hydrothermal process which were deposited on cotton fabric with acacia gum as binder for antibacterial activity [74, 100]. A typical example of flower like structures is shown in Figure 1-15.

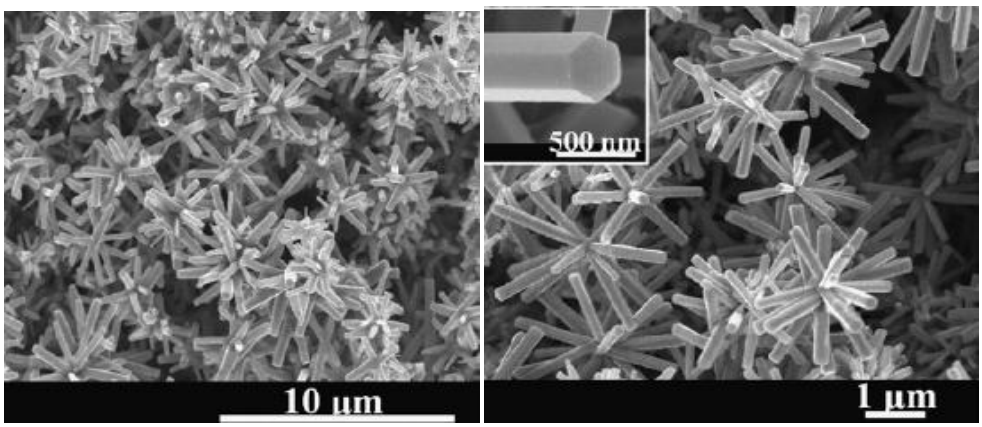

Figure 1-15: SEM images of flower like structures [158]

III.3.3.2 Nanorods

The nanorods are one of the ZnO nanostructures which have been most commonly used to functionalize surfaces for different purposes like to generate nano-roughness on textiles for hydrophobicity [148], to exploit its ability to absorb UV light for protective clothing [100], to prepare dye sensitized cells [159] and to prepare antibacterial surfaces [160]. The low temperature hydrothermal method is commonly used for the growth of ZnO nanorods with zinc nitrate hexahydrate and hexamethylenetetramine (HMT) at 90°C and at pH around 7. At this pH, as soon as nucleation takes place, the ZnO crystal grows along (0001) very quickly because this facet has highest surface free energy. This would minimize the total surface energy since the total surface area of the (0001) facet would be limited to the tips and hence very low [161, 162]. HMT is used as a precursor for the growth of ZnO nanorods. The HMT first hydrolyzes to produce the hydroxide ions (OH^-) and ammonia (as described in section III.4). The OH^- then forms complex ions with Zn^{2+} and then it decomposes into ZnO [163]. In another explanation for the growth mechanism of ZnO nanorods, Sugunan, A., et al. studied the role of hexamethylenetetramine. They argued that ZnO crystal exhibits partial polar characteristics, and in a typical Wurtzite structure the (001) plane is the basal polar plane (Figure 1-16a). One end of the basal polar plane terminates with partially positive Zn lattice points and the other end terminates in partially negative oxygen lattice points. It is believed that, in the chemical bath, hexamine being a non-polar chelating agent would preferentially attach to the non-polar facets of the nanorods, thereby exposing only the (001) plane for epitaxial growth (Figure 1-16b). Thus a preferential growth along the [0001] direction is made possible [164].

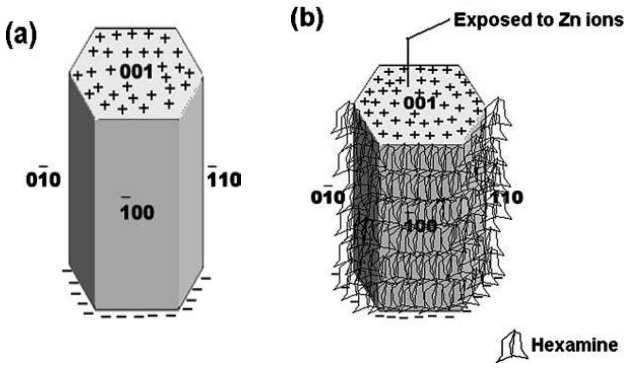

Figure 1-16: Explanation of growth of nanorods along (001) facet

III.3.3.3 Nanowires

The nano wires have shape like nanorods but have much longer length. They grew under hydrothermal conditions with pH higher than 7.2 and at temperature around 90°C [165, 166]. The addition of polyethyleneimine(PEI) in growth solution plays an important role to obtain long nano wires. The PEI can get protonated over wide range of pH (3-11) [167]. This protonation produces two results: the positively charged PEI molecules and the increase of the solution pH. PEI molecules adsorb on the lateral plane of the rods by the electrostatic attraction. This adsorption of PEI inhibits the lateral but promote the longitudinal growth of nanowires [168]. The growth mechanism of nanobelts is approximately same as of nanorods, the only difference is the growth time and precursor concentration.

III.3.3.4 Nanobelts

The most intriguing nanostructures of ZnO grown by hydrothermal process are nano belts. The growth of nano belts takes place at pH 7 with $ZnCl_2$ and Na_2CO_3. The growth is greatly influenced by the presence of some surfactant like sodium dodecyl sulfonate which deposit on certain facets and inhibits their growth [169]. Owing to the anisotropic growth property of wurtzite ZnO, the nanoparticles undergo an oriented attachment process to lower the overall system energy by piling up and then fusing with the adjacent nanoplates. This eventually leads to the formation of unique 1D rectangular cross-sectional ZnO nanobelts. This oriented attachment based growth mechanism dominates when the concentration of the precursors is high [139]. The nano belts grow either in the solution or stand perpendicularly on substrate [169, 170]. Xi, Y., *et al* grew the nano belts and studied their gas sensitivity. They found high sensitivities with an operating temperature of only 220° C for the oxidative gas O_2, and 305° C for the gas N_2 [171].

III.3.3.5 Nanoparticles

ZnO particles can be synthesized in powder form or can be deposited directly on the surfaces to functionalize them by different methods like hydrothermal with zinc chloride and sodium hydroxide [172], and with zinc acetate dihydrate and ammonium hydroxide [173], sol-gel method [174]. Zinc oxide nanoparticles prepared by hydrothermal and solvothermal methods are extensively used to functionalize surfaces for different purposes like functionalization of textile for antibacterial activity and UV protection [175]. They also appeared for enhancement wear resistant fabrics. The application of ZnO nanoparticles on wool fabric increases the maximum force, both in the warp and weft direction [98]. Li *et al* have investigated the durability of anti-bacterial activity of nano-ZnO functionalized cotton fabric to sweat. They treated cotton fabrics at a

concentration of 11 g/l ZnO in finishing agent ZPU-1 (commercial name) and padded them to 100% wet pick-up. The durability of anti-bacterial activity of the finished fabric in alkaline, acidic and inorganic salt artificial sweat solution has been evaluated. Results showed better salt and alkaline resistances than acid resistances for the treated fabrics A negative surface charge has been deduced for ZnO nanoparticles and illumination can increase anti-bacterial performance compared to normal conditions [75]. Applerot, G., *et al* deposited the ZnO nanoparticles on glass slide which showed excellent inhibition of bacterial colonization [176]. The photocatalytic effect was also studied by degradation of chrysophenine with immobilized ZnO nanoparticles deposited on glass slides. The results showed an excellent removal of dye from solution [177].

IV Conclusion

This study shows that physical self-cleaning (lotus effect) is the combination of two indispensible properties; superhydrophobicity ($\Theta > 150°$) and water roll off angle ($\Phi < 5°$). To develop physical self-cleaning, the surface should have hierarchical micro and nano-roughness structures covered with hydrophobic chemical. This hierarchical roughness structure not only increases the superhydrophobicity but also enhances the self-cleaning of a surface (by reducing the roll off angle). For chemical and biological self-cleanings, no specific structure is required.

Two different studies were conducted to find the functionalizing material and the methods of surface functionalization so that the nanoroughness could be generated on textile surface. The ZnO appears to be a good candidate as functionalizing material due to following reasons;

- Possibility to be grown different nanostructures: nanorods, nanocages, nanobelts, nanowires etc
- Excellent photocatalytic properties (absorb large part of spectrum)
- Antibacterial characteristics
- Human friendly, selective toxicity for pathogens

As far as functionalizing method is concerned, the hydrothermal process has potential to be used to functionalize textiles due to following reasons

- Working temperature is around 90°C which is good for textiles
- Water is used as solvent, therefore, it poses minimum environmental problem
- Various kind of nanostructures can be grown by changing the process conditions

By using ZnO as functionalizing under hydrothermal process conditions, it seems quite possible that all self-cleanings could be integrated into one fabric

References

1. Z. Guo and W. Liu, *Biomimic from the Superhydrophobic Plant Leaves in Nature: Binary Structure and Unitary Structure*. Plant Science, 2007. **172**(6): p. 1103-1112.

2. H. Morkoç and Ü. Özgür, *General Properties of ZnO*, Zinc Oxide: Fundamentals, Materials and Device Technology, Wiley-VCH Verlag GmbH & Co. KGaA, 2009. p. 1-76.

3. Y. Liu , X. Chen and JH. Xin , *Hydrophobic Duck Feathers and Their Simulation on Textile Substrates for Water Repellent Treatment*. Bioinspiration & Biomimetics, 2008. **3**(4): p. 046007.

4. J. Kiwi and C. Pulgarin, *Innovative Self-Cleaning and Bactericide Textiles*. Catalysis Today, 2010. **151**(1-2): p. 2-7.

5. C. Su, *Facile Fabrication of a Lotus-Effect Composite Coating Via Wrapping Silica with Polyurethane*. Applied Surface Science, 2010. **256**(7): p. 2122-2127.

6. X.-M. Li, D. Reinhoudt and M. Crego-Calama, *What Do We Need for a Superhydrophobic Surface? A Review on the Recent Progress in the Preparation of Superhydrophobic Surfaces*. Chemical Society Reviews, 2007. **36**(8): p. 1350-1368.

7. N. Michael and B. Bhushan, *Hierarchical Roughness Makes Superhydrophobic States Stable*. Microelectronic Engineering, 2007. **84**(3): p. 382-386.

8. B. Bhushan and Y. C. Jung, *Natural and Biomimetic Artificial Surfaces for Superhydrophobicity, Self-Cleaning, Low Adhesion, and Drag Reduction*. Progress in Materials Science, 2011. **56**(1): p. 1-108.

9. B. Bharat and J. Yong Chae, *Wetting, Adhesion and Friction of Superhydrophobic and Hydrophilic Leaves and Fabricated Micro/Nanopatterned Surfaces*. Journal of Physics: Condensed Matter, 2008. **20**(22): p. 225010.

10. B. Bhushan, Y. C. Jung and K. Koch, *Self-Cleaning Efficiency of Artificial Superhydrophobic Surfaces*. Langmuir, 2009. **25**(5): p. 3240-3248.

11. B. Bhushan and Y.C. Jung, *Biomimetics Inspired Surfaces for Superhydrophobicity, Self-cleaning, Low Adhesion, and Drag Reduction Nanotribology and Nanomechanics II*, Springer Berlin Heidelberg. 2011 p. 533-699.

12. K. Koch, B. Bhushan and W. Barthlott, *Diversity of Structure, Morphologyand Wetting of Plant Surfaces*. Soft Matter, 2008. **4**(10): p. 1943-1963.

13. K. Koch, H. F. Bohn and W. Barthlott, *Hierarchically Sculptured Plant Surfaces and Superhydrophobicity*. Langmuir, 2009. **25**(24): p. 14116-14120.

14. K. Koch, B. Bhushan, Y. C. Jung and W. Barthlott, *Fabrication of Artificial Lotus Leaves and Significance of Hierarchical Structure for Superhydrophobicity and Low Adhesion*. Soft Matter, 2009. **5**(7): p. 1386-1393.

15. W. Barthlott, T. Schimmel, S. Wiersch, K. Koch, M. Brede, M. Barczewski, S. Walheim, A. Weis, A. Kaltenmaier, A. Leder and H. F. Bohn, *The Salvinia Paradox: Superhydrophobic Surfaces with Hydrophilic Pins for Air Retention Under Water*. Advanced Materials, 2010. **22**(21): p. 2325-2328.

16. J. Hunt and B. Bhushan, *Nanoscale Biomimetics Studies of Salvinia Molesta for Micropattern Fabrication*. Journal of Colloid and Interface Science, 2011. **363**(1): p. 187-192.

17. T. Onda, S. Shibuichi, N. Satoh and K. Tsujii, *Super-Water-Repellent Fractal Surfaces*. Langmuir, 1996. **12**(9): p. 2125-2127.

18. S. Shibuichi, T. Onda, N. Satoh and K. Tsujii, *Super Water-Repellent Surfaces Resulting from Fractal Structure*. The Journal of Physical Chemistry, 1996. **100**(50): p. 19512-19517.

19. X. Yonghao, D. W. Hess and C. P. Wong, *Hierarchically Etched Silicon Lotus Effect Surface Structures for Reduced Light Reflection*. in *Electronics Packaging Technology Conference, 2008. EPTC 2008. 10th*. 2008: p**.** 916-922.

20. M. K. Dawood, H. Zheng, T. H. Liew, K. C. Leong, Y. L. Foo, R. Rajagopalan, S. A. Khan and W. K. Choi, *Mimicking Both Petal and Lotus Effects on a Single Silicon Substrate by Tuning the Wettability of Nanostructured Surfaces*. Langmuir, 2011. **27**(7): p. 4126-4133.

21. H. Liu, S. Szunerits, M. Pisarek, W. Xu and R. Boukherroub, *Preparation of Superhydrophobic Coatings on Zinc, Silicon, and Steel by a Solution-Immersion Technique*. ACS Applied Materials & Interfaces, 2009. **1**(9): p. 2086-2091.

22. K.-Y. Yeh, K.-H. Cho and L.-J. Chen, *Preparation of Superhydrophobic Surfaces of Hierarchical Structure of Hybrid from Nanoparticles and Regular Pillar-Like Pattern*. Langmuir, 2009. 25 (24), p. 14187–14194

23. J. Xiong, S. N. Das, B. Shin, J. P. Kar, J. H. Choi and J.-M. Myoung, *Biomimetic Hierarchical ZnO Structure with Superhydrophobic and Antireflective Properties*. Journal of Colloid and Interface Science, 2010. **350**(1): p. 344-347.

24. C. R. Crick and I. P. Parkin, *Superhydrophobic Silica Films on Glass Formed by Hydrolysis of an Acidic Aerosol of Tetraethylorthosilicate*. Journal of Materials Chemistry, 2011. **21**(25): p. 9362-9366.

25. M. Guo, P. Diao and S. Cai, *Highly Hydrophilic and Superhydrophobic ZnO Nanorod Array Films*. Thin Solid Films, 2007. **515**(18): p. 7162-7166.

26. F. Guo, X. Su, G. Hou, Z. Liu and Z. Mei, *Fabrication of Superhydrophobic TiO2 Surface with Cactus-Like Structure by a Facile Hydrothermal Approach*. Colloids and Surfaces A: Physicochemical and Engineering Aspects, 2012. **395**(0): p. 70-74.

27. M. Ma, Y. Mao, M. Gupta, K. K. Gleason and G. C. Rutledge, *Superhydrophobic Fabrics Produced by Electrospinning and Chemical Vapor Deposition*. Macromolecules, 2005. **38**(23): p. 9742-9748.

28. W. Xufeng and S. Gaoquan, *Fabrication of a Lotus-Like Micro-Nanoscale Binary Structured Surface and Wettability Modulation From Superhydrophilic To Superhydrophobic*. Nanotechnology, 2005. **16**(10): p. 2056.

29. C.-H. Xue, S.-T. Jia, J. Zhang and L.-Q. Tian, *Superhydrophobic Surfaces on Cotton Textiles by Complex Coating of Silica Nanoparticles and Hydrophobization*. Thin Solid Films, 2009. **517**(16): p. 4593-4598.

30. M. Yu, G. Gu, W.-D. Meng and F.-L. Qing, *Superhydrophobic Cotton Fabric Coating Based on a Complex Layer of Silica Nanoparticles and Perfluorooctylated Quaternary Ammonium Silane Coupling Agent*. Applied Surface Science, 2007. **253**(7): p. 3669-3673.

31. B. Zhang, B. Liu, X. Deng, S. Cao, X. Hou and H. Chen, *Fabricating Superhydrophobic Surfaces by Molecular Accumulation of Polysiloxane on the Wool Textile Finishing*. Colloid & Polymer Science, 2008. **286**(4): p. 453-457.

32. J. Zimmermann, F. A. Reifler, G. Fortunato, L.-C. Gerhardt and S. Seeger, *A Simple, One-Step Approach to Durable and Robust Superhydrophobic Textiles*. Advanced Functional Materials, 2008. **18**(22): p. 3662-3669.

33. D. Wu, M. Long, J. Zhou, W. Cai, X. Zhu, C. Chen and Y. Wu, *Synthesis and Characterization of Self-Cleaning Cotton Fabrics Modified by TiO2 Through a Facile Approach*. Surface and Coatings Technology, 2009. **203**(24): p. 3728-3733.

34. A. Mills and S. Le Hunte, *An Overview of Semiconductor Photocatalysis*. Journal of Photochemistry and Photobiology A: Chemistry, 1997. **108**(1): p. 1-35.

35. R. Thiruvenkatachari, S. Vigneswaran and I. Moon, *A review on UV/TiO2 Photocatalytic Oxidation Process (Journal Review)*. Korean Journal of Chemical Engineering, 2008. **25**(1): p. 64-72.

36. J.-M. Herrmann, *Photocatalysis Fundamentals Revisited to Avoid Several Misconceptions*. Applied Catalysis B: Environmental, 2010. **99**(3–4): p. 461-468.

37. Y. Wang, F. Huang, D. Pan, B. Li, D. Chen, W. Lin, X. Chen, R. Li and Z. Lin, *Ultraviolet-Light-Induced Bactericidal Mechanism on ZnO Single Crystals*. Chemical Communications, 2009. **0**(44): p. 6783-6785.

38. N. Daneshvar, D. Salari and A. R. Khataee, *Photocatalytic Degradation of Azo Dye Acid Red 14 in Water on ZnO as an Alternative Catalyst to TiO2*. Journal of Photochemistry and Photobiology A: Chemistry, 2004. **162**(2-3): p. 317-322.

39. S. H. Zeronian and M. K. Inglesby, *Bleaching of Cellulose by Hydrogen Peroxide*. Cellulose, 1995. **2**(4): p. 265-272.

40. S. Wang, W. Hou, L. Wei, H. Jia, X. Liu and B. Xu, *Antibacterial Activity of Nano-SiO2 Antibacterial Agent Grafted on Wool Surface*. Surface and Coatings Technology, 2007. **202**(3): p. 460-465.

41. X.-Y. Ma and W.-D. Zhang, *Effects of Flower-Like ZnO Nanowhiskers on the Mechanical, Thermal and Antibacterial Properties of Waterborne Polyurethane*. Polymer Degradation and Stability, 2009. **94**(7): p. 1103-1109.

42. O. Akhavan, M. Mehrabian, K. Mirabbaszadeh and R. Azimirad, *Hydrothermal Synthesis Of ZnO Nanorod Arrays for Photocatalytic Inactivation of Bacteria*. Journal of Physics D: Applied Physics, 2009. **42**(22): p. 225305.

43. J. H. Li, R. Y. Hong, M. Y. Li, H. Z. Li, Y. Zheng and J. Ding, *Effects of ZnO Nanoparticles on the Mechanical and Antibacterial Properties of Polyurethane Coatings*. Progress in Organic Coatings, 2009. **64**(4): p. 504-509.

44. R. Wahab, A. Mishra, S.-I. Yun, Y.-S. Kim and H.-S. Shin, *Antibacterial activity of ZnO Nanoparticles Prepared Via Non-Hydrolytic Solution Route*. Applied Microbiology and Biotechnology, 2010. **87**(5): p. 1917-1925.

45. C. Lu, Y. Wu, F. Mai, W. Chung, C. Wu, W. Lin and C. Chen, *Degradation Efficiencies and Mechanisms of the ZnO-Mediated Photocatalytic Degradation of Basic Blue 11 Under Visible Light Irradiation*. Journal of Molecular Catalysis A: Chemical, 2009. **310**(1-2): p. 159-165.

46. R. Ullah and J. Dutta, *Photocatalytic Degradation of Organic Dyes With Manganese-Doped ZnO Nanoparticles*. Journal of Hazardous Materials, 2008. **156**(1-3): p. 194-200.

47. D. Chatterjee and S. Dasgupta, *Visible Light Induced Photocatalytic Degradation of Organic Pollutants*. Journal of Photochemistry and Photobiology C: Photochemistry Reviews, 2005. **6**(2-3): p. 186-205.

48. K. T. Meilert, D. Laub and J. Kiwi, *Photocatalytic Self-Cleaning of Modified Cotton Textiles by TiO2 Clusters Attached by Chemical Spacers*. Journal of Molecular Catalysis A: Chemical, 2005. **237**(1-2): p. 101-108.

49. A. Bozzi, T. Yuranova, I. Guasaquillo, D. Laub and J. Kiwi, *Self-Cleaning Of Modified Cotton Textiles by TiO2 at Low Temperatures Under Daylight Irradiation*. Journal of Photochemistry and Photobiology A: Chemistry, 2005. **174**(2): p. 156-164.

50. H. Zhang, H. Zhu and R. Sun, *Fabrication of Photocatalytic TiO2 Nanoparticle Film on PET Fabric by Hydrothermal Method*. Textile Research Journal, 2012. **82**(8): p. 747-754.

51. D.G.Kaiser, *A. Sizes, Shapes, And Arrangements Of Bacteria*. The Prokaryotic Cell: BACTERIA, June 28, 2006. Available from: http://faculty.ccbcmd.edu/courses/bio141/lecguide/unit1/shape/shape.html

52. Cooke, R.-l., *Bacterial Shapes and Classification*. 2000. Available from: http://water.me.vccs.edu/courses/env108/lesson5_2.htm

53. Terry, T.M. *Anatomy of a bacterial cell*. 1998; Available from: http://www.biologie.uni-hamburg.de/b-online/library/micro229/terry/229sp00/lectures/bactanat.html.

54. Cooke, R.-l. *Bacterial Shapes and Classification*. 2000; Available from: http://water.me.vccs.edu/courses/env108/lesson5_2.htm.

55. The McGraw-Hill Companies, I., *cell walls of gram positive and gram negative bacteria*. 2008. Available from: bhttp://water.me.vccs.edu/courses/ENV108/Lesson5_print.htm

56. K.Todar, *Mechanisms of Bacterial Pathogenicity*. 2012; Available from: http://textbookofbacteriology.net/pathogenesis.html.

57. M. Patino, *List of Gram positive and Gram Negative Bacteria*. 2011; Available from: http://quizlet.com/5349160/list-of-gram-positive-and-gram-negative-bacteria-flash-cards/.

58. J. W. Costerton, Z. Lewandowski, D. E. Caldwell, D. R. Korber and H. M. Lappin-Scott, *Microbial Biofilms*. Annual Review of Microbiology, 1995. **49**(1): p. 711-745.

59. R. Van Houdt and C. W. Michiels, *Role of Bacterial Cell Surface Structures in Escherichia Coli Biofilm Formation*. Research in Microbiology, 2005. **156**(5-6): p. 626-633.

60. P. Stoodley, K. Sauer, D. G. Davies and J. W. Costerton, *Biofilms as Complex Differentiated Communities*. Annual Review of Microbiology, 2002. **56**(1): p. 187-209.

61. F. Siedenbiedel and J. C. Tiller, *Antimicrobial Polymers in Solution and on Surfaces: Overview and Functional Principles*. Polymers, 2012. **4**(1): p. 46-71.

62. K. Page, M. Wilson and I. P. Parkin, *Antimicrobial Surfaces and Their Potential in Reducing the Role of the Inanimate Environment in the Incidence of Hospital-Acquired Infections*. Journal of Materials Chemistry, 2009. **19**(23): p. 3819-3831.

63. W. Barthlott and C. Neinhuis, *Purity of the Sacred Lotus, or Escape from Contamination in Biological Surfaces*. Planta, 1997. **202**(1): p. 1-8.

64. J. G. K. EFIMENKO, *Recent Developments in Superhydrophobic Surfaces and Their Relevance to Marine Fouling: a review*. Biofouling, 2006. **22**(5): p. 339 – 360.

65. J. Tiller, H. G. Börner and J.-F. Lutz, *Antimicrobial Surfaces Bioactive Surfaces*, Springer Berlin / Heidelberg, 2011. p. 193-217.

66. J. C. Tiller, C.-J. Liao, K. Lewis and A. M. Klibanov, *Designing Surfaces That Kill Bacteria on Contact*. Proceedings of the National Academy of Sciences, 2001. **98**(11): p. 5981-5985.

67. N. M. Milović, J. Wang, K. Lewis and A. M. Klibanov, *Immobilized N-Alkylated Polyethylenimine Avidly Kills Bacteria by Rupturing Cell Membranes with No Resistance Developed*. Biotechnology and Bioengineering, 2005. **90**(6): p. 715-722.

68. J. Lin, S. Qiu, K. Lewis and A. M. Klibanov, *Mechanism of bactericidal and fungicidal activities of textiles covalently modified with alkylated polyethylenimine*. Biotechnology and Bioengineering, 2003. **83**(2): p. 168-172.

69. G. McDonnell and A. D.Russell, *Antiseptics and Disinfectants: Activity, Action, and Resistance*. Clinical Microbiology Reviews, 1999. **12**(1): p. 147–179.

70. G. Yuan and R. Cranston, *Recent Advances in Antimicrobial Treatments of Textiles*. Textile Research Journal, 2008. **78**(1): p. 60-72.

71. F. Özyıldız, M. Güden, A. Uzel, I. Karaboz, O. Akil and H. Bulut, *Antimicrobial Activity of TiO_2-Coated Orthodontic Ceramic Brackets Against Streptococcus Mutans and Candida Albicans*. Biotechnology and Bioprocess Engineering, 2010. **15**(4): p. 680-685.

72. C. Maneerat and Y. Hayata, *Antifungal activity Of TiO2 Photocatalysis against Penicillium Expansum in Vitro and in Fruit Tests*. International Journal of Food Microbiology, 2006. **107**(2): p. 99-103.

73. F. d. r. Leroux, C. Campagne, A. Perwuelz and L. o. Gengembre, *Polypropylene Film Chemical and Physical Modifications by Dielectric Barrier Discharge Plasma Treatment at Atmospheric Pressure*. Journal of Colloid and Interface Science, 2008. **328**(2): p. 412-420.

74. P. M. Sivakumar, S. Balaji, V. Prabhawathi, R. Neelakandan, P. T. Manoharan and M. Doble, *Effective Antibacterial Adhesive Coating on Cotton Fabric Using ZnO Nanorods and Chalcone*. Carbohydrate Polymers, 2010. **79**(3): p. 717-723.

75. Q. Li, S.-L. Chen, and W.-C. Jiang, *Durability of Nano ZnO Antibacterial Cotton Fabric to Sweat*. Journal of Applied Polymer Science, 2007. **103**(1): p. 412-416.

76. R. Dastjerdi and M. Montazer, *A Review on the Application of Inorganic Nano-Structured Materials in the Modification of Textiles: Focus On Anti-Microbial Properties*. Colloids and Surfaces B: Biointerfaces,2010. **79**(1): p. 5-18.

77. M. Ashraf, C. Campagne, A. Perwuelz, P. Champagne, A. Leriche and C. Courtois, *Development of Superhydrophilic and Superhydrophobic Polyester Fabric by Growing ZnO Nanorods*. Journal of Colloid and Interface Science, 2012. (0) in press

78. R. Dastjerdi and M. Montazer, *Nano-colloidal functionalization of textiles based on polysiloxane as a novel photo-catalyst assistant: Processing design*. Colloids and Surfaces B: Biointerfaces, 2011. **88**(1): p. 381-388.

79. B. A. Çakır, L. Budama, Ö. Topel and N. Hoda, *Synthesis of ZnO Nanoparticles Using PS-B-PAA Reverse Micelle Cores for UV Protective, Self-Cleaning and Antibacterial Textile Applications*. Colloids and Surfaces A: Physicochemical and Engineering Aspects, 2012. **414**(0): p. 132-139.

80. R. Lindberg, J. Sjoblom, and G.r. Sundholm, *Preparation of Silica Particles Utilizing the Sol-Gel and the Emulsion-Gel Processes*. Colloids and Surfaces A: Physicochemical and Engineering Aspects, 1995. **99**(1): p. 79-88.

81. T. K. Tseng, Y. S. Lin, Y. J. Chen and H. Chu, *A Review of Photocatalysts Prepared by Sol-Gel Method for VOCs Removal*. International Journal of Molecular Sciences, 2010. **11**(6): p. 2336-2361.

82. T.M.Racheva and G.W. Critchlow, *SnO2 Thin Films Prepared by the Sol-Gel Process*. Thin Solid Films, 1997. **292**(1-2): p. 299-302.

83. G. Y. Bae, B. G. Min, Y. G. Jeong, S. C. Lee, J. H. Jang and G. H. Koo, *Superhydrophobicity of Cotton Fabrics Treated With Silica Nanoparticles and Water-Repellent Agent*. Journal of Colloid and Interface Science, 2009. **337**(1): p. 170-175.

84. X. Chen and S.S. Mao, *Titanium Dioxide Nanomaterials: Synthesis, Properties, Modifications, and Applications*. ChemInform, 2007. **38**(41): p. 2891–2959.

85. T. Pauporte and J. Rathousky, *Electrodeposited Mesoporous ZnO Thin Films as Efficient Photocatalysts for the Degradation of Dye Pollutants*. The Journal of Physical Chemistry C, 2007. **111**(21): p. 7639-7644.

86. L.-C. Jiang and W.-D. Zhang, *Electrodeposition of TiO2 Nanoparticles on Multiwalled Carbon Nanotube Arrays for Hydrogen Peroxide Sensing*. Electroanalysis, 2009. **21**(8): p. 988-993.

87. Y. Sheng, W. Yiting, Z. Xiangyu and Z. Jia. *Fabrication and Analysis of Super-Hydrophobic ZnO Film for Microfluidic Devices*. in *Solid-State and Integrated Circuit Technology (ICSICT), 2010. 10th IEEE International Conference on*. p. 1428 - 1430

88. T. Loewenstein, M. Rudolph, M. Mingebach, K. Strauch, Y. Zimmermann, A. Neudeck, S. Sensfuss and D. Schlettwein, *Textile-Compatible Substrate Electrodes with Electrodeposited ZnO—A New Pathway to Textile-Based Photovoltaics*. ChemPhysChem, 2010. **11**(4): p. 783-788.

89. K. Byrappa and T. Adschiri, *Hydrothermal Technology for Nanotechnology*. Progress in Crystal Growth and Characterization of Materials, 2007. **53**(2): p. 117-166.

90. W. Tan, J. Chen, X. Zhou, J. Zhang, Y. Lin, X. Li and X. Xiao, *Preparation of Nanocrystalline TiO_2 Thin Film at Low Temperature and its Application in Dye-Sensitized Solar Cell*. Journal of Solid State Electrochemistry, 2009. **13**(5): p. 651-656.

91. B. Liu and E.S. Aydil, *Growth of Oriented Single-Crystalline Rutile TiO2 Nanorods on Transparent Conducting Substrates for Dye-Sensitized Solar Cells*. Journal of the American Chemical Society, 2009. **131**(11): p. 3985-3990.

92. H. Chen, W. Fu, H. Yang, P. Sun, Y. Zhang, L. Wang, W. Zhao, X. Zhou, H. Zhao, Q. Jing, X. Qi and Y. Li, *Photosensitization of TiO2 nanorods with CdS quantum dots for photovoltaic devices*. Electrochimica Acta, 2010. **56**(2): p. 919-924.

93. L. Liu, H. Liu, Y.-P. Zhao, Y. Wang, Y. Duan, G. Gao, M. Ge and W. Chen, *Directed Synthesis of Hierarchical Nanostructured TiO2 Catalysts and their Morphology-Dependent Photocatalysis for Phenol Degradation*. Environmental Science & Technology, 2008. **42**(7): p. 2342-2348.

94. Hari, P. and D. Spencer, *Surface Morphology of Zinc Oxide Nanorods Grown by Hydrothermal Deposition Technique*. physica status solidi (c), 2009. **6**(S1): p. S150-S153.

95. Y. Lee, Y. Zhang, S. L. G. Ng, F. C. Kartawidjaja and J. Wang, *Hydrothermal Growth of Vertical ZnO Nanorods*. Journal of the American Ceramic Society, 2009. **92**(9): p. 1940-1945.

96. D. Pradhan, M. Kumar, Y. Ando and K. T. Leung, *One-Dimensional and Two-Dimensional ZnO Nanostructured Materials on a Plastic Substrate and Their Field Emission Properties*. The Journal of Physical Chemistry C, 2008. **112**(18): p. 7093-7096.

97. R. H. Wang, J. H. Xin and X. M. Tao, *UV-Blocking Property of Dumbbell-Shaped ZnO Crystallites on Cotton Fabrics*. Inorganic Chemistry, 2005. **44**(11): p. 3926-3930.

98. A. Becheri, M. Dürr, P. Lo Nostro and P. Baglioni, *Synthesis and Characterization of Zinc Oxide Nanoparticles: Application to Textiles as UV-Absorbers*. Journal of Nanoparticle Research, 2008. **10**(4): p. 679-689.

99. S.A.Morin, F.F. Amos, and S. Jin, *Biomimetic Assembly of Zinc Oxide Nanorods onto Flexible Polymers*. Journal of the American Chemical Society, 2007. **129**(45): p. 13776-13777.

100. R. Wang, J. H. Xin, X. M. Tao and W. A. Daoud, *Zno Nanorods Grown on Cotton Fabrics at Low Temperature*. Chemical Physics Letters, 2004. **398**(1-3): p. 250-255.

101. G. Demazeau, *Solvothermal Processes: New Trends in Materials Chemistry*. Journal of Physics: Conference Series, 2008. **121**(8): p. 082003.

102. F. Yuan, P. Hu, L. Yu, S. Li and J. Ke, *Deposition Of ZnO on the Surface of Al Metal Particles by Esterification Reaction under Solvothermal Conditions.* Journal of Materials Science, 2008. **43**(7): p. 2397-2401.

103. A. Ranga Rao and V. Dutta, *Low-Temperature Synthesis of TiO2 Nanoparticles and Preparation of TiO2 Thin Films by Spray Deposition*. Solar Energy Materials and Solar Cells, 2007. **91**(12): p. 1075-1080.

104. C.-H. Chao. J.-S. Huang, and C.-F. Lin, *Low-Temperature Growth of Surface-Architecture-Controlled ZnO Nanorods on Si Substrates.* The Journal of Physical Chemistry C, 2008. **113**(2): p. 512-517.

105. R. Velmurugan and M. Swaminathan, *An Efficient Nanostructured ZnO For Dye Sensitized Degradation Of Reactive Red 120 Dye Under Solar Light*. Solar Energy Materials and Solar Cells, 2011. **95**(3): p. 942-950.

106. M. Quintana, T. Marinado, K. Nonomura, G. Boschloo and A. Hagfeldt, *Organic Chromophore-Sensitized ZnO Solar Cells: Electrolyte-Dependent Dye Desorption and Band-Edge Shifts.* Journal of Photochemistry and Photobiology A: Chemistry, 2009. **202**(2-3): p. 159-163.

107. M.A. Behnajady, N. Modirshahla, and R. Hamzavi, *Kinetic Study on Photocatalytic Degradation of C.I. Acid Yellow 23 by Zno Photocatalyst.* Journal of Hazardous Materials, 2006. **133**(1-3): p. 226-232.

108. S. H. S. Chan, T. Yeong Wu, J. C. Juan and C. Y. Te, *Recent Developments of Metal Oxide Semiconductors as Photocatalysts in Advanced Oxidation Processes (Aops) for Treatment of Dye Waste-Water.* Journal of Chemical Technology & Biotechnology, 2011. **86**(9): p. 1130-1158.

109. K. M. Reddy, K. Feris, J. Bell, D. G. Wingett, C. Hanley and A. Punnoose, *Selective Toxicity of Zinc Oxide Nanoparticles to Prokaryotic and Eukaryotic Systems.* Applied Physics Letters, 2007. **90**(21): p. 213902-213903.

110. Y. Xie, Y. He, P. L. Irwin, T. Jin and X. Shi, *Antibacterial Activity and Mechanism of Action of Zinc Oxide Nanoparticles against Campylobacter jejuni*. Applied and Environmental Microbiology, 2011. **77**(7): p. 2325-2331.

111. A. A. Ansari, R. Singh, G. Sumana and B. D. Malhotra, *Sol-Gel Derived Nano-Structured Zinc Oxide Film for Sexually Transmitted Disease Sensor.* Analyst, 2009. **134**(5): p. 997-1002.

112. Y. Jiang, M. Wu, X. Wu, Y. Sun and H. Yin, *Low-Temperature Hydrothermal Synthesis of Flower-Like ZnO Microstructure and Nanorod Array on Nanoporous TiO2 Film.* Materials Letters, 2009. **63**(2): p. 275-278.

113. X. Gao, X. Li, and W. Yu, *Flowerlike ZnO Nanostructures via Hexamethylenetetramine-Assisted Thermolysis of Zinc-Ethylenediamine Complex*. The Journal of Physical Chemistry B, 2005. **109**(3): p. 1155-1161.

114. Z. Wang, X.-f. Qian, J. Yin and Z.-k. Zhu, *Large-Scale Fabrication of Tower-like, Flower-like, and Tube-like ZnO Arrays by a Simple Chemical Solution Route*. Langmuir, 2004. **20**(8): p. 3441-3448.

115. R. Wahab, I. H. Hwang, Y.-S. Kim and H.-S. Shin, *Photocatalytic Activity of Zinc Oxide Micro-Flowers Synthesized Via Solution Method*. Chemical Engineering Journal, 2011. **168**(1): p. 359-366.

116. H.-K. Ni, Q. Zou, X. Fu, S. Wu, H. Wang and T. Xue, *Production of ZnO Nanobelts and Meso-Scale Study of Mechanical Properties.* Chinese Physics Letters, 2010. **27**(11): p. 116801.

117. L. Castañeda, *Synthesis and Characterization of ZnO Micro- and Nano-Cages.* Acta Materialia, 2009. **57**(5): p. 1385-1391.

118. Q. Li, V. Kumar, Y. Li, H. Zhang, T. J. Marks and R. P. H. Chang, *Fabrication of ZnO Nanorods and Nanotubes in Aqueous Solutions.* Chemistry of Materials, 2005. **17**(5): p. 1001-1006.

119. C.-H. Xue, R.-L. Wang, J. Zhang, S.-T. Jia and L.-Q. Tian, *Growth of ZnO Nanorod Forests and Characterization of Zno-Coated Nylon Fibers*. Materials Letters, 2010. **64**(3): p. 327-330.

120. X. Hou, L. Wang, B. Yu, F. Zhou and W. Liu, *Synthesis of Branched ZnO Nanorods on Various Substrates Via a Wet-Chemistry Route*. Particuology, 2010. **8**(5): p. 458-462.

121. H. Q. Le, S. J. Chua, Y. W. Koh, K. P. Loh and E. A. Fitzgerald, *Systematic Studies of the Epitaxial Growth of Single-Crystal ZnO Nanorods on Gan Using Hydrothermal Synthesis*. Journal of Crystal Growth, 2006. **293**(1): p. 36-42.

122. J.H. Lee, I.C. Leu, and M.H. Hon, *Substrate Effect on the Growth of Well-Aligned ZnO Nanorod Arrays from Aqueous Solution*. Journal of Crystal Growth, 2005. **275**(1-2): p. e2069-e2075.

123. N. Liu, G. Fang, W. Zeng, H. Zhou, F. Cheng, Q. Zheng, L. Yuan, X. Zou and X. Zhao, *Direct Growth of Lateral ZnO Nanorod UV Photodetectors with Schottky Contact by a Single-Step Hydrothermal Reaction*. ACS Applied Materials & Interfaces, 2010. **2**(7): p. 1973-1979.

124. S.-F. Wang, T.-Y. Tseng, Y.-R. Wang, C.-Y. Wang and H.-C. Lu, *Effect of ZnO Seed Layers on the Solution Chemical Growth of ZnO Nanorod Arrays*. Ceramics International, 2009. **35**(3): p. 1255-1260.

125. F. Xu, Y. Lu, L. Xia, Y. Xie, M. Dai and Y. Liu, *Seed Layer-Free Electrodeposition of Well-Aligned Zno Submicron Rod Arrays Via a Simple Aqueous Electrolyte*. Materials Research Bulletin, 2009. **44**(8): p. 1700-1708.

126. J. Zhao, Z.-G. Jin, T. Li and X.-X. Liu, *Nucleation and Growth of ZnO Nanorods on the ZnO-Coated Seed Surface by Solution Chemical Method*. Journal of the European Ceramic Society, 2006. **26**(13): p. 2769-2775.

127. Z. Zhou, Y. Zhao, and Z. Cai, *Low-Temperature Growth of ZnO Nanorods on PET Fabrics with Two-Step Hydrothermal Method*. Applied Surface Science, 2010. **256**(14): p. 4724-4728.

128. J. Anderson and G.V.d.W. Chris, *Fundamentals of Zinc Oxide as a Semiconductor*. Reports on Progress in Physics, 2009. **72**(12): p. 126501.

129. T. Pauporté and Z.M. Wang, *Design of Solution-Grown ZnO Nanostructures. Toward Functional Nanomaterials*, 2009, Springer US. p. 77-125.

130. B. Sunandan and D. Joydeep, *Hydrothermal Growth of ZnO Nanostructures*. Science and Technology of Advanced Materials, 2009. **10**(1): p. 013001.

131. T. Song, J. W. Choung, J.-G. Park, W. I. Park, J. A. Rogers and U. Paik, *Surface Polarity and Shape-Controlled Synthesis of ZnO Nanostructures on GaN Thin Films Based on Catalyst-Free Metalorganic Vapor Phase Epitaxy*. Advanced Materials, 2008. **20**(23): p. 4464-4469.

132. W. Zhong Lin, *Zinc Oxide Nanostructures: Growth, Properties and Applications*. Journal of Physics: Condensed Matter, 2004. **16**(25): p. R829.

133. A.-J. Cheng, Y. Tzeng, Y. Zhou, M. Park, T.-h. Wu, C. Shannon, D. Wang and W. Lee, *Thermal Chemical Vapor Deposition Growth of Zinc Oxide Nanostructures for Dye-Sensitized Solar Cell Fabrication*. Applied Physics Letters, 2008. **92**(9): p. 092113-092116.

134. A. A. Scalisi, R. G. Toro, G. Malandrino, M. E. Fragalà and G. Pezzotti, *Growth of ZnO Nanostructures Produced by MOCVD: A Study of the Effect of the Substrate*. Chemical Vapor Deposition, 2008. **14**(5-6): p. 115-122.

135. Z. Zhang, G. Meng, Q. Xu, Y. Hu, Q. Wu and Z. Hu, *Aligned ZnO Nanorods with Tunable Size and Field Emission on Native Si Substrate Achieved via Simple Electrodeposition*. The Journal of Physical Chemistry C, 2009. **114**(1): p. 189-193.

136. J. Li, S. Srinivasan, G. N. He, J. Y. Kang, S. T. Wu and F. A. Ponce, *Synthesis and Luminescence Properties of ZnO Nanostructures Produced by the Sol-Gel Method*. Journal of Crystal Growth, 2008. **310**(3): p. 599-603.

137. L. Wang, X. Zhang, C. Shao, X. Hong, Q. Qiao and Y. Liu, *Hexamethylenediamine-Assisted Hydrothermal Preparation of Uniform ZnO Particles and Their Morphology-Dependent Photoluminescent Properties*. Materials Chemistry and Physics, 2009. **115**(2-3): p. 547-550.

138. J. Zang, C. M. Li, X. Cui, J. Wang, X. Sun, H. Dong and C. Q. Sun, *Tailoring Zinc Oxide Nanowires for High Performance Amperometric Glucose Sensor*. Electroanalysis, 2007. **19**(9): p. 1008-1014.

139. S. Xu and Z. Wang, *One-Dimensional ZnO Nanostructures: Solution Growth and Functional Properties*. Nano Research. 2011, 4(11): p.1013–1098

140. S. Baruah and J. Dutta, *Ph-Dependent Growth of Zinc Oxide Nanorods*. Journal of Crystal Growth, 2009. **311**(8): p. 2549-2554.

141. L.N. Dem'yanets, D.V. Kostomarov, and I.P. Kuz'mina, *Chemistry and Kinetics of ZnO Growth from Alkaline Hydrothermal Solutions*. Inorganic Materials, 2002. **38**(2): p. 124-131.

142. R. Wahab, Y.-S. Kim, K. Lee and H.-S. Shin, *Fabrication and Growth Mechanism of Hexagonal Zinc Oxide Nanorods Via Solution Process*. Journal of Materials Science, 2010. **45**(11): p. 2967-2973.

143. C. Liu, Y. Masuda, Z. Li, Q. Zhang and T. Li, *Site-Selective Growth of Highly Oriented ZnO Rod Arrays on Patterned Functionalized Si Substrates from Aqueous Solution*. Crystal Growth & Design, 2009. **9**(5): p. 2168-2172.

144. J. W. P. Hsu, Z. R. Tian, N. C. Simmons, C. M. Matzke, J. A. Voigt and J. Liu, *Directed Spatial Organization of Zinc Oxide Nanorods*. Nano Letters, 2004. **5**(1): p. 83-86.

145. J.J. De Yoreoand P.G. Vekilov, *Principles of Crystal Nucleation and Growth*. Reviews in Mineralogy and Geochemistry, 2003. **54**(1): p. 57-93.

146. R.B. Peterson, C.L. Fields, and B.A. Gregg, *Epitaxial Chemical Deposition of ZnO Nanocolumns from NaOH Solutions*. Langmuir, 2004. **20**(12): p. 5114-5118.

147. J. Zhao, Z.-G. Jin, X.-X. Liu and Z.-F. Liu, *Growth and Morphology of ZnO Nanorods Prepared from $Zn(NO_3)_2$/NaOH solutions*. Journal of the European Ceramic Society, 2006. **26**(16): p. 3745-3752.

148. B. Xu and Z. Cai, *Fabrication of a Superhydrophobic ZnO Nanorod Array film on Cotton Fabrics Via a Wet Chemical Route and Hydrophobic Modification*. Applied Surface Science, 2008. **254**(18): p. 5899-5904.

149. N.G. Ndifor-Angwafor and D.J. Riley, *Synthesis of ZnO Nanorod/Nanotube Arrays Formed by Hydrothermal Growth at a Constant Zinc Ion Concentration*. physica status solidi (a), 2008. **205**(10): p. 2351-2354.

150. S. H. Yi, S. K. Choi, J. M. Jang, J. A. Kim and W. G. Jung, *Low-Temperature Growth of ZnO Nanorods by Chemical Bath Deposition*. Journal of Colloid and Interface Science, 2007. **313**(2): p. 705-710.

151. Z. Hui, Y. Deren, M. Xiangyang, J. Yujie, X. Jin and Q. Duanlin, *Synthesis of Flower-Like ZnO Nanostructures by an Organic-Free Hydrothermal Process*. Nanotechnology, 2004. **15**(5): p. 622.

152. J. Wu, J. Xia, C. Jing, W. Lei and B.-p. Wang, *Formation of Hierarchical ZnO Nanostructure on Tinfoil Substrate and the Application on Wetting Repellency*. Applied Physics A: Materials Science & Processing, 2011. **105**(1): p. 221-224.

153. H. Wang, J. Xie, K. Yan and M. Duan, *Growth Mechanism of Different Morphologies of ZnO Crystals Prepared by Hydrothermal Method*. Journal of Materials Science & Technology, 2011. **27**(2): p. 153-158.

154. Q. Ahsanulhaq, S. H. Kim, J. H. Kim and Y. B. Hahn, *Structural Properties and Growth Mechanism of Flower-Like ZnO Structures Obtained by Simple Solution Method*. Materials Research Bulletin, 2008. **43**(12): p. 3483-3489.

155. Z. Han, L. Liao, Y. Wu, H. Pan, S. Shen and J. Chen, *Synthesis and Photocatalytic Application of Oriented Hierarchical ZnO Flower-Rod Architectures*. Journal of Hazardous Materials, 2012. **217–218**(0): p. 100-106.

156. Y. Sun, R. Zou, W. Li, Q. Tian, J. Wu, Z. Chen and J. Hu, *A Controllable Hydrothermal Synthesis of Uniform Three-Dimensional Hierarchical Microstructured ZnO Films*. CrystEngComm, 2011. **13**(20): p. 6107-6113.

157. J. Li, Y. Yang, F. Zha and Z. Lei, *Facile Fabrication of Superhydrophobic ZnO Surfaces from High to Low Water Adhesion*. Materials Letters, 2012. **75**(0): p. 71-73.

158. A. Umar, M. M. Rahman, A. Al-Hajry and Y. B. Hahn, *Highly-Sensitive Cholesterol Biosensor Based on Well-Crystallized Flower-Shaped ZnO Nanostructures*. Talanta, 2009. **78**(1): p. 284-289.

159. I. Gonzalez-Valls and M. Lira-Cantu, *Dye Sensitized Solar Cells Based on Vertically-Aligned ZnO Nanorods: Effect Of UV Light on Power Conversion Efficiency and Lifetime*. Energy & Environmental Science, 2010. **3**(6): p. 789-795.

160. K. H. Tam, A. B. Djurisic, C. M. N. Chan, Y. Y. Xi, C. W. Tse, Y. H. Leung, W. K. Chan, F. C. C. Leung and D. W. T. Au, *Antibacterial Activity of ZnO Nanorods Prepared by a Hydrothermal Method*. Thin Solid Films, 2008. **516**(18): p. 6167-6174.

161. S. Cho, S.-H. Jung, and K.-H. Lee, *Morphology-Controlled Growth of ZnO Nanostructures Using Microwave Irradiation: from Basic to Complex Structures*. The Journal of Physical Chemistry C, 2008. **112**(33): p. 12769-12776.

162. J.H. Park, P. Muralidharan, and D.K. Kim, *Solvothermally Grown ZnO Nanorod Arrays on (101) and (002) Single- and Poly-Crystalline Zn Metal Substrates*. Materials Letters, 2009. **63**(12): p. 1019-1022.

163. M. Willander, K. ul Hasan, O. Nur, A. Zainelabdin, S. Zaman and G. Amin, *Recent Progress On Growth And Device Development Of Zno and CuO Nanostructures And Graphene Nanosheets*. Journal of Materials Chemistry, 2011. **22**(6): p. 2337-2350.

164. A. Sugunan, H. Warad, M. Boman and J. Dutta, *Zinc Oxide Nanowires in Chemical Bath on Seeded Substrates: Role of Hexamine*. Journal of Sol-Gel Science and Technology, 2006. **39**(1): p. 49-56.

165. C. Xu and D. Gao, *Two-Stage Hydrothermal Growth of Long ZnO Nanowires for Efficient TiO2 Nanotube-Based Dye-Sensitized Solar Cells*. The Journal of Physical Chemistry C, 2012. **116**(12): p. 7236-7241.

166. T. Jing-Hua, H. Jie, L. Si-Si, Z. Fan, L. Jun, S. Jian, L. Xin, T. Zhong-Qun and C. Yong, *Improved Seedless Hydrothermal Synthesis of Dense and Ultralong ZnO Nanowires*. Nanotechnology, 2011. **22**(24): p. 245601.

167. Y. Zhou, W. Wu, G. Hu, H. Wu and S. Cui, *Hydrothermal synthesis of ZnO nanorod arrays with the addition of polyethyleneimine*. Materials Research Bulletin, 2008. **43**(8-9): p. 2113-2118.

168. W. Wu, G. Hu, S. Cui, Y. Zhou and H. Wu, *Epitaxy of Vertical ZnO Nanorod Arrays on Highly (001)-Oriented ZnO Seed Monolayer by a Hydrothermal Route*. Crystal Growth & Design, 2008. **8**(11): p. 4014-4020.

169. H. Hu, X. Huang, C. Deng, X. Chen and Y. Qian, *Hydrothermal Synthesis of ZnO Nanowires and Nanobelts on a Large Scale*. Materials Chemistry and Physics, 2007. **106**(1): p. 58-62.

170. J. P. Kar, M. H. Ham, S. W. Lee and J. M. Myoung, *Fabrication of ZnO Nanostructures of Various Dimensions Using Patterned Substrates*. Applied Surface Science, 2009. **255**(7): p. 4087-4092.

171. Y. Xi, C. G. Hu, X. Y. Han, Y. F. Xiong, P. X. Gao and G. B. Liu, *Hydrothermal Synthesis of ZnO Nanobelts and Gas Sensitivity Property*. Solid State Communications, 2007. **141**(9): p. 506-509.

172. S. B. Khan, M. Faisal, M. M. Rahman and A. Jamal, *Low-Temperature Growth of ZnO Nanoparticles: Photocatalyst and Acetone Sensor*. Talanta,2011. **85**(2): p. 943-949.

173. R. Y. Hong, J. H. Li, L. L. Chen, D. Q. Liu, H. Z. Li, Y. Zheng and J. Ding, *Synthesis, Surface Modification and Photocatalytic Property of ZnO Nanoparticles*. Powder Technology, 2009. **189**(3): p. 426-432.

174. M. S. Tokumoto, V. Briois, C. V. Santilli and S. H. Pulcinelli, *Preparation of ZnO Nanoparticles: Structural Study of the Molecular Precursor*. Journal of Sol-Gel Science and Technology, 2003. **26**(1): p. 547-551.

175. V. Nadanathangam, K. Sampath, A. A. Kathe, P. V. Varadarajan and P. Virendra, *Functional Finishing of Cotton Fabrics Using Zinc Oxide-Soluble Starch Nanocomposites*. Nanotechnology, 2006. **17**(20): p. 5087.

176. G. Applerot, J. Lellouche, N. Perkas, Y. Nitzan, A. Gedanken and E. Banin, *Zno Nanoparticle-Coated Surfaces Inhibit Bacterial Biofilm Formation and Increase Antibiotic Susceptibility*. RSC Advances,2011. **2**(6): p. 2314-2321.

177. A.R. Khataee and M. Zarei, *Photocatalysis of a Dye Solution Using Immobilized ZnO Nanoparticles Combined with Photoelectrochemical Process*. Desalination, 2011. **273**(2-3): p. 453-460.

CHAPTER 2

Growth of nanorods

Introduction

This chapter covers the methods of nanorods growth to functionalize the fabric surface to generate hierarchical roughness structure. The characterization of nanorods as well as surface roughness is done by using the different techniques; scanning electron microscopy, profilometery, AFM, XRD spectroscopy, transmission electron microscopy, XPS spectroscopy and atomic absorption spectroscopy. The effect of nano seeds on roughness is also studied.

I Nanostructuration

To develop the nano-roughness on textile surface, ZnO nanorods were grown by using hydrothermal process. As discussed in section III.4 of chapter 1, the nanorods can be grown by seedless and seeding methods. The both methods were tested to functionalize the textiles. Both processes are summarized below.

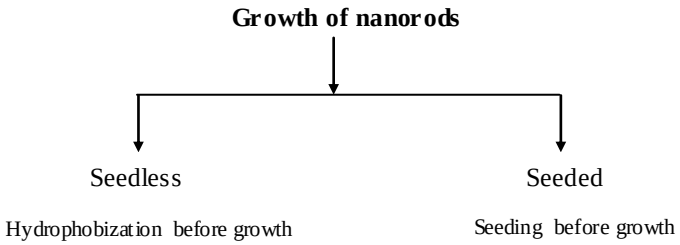

The scanning electron microscope (SEM) was used to observe the growth of nanorods on fabric. Hitachi S-3500N scanning electron microscope was used in this study. The samples were mounted on aluminum stubs using conductive carbon tape. As our samples were nonconducting, in order to avoid the accumulation of static charges on surface and to obtain high resolution images, the samples were metalized with ultrathin coating of gold.

I .1 Seedless growth

To grow the nanorods, equimolar solutions of zinc nitrate hexahydrate (ACS reagent grade with assay ≥ 98%, Sigma Aldrich) and hexamethylenetetramine (ACS reagent grade with assay ≥99.0%, Sigma Aldrich) were used. The fabric sample was held vertically in Teflon bottle with 250mL solution of each reagent at pH 7 and agitated with continuous stirring at 90°C for 4 hours, and then the sample was washed in distilled water and dried at 120°C for 5 minutes. The equimolar concentration of reagents varied from 25mM/l to 100mM/l. The details are available in annexe.

I .1.1 Growth of ZnO nanorods on cotton

The plain woven cotton fabric weight of 123±2g/m^2 was used to grow the nanorods. The cleaned fabric was mercerized with 400g/l caustic soda at room temperature and subsequently washed several times with water and mild acidified water to neutralize it. This treatment swells the fibers and makes them very uniform. The growth process was carried out under the above mentioned conditions the details of process are available in annexe.

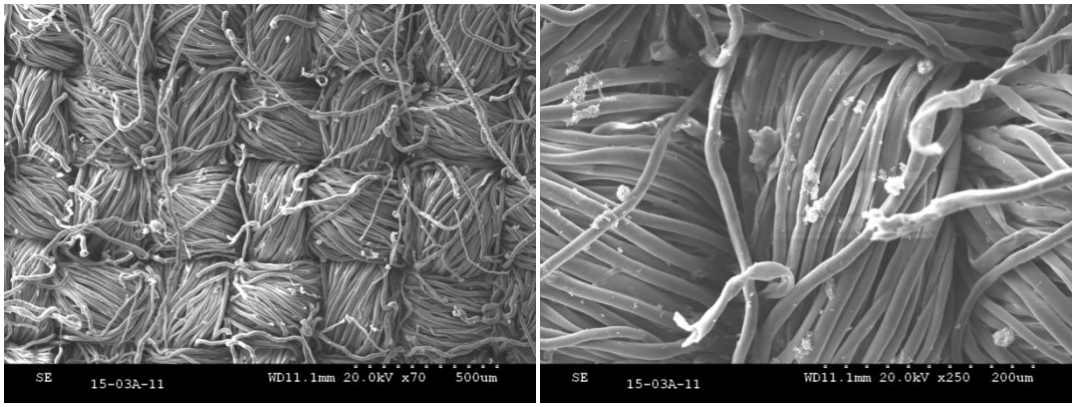

Figure 2-1: Cotton fabric treated with 100mM/l zinc nitrate hexahydrate and hexamethylenetetramine for growth of nanorods

It was found that nanorods did not grow on cotton fabric whatever was the precursor concentration (Figure 2-1). It is because of the hydrophilicity of cotton fabric (water contact angle is 0°). According to equation discussed in section I.1.1.1 of chapter 1, the solution spreads over the fabric surface and could not create the nucleus. In order to have the nucleation, the surface should be hydrophobic. As discussed in section III.4.1 of chapter 1, the hydrophobicity favors the nucleation and growth of nanorods.

In order to modify the cotton fabric to make it hydrophobic so that nucleation and growth of nanorods could take place, different chemicals were used. The synthesis and application of these chemicals, and subsequently the growth of nanorods on these modified samples are discussed below.

I .1.1.1 Hydrophobic pretreatment with methyltrimethoxysilane based silica gel

A silica gel was prepared from methyltrimethoxysilane (MTMS) (95% assay, Sigma Aldrich), $H_3C\text{-}Si\text{-}(OCH_3)_3$. We wanted to coat the surface of textile with a usual hydrophobic alkyl polysilane to induce the growth of zinc oxide nanorods. To prepare the gel, the acidic catalysis was used to accelerate hydrolysis of this MTMS. The molar ratio MTMS/H_2O equal to 1/3 allowed the complete hydrolysis of MTMS at room temperature and helped its polymerization. The methanol was chosen as solvent because of its compatibility with methoxysilane which maintained a homogenous solution during hydrolysis and cross-linking steps. Heating of the clear solution accelerate the gelation step. Thanks to dilution of MTMS in methanol (MTMS/CH_3OH=1/4), we obtained a

good control of temperature (boiled point: 65°C) giving appropriate viscosity to the final gel (for coating of textile). The following experimental procedure was used:

MTMS	*= 35.5ml (0.249 mole)*
Methanol(absolute) :	*= 10 ml (0.247 mole)*
Distilled Water	*= 13.5ml (0.75 mole)*
65% HNO_3	*= 50µl*

The above mentioned chemicals were added in a flask respectively and stirred at room temperature for 1 hour then refluxed at 60°C for 3 hours. MTMS was hydrolyzed and cross linked to give gel. eq 1

$$H_3C\text{-}Si\text{-}(OCH_3)_3 \rightarrow [(OR)_2Si(CH_3)\text{–}O\text{–}(CH_3)Si(OR)_2] \qquad \text{eq 1}$$

The prepared gel was applied to fabric by padding. The fabric was immersed in the gel for 5 minutes then squeezed between two rollers at nip pressure of 2 bars with 100% expression. This process was repeated twice. The sample was dried and cured at 120°C for 1 hour (details are available in annexe). The water contact angle measured on this treated fabric was 120°. Therefore, the value of spreading coefficient "S" would be negative and the solution would not spread over the fabric. This helps formation of nuclei on the surface.

The Figure 2-2 presents the SEM images of treated sample after growth of nanorods when precursor concentration was 25mM/l. It shows that nanorods grew on scattered places in form of flower like structures. This problem of scattered growth can be due to nonuniformity of surface modified with MTMS gel. The fabric became very stiff after the application of MTMS gel. Due to this stiffness, the possibility of cross linked gel to be broken was high causing the nonuniformity of the surface.

It is believed that the reason for growth of flower like structure in this study is similar to the one discussed in section III.4.3.1 of chapter 1. Although the initial pH of solution is 7, but on heating more and more hydroxyl groups are produced by the reaction between hexamethylenetetramine and water as shown in reaction 2 and 3, and as results the growth units $[Zn(OH)_4]^{2-}$. But its consumption for the growth is low due to availability of less number of nuclei on fabric surface. Due to this imbalance, the growth units start depositing on same nucleus in different direction leading to growth of flower like structures.

$$(CH_2)_6N_4 + 6H_2O \rightarrow 6HCHO + 4NH_3 \qquad \text{eq.2}$$

$$NH_3 + H_2O \rightarrow NH_4^+ + {}^-OH \qquad \text{eq.3}$$

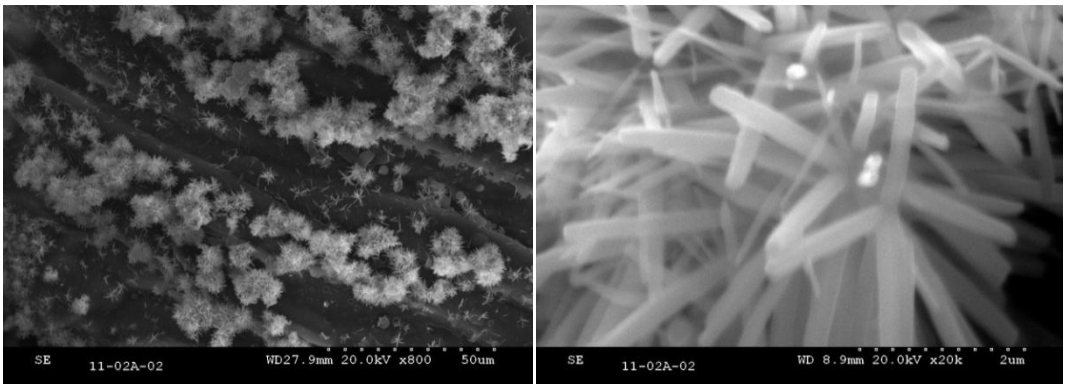

Figure 2-2: MTMS gel modified cotton fabric treated with 25mM/l zinc nitrate hexahydrate and hexamethylenetetramine for growth of nanorods

I .1.1.2 Hydrophobic pretreatment with isobutyl(trimethoxy)silane based silica gel

In order to avoid above mentioned problem, Isobutyl(trimethoxy)silane $(CH_3)_2CHCH_2Si(OCH_3)_3$ was used as precursor to prepare the gel. As it has long carbon chain made of 4 carbon atoms, the application of relatively low quantity of gel prepared from it will give the higher hydrophobicity with less stiffness. Isobutyl(trimethoxy)silane (97% assay, Sigma Aldrich) gel was prepared by using the following conditions.

ISBTMOS	*= 10ml (0.052 mole)*
Methanol(Absolute)	*= 20ml (0.50 mole)*
Water	*= 10ml (0.55 mole)*
65%HNO3	*= 50µl*

All the above ingredients were mixed respectively in round bottom flask and stirred at 60°C for one hour. ISBTMOS was hydrolyzed and cross linked to give gel.

$$C_4H_9\text{-}Si\text{-}(OCH_3)_3 \rightarrow [(OR)_2Si(C_4H_9)\text{–}O\text{–}(C_4H_9)Si(OR)_2] \quad \text{eq 4}$$

This gel was applied to fabric by padding method with 100% expression. The sample was dried and cured at 120°C for 1 hour.

The Figure 2-3 presents the SEM images of treated sample when the precursors concentrations were 50mM/l. It shows that the flower like structures grew with nanorods as their petals. The fabric was relatively less stiff with water contact angle 125° but the nanorods did grow uniformly perpendicular to fiber surface. Again due to probably the same reasons mentioned above in case of MTMS gel.

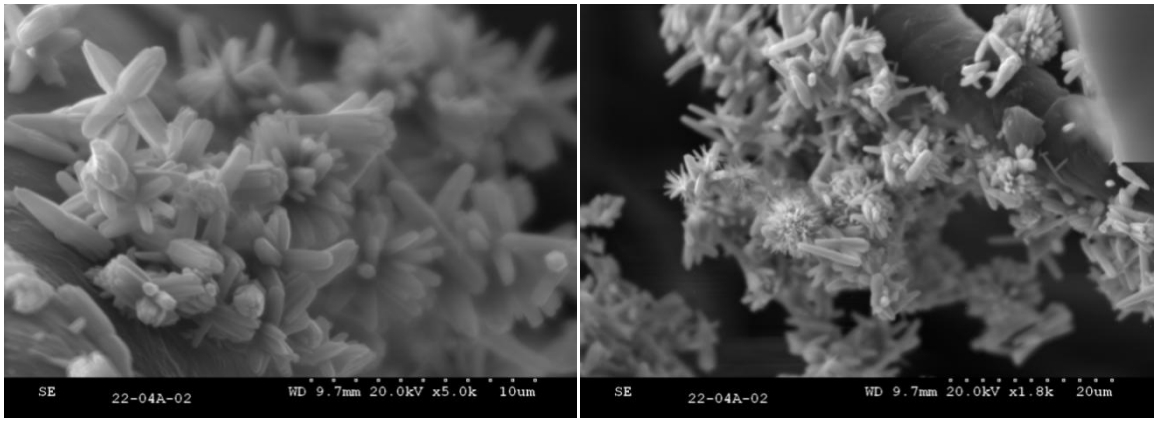

Figure 2-3: IBTMOS gel modified cotton fabric treated with 50mM/l zinc nitrate hexahydrate and hexamethylenetetramine for growth of nanorods

I.1.1.3 Hydrophobic pretreatment with octadecyltrimethoxysilane (ODS)

To avoid the problem of stiffness and to obtain uniformity of the hydrophobic treatment, Octadecyltrimethethoxysilane (90% Assay, Sigma Aldrich) $CH_3(CH_2)_{17}Si(OCH_3)_3$ was deposited on fabric by vapor deposition method. It has very long chain of carbon atoms which impart hydrophobicity, therefore, only a monolayer of it will give sufficient hydrophobicity. The fabric was held vertically in Teflon bottle with 200µl of ODS placed at its bottom details are available in annexe. The closed bottle was heated at 150°C for 2 hours. The water contact angle was measured to be 132°. It has relatively lower spreading coefficient as compared to the previous cases.

The Figure 2-4 presents the images of treated sample (precursor's concentrations 100mM/l). It shows that nanorods were grown in solution and just deposited on fibers but there is also little nucleation on surface due to which flower like structures grows.

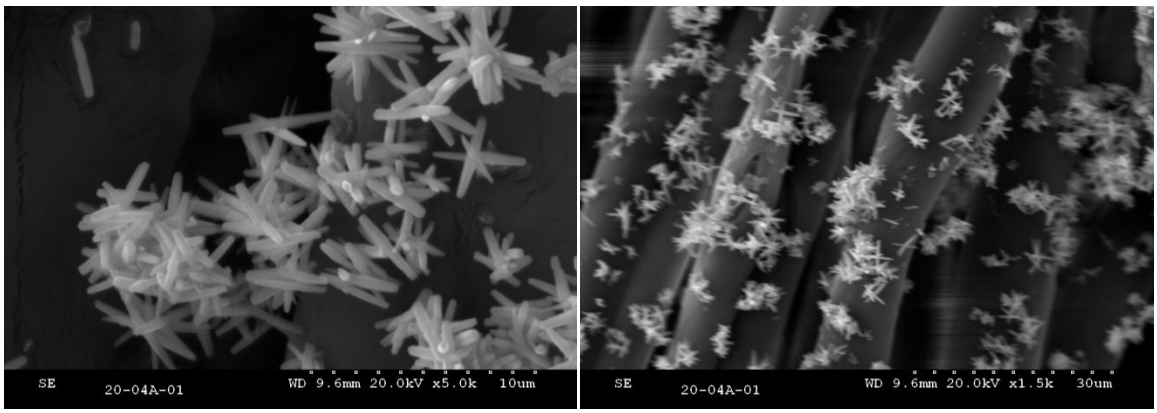

Figure 2-4: ODS modified cotton fabric treated with 100mM/l zinc nitrate hexahydrate and hexamethylenetetramine for growth of nanorods

I .1.1.4 Hydrophobic pretreatment with fluorinated polymer (Oleophobol CO)

In order to further enhance the hydrophobicity to obtain nucleation and growth of nanorod on fabric, it was treated with Oleophobol CO (product details are in annexe) which is a commercial fluorinated polymer. The fabric was padded in solutions containing 2g/l to 10g/l of Oleophobol CO with 100% expression, dried and cured at 150°C for 5 minutes. The water contact angles measured on these samples were 120° to 135°.

The Figure 2-5 presents the images of a treated sample (precursor's concentration 50mM/l) when the Oleophol CO concentration was 8g/l. Approximately, the same result was obtained as in previous cases.

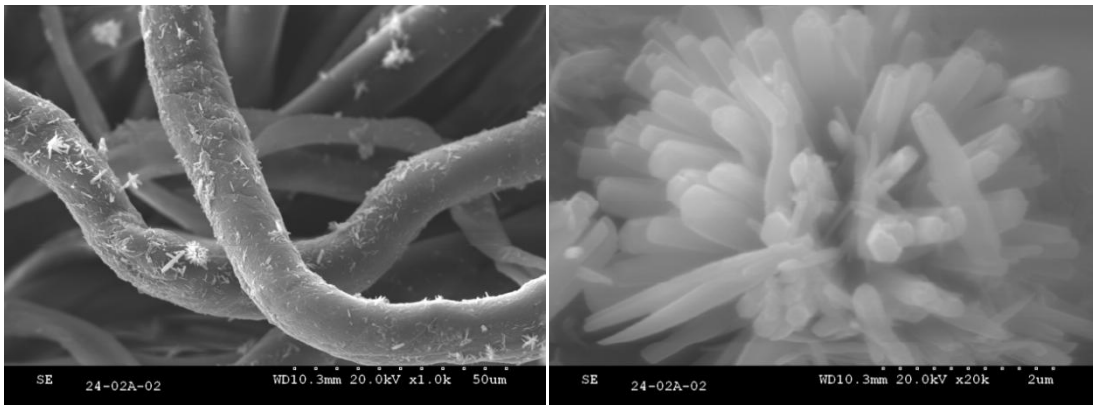

Figure 2-5: Oleophobol CO modified cotton fabric treated with 50mM/l zinc nitrate hexahydrate and hexamethylenetetramine for growth of nanorods

As a conclusion, it can be said that on modified cotton fabric, the nanorods grow on scattered places in flower like structures. The scattered growth is probably due to nonuniformity of cotton fabric. The cotton fabric is made up of natural fibers which have lot of variations in their size, presence of contamination, organic and inorganic impurities etc, which add to the nonuniformity of hydrophobic treatment. Perhaps, it was the reason for not obtaining the uniform of growth of nanorods.

I .1.2 Growth of nanorods on poly(ethyleneterephtalate)

To avoid the nonuniformity of fibers and the hydrophobization process, the polyester fabric was chosen for the growth of nanorods due to uniformity of fibers and inherent hydrophobicity. Plane woven fabric made of micro fibers (9-10µm) was used in this process. The water contact angle (WCA) on this fabric (without impurities) measured by sessile drop method was 88°. The details of fabric cleaning and checking of impurities are available in annexe.

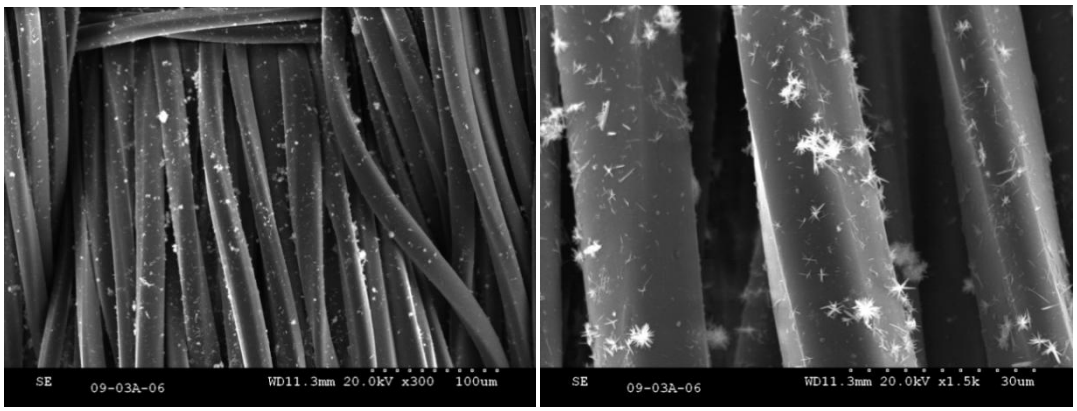

Figure 2-6: Polyester fabric treated with 100mM/l zinc nitrate hexahydrate and hexamethylenetetramine for growth of nanorods

The nanorods were grown by equimolar concentrations (25mM/l to100mM/l) of zinc nitrate hexahydrate and hexamethylenetetramine at 90°C for 4 hours. The SEM images show that there is no growth of nanorods (Figure 2-6). There is only deposition of nanostructures which grew in solution. The same results were obtained for all precursors concentrations (25mM/l to 100mM/l). The nanorods did not grow on fabric, perhaps the surface was not enough hydrophobic to have the nucleation of the surface

To increase the hydrophobicity, the polyester fabric was treated with same chemicals as for cotton fabric described in previous section, in the same conditions.

I .1.2.1 Hydrophobic pretreatment with methyltrimethoxysilane based silica gel

The water contact angle measured on fabric treated with silica gel described in section I .1.1.1 of this chapter was 110°. The contact angle for polyester fabric is lower than that of cotton treated with same gel. The cotton fabric has protruding fibers as it has lot of long and short fibers which increase the surface roughness and contact angle. The polyester fabric is made of long filaments therefore, there are no protruding fibers.

The Figure 2-7 presents the SEM images of treated sample when precursor concentration was 50mM/l. It shows that either nanorods grew on scattered places or just deposited which were grown in solution. The growth is in the form of flower like structures as they grew in case of cotton fabric treated with MTMS.

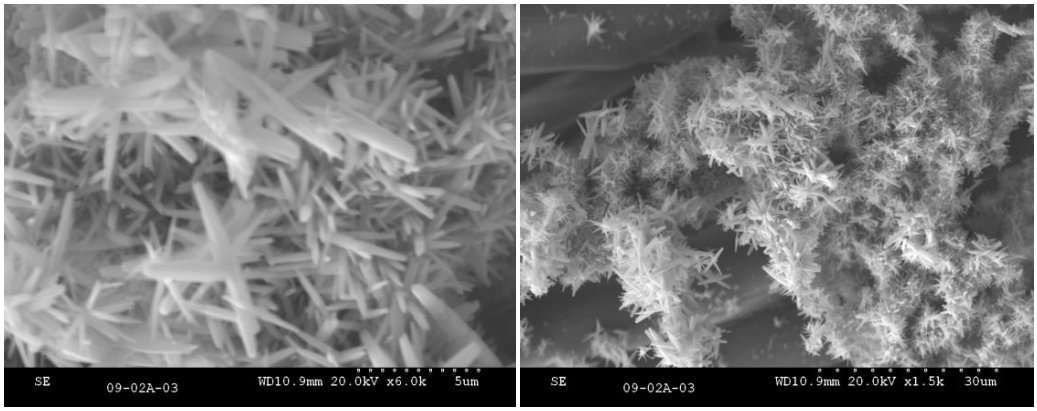

Figure 2-7: MTMS gel modified Polyester fabric treated with 50mM/l zinc nitrate hexahydrate and hexamethylenetetramine for growth of nanorods

I .1.2.2 Hydrophobic pretreatment with isobutyl(trimethoxy)silane based silica gel

The Figure 2-8 presents the SEM images of treated sample with 75mM/l precursor concentrations. It shows that the nanorods grew as flower like structures in solution and are deposited on scattered places on fabric.

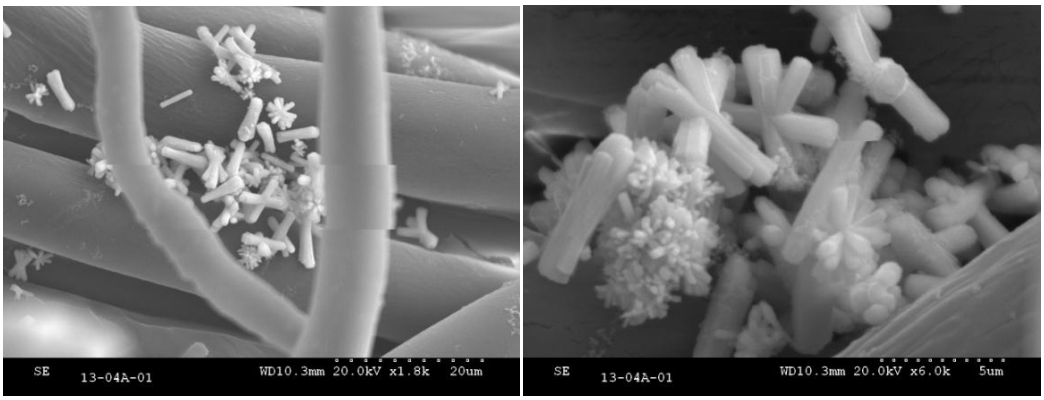

Figure 2-8: ISBTMOS gel modified Polyester fabric treated with 75mM/l zinc nitrate hexahydrate and hexamethylenetetramine for growth of nanorods

I .1.2.3 Oleophobol CO

Oleophobol CO was applied to polyester fabric under the same conditions as it was applied to cotton fabric. The water contact angle measured on this sample was 120° to 130° when the expression was 100%.

Although the nanorods grew perpendicular to surface of fibers with 50mM/l precursors concentrations as it was required when the Oleophobol CO concentration was 6g/l but their growth is on scattered placed (Figure 2-9).

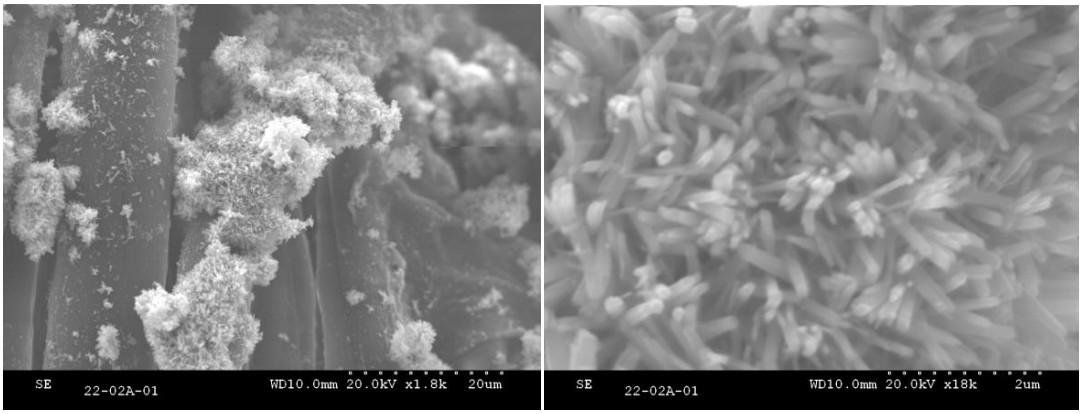

Figure 2-9: Oleophobol CO modified Polyester fabric treated with50mM/l zinc nitrate hexahydrate and hexamethylenetetramine for growth of nanorods

I .1.3 Comparison with Literature

The results obtained in the present study are different than previous work which was carried out on Si wafer. For instance, the nanorods were grown on Si substrate modified with octadecyltrimethoxysilane to make the substrate hydrophobic [1]. In another study, it was once again demonstrated that the presence of CH_3- at the surface favors the growth of ZnO nanorods [2]. The textile structures are very different than the flat surfaces. It is relatively easier to modify flat surfaces uniformly with different chemicals to obtain nucleation but in case of textiles, uniform treatment is very difficult due to complex structure which is responsible for the flower like structures and scattered growth of nanorods.

I .1.4 Conclusion

In conclusion, it can be said that the growth of nanorods are affected by surface characteristics. They do not grow on hydrophilic surface like cotton fabric because the solution spreads over the surface. The hydrophobicity is the pre-requisite to nucleation and growth of nanorods. Although the nucleation and growth of nanorods took place when both cotton and polyester fabrics were treated with hydrophobic chemicals but they were not uniform. They grew either as flower like structures with nanorods as their petals like on MTMS silica gel treated cotton fabric or as nano needles perpendicular to the fiber surface on Oleophobol CO treated polyester fabric on scattered places. It is believed that the scattered growth of nanorods is due to the nonuniformity of fabric pre-treatment which affects the nucleation of nanorods.

I .2 Seeded growth

The growth of nanorods is sensitive to the nucleation step which caused the scattered growth. In order to overcome this problem, the nano seeds were deposited on fabric which provided the site for the growth of nanorods.

In the first step nano seeds are prepared and deposited on fabric. The nano seeds were prepared by using 90mM/l of zinc acetate dihydrate (ACS assay ≥ 98%, Sigma Aldrich) and 75 mM/l sodium hydroxide (ACS reagent pellets, Sigma Aldrich). The solutions of both reagents were prepared in absolute methanol. Then, sodium hydroxide solution was added slowly to solution of zinc acetate dihydrate while stirring at 60°C and the mixture was refluxed. After 3 hours a transparent seed solution was obtained.

When the seed solution cooled down at room temperature, the fabric was immersed in it for 5 minutes, then squeezed between two rollers at nip pressure of 2 bars and dried at 120°C for 2 minutes. This process was repeated 5 times to ensure uniform application of seeds on each fiber. Finally, the seeded fabric was cured at 170°C for 8 minutes.

In the 2nd step, equimolar (100mM/l) solutions of hexamethyleneteramine and zinc nitrate hexahydrate were used to grow nanorods. Seeded PET fabric was held perpendicularly in Teflon bottle and 250ml of each solution was added. The pH of the solution was maintained at 7. The mixture was agitated at 90°C for 4 hours. Then, the samples were washed in distilled water for 3 times and dried at 120°C for 10 minutes

I .2.1 Untreated Polyester fabric

The clean polyester fabric without any pretreatment was seeded with seed solution described in section I .2 and placed in Teflon bottle containing reagent solutions for the growth of nanorods. The Figure 2-10 shows that nanorods grow only on scattered places. This means that the seeds do not attach on the surface very well and during growth process, they transfer from fabric to solution which causes the loss of nucleating sites for the growth of nanorods.

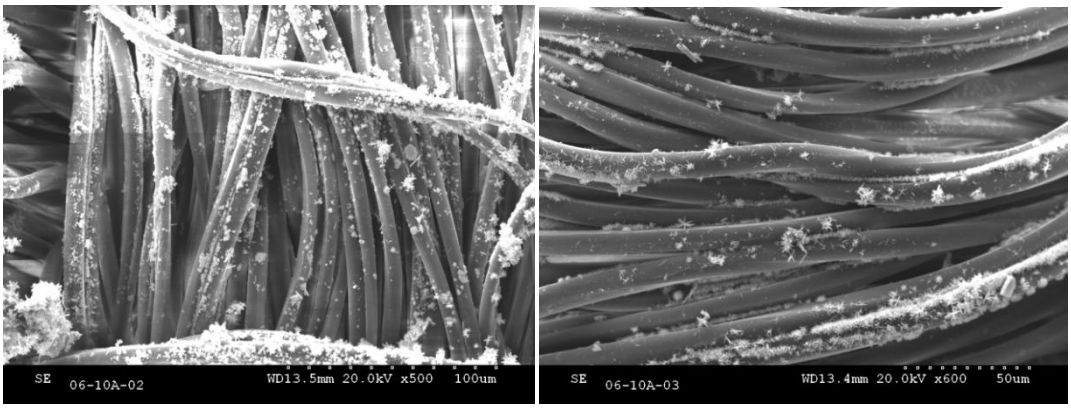

Figure 2-10: Seeded polyester fabric treated with zinc nitrate hexahydrate and hexamethylenetetramine for growth of nanorods

I .2.2 Plasma treated polyester fabric

In order to overcome the problem of detachment of nano seeds from the fiber surface, the atmospheric plasma treatment was carried out to generate the polar groups so that nano seeds could attach on it.

The atmospheric air plasma device used in this study was the "Coating Star" Systems. Dielectric Barrier Discharge (DBD) was created in air at atmospheric pressure. The following machine parameters were used: speed of 2 $m.min^{-1}$, electrical power of 750 W, frequencies of 26 kHz. The sample was treated twice on each side. The Figure 2-11 shows the schematic diagram of plasma treatment machine.

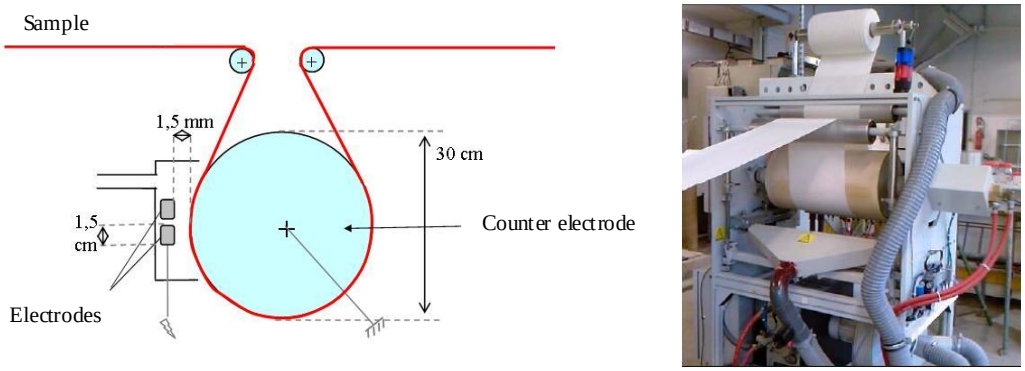

Figure 2-11: A. Schematic diagram of plasma machine, B. image of Coating Star plasma treatment machine.

To check the effectiveness of plasma treatment, the water contact angle was measured by tensiometric method on GBX-3S (details in chapter 3). The water contact angle on PET surface before treatment was 88° and decreased to 33° for functionalized PET surface. This result confirms the creation of polar groups at the surface of PET. In order to check the presence of weak layer of oligomer if any, formed during plasma treatment, we carried out tensiometric test i.e. the surface tension of water was checked before and after immersion of a small piece of plasma treated PET fabric in water for 5 minutes. It was found that there was no change in surface

tension of water before and after. Therefore no oligomer was present on surface because if an organic impurities move from fabric to water, the surface tension of water reduces.

This plasma treated fabric was seeded with seeding solution prepared with same concentrations of zinc acetate dihydrate and sodium hydroxide as described in section I.2. The nanorods were grown with equimolar concentrations (100mM/l) of zinc nitrate hexahydate and hexamethylenetetramine. The Figure 2-12 shows that the nanorods grew all over the fibers uniformly. It means that presence of polar group on fabric surface is imperative to bind the seeds and to obtain uniform growth of nanorods at the PET surface.

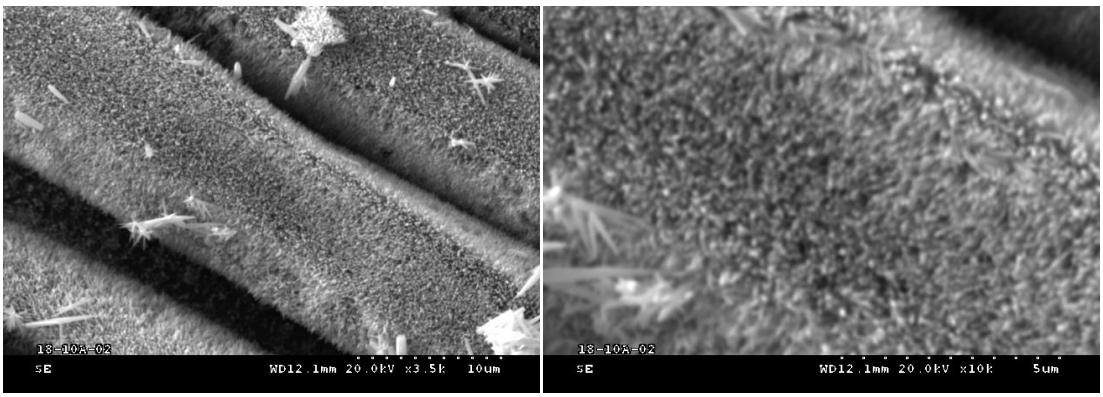

Figure 2-12: Nanorods grown on plasma treated seeded polyester fabric

The results of seeded growth are summarized below.

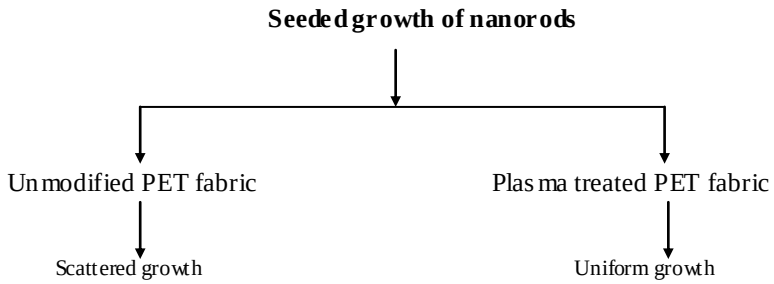

As the nanorods have been successfully grown on PET fabric, the rest of study will be carried out on only this fabric.

I .2.3 Characterization of surface

I .2.3.1 Profilometery

The surface structure of fabric was characterized by using profilometer AltiSurf® 500. The AltiSurf® 500 is a multi-sensor system created to read accurately component surfaces. It measures several profiles, which,

automatically put together, allow rebuilding the morphology of the sample. Then post-treatment software enables to apply analysis parameters such as roughness, tribology, forms and dimensions as well as topographic phenomenon. It was used to characterize the surface morphology of PET fabric before growth of nanorods. The details of process are available in annexe.

The Figure 2-13 presents the profile of the fabric. The protruding fibers are responsible for the micro-roughness. The average roughness calculated on this fabric was 18±2µm after carrying out the test on three different places.

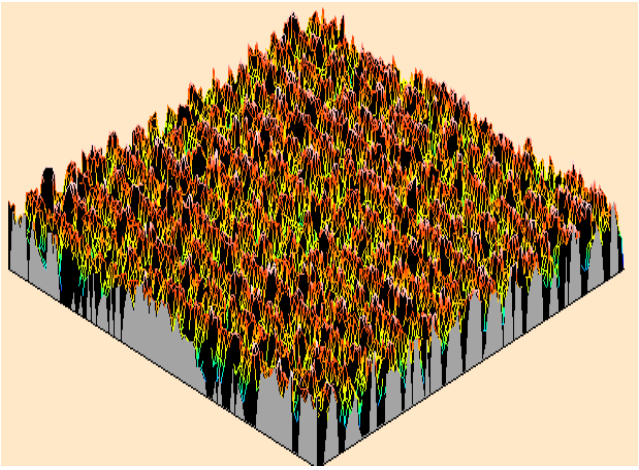

Figure 2-13: Profile of the fabric

I .2.3.2 Atomic absorption spectroscopy

To determine the amount of ZnO deposited on fabric in the form of nanorods, atomic absorption spectroscopy (AAS) was carried out, because it is frequently used for quantitative analyses of elements. The basis of AAS is the absorption of discrete wavelengths of light by ground state, gas phase free atoms. Atomic absorption is the process that occurs when a ground state atom absorbs energy in the form of light of a specific wavelength and is elevated to an excited state. The amount of light energy absorbed at this wavelength will increase as the number of atoms of the selected element in the light path increases. The relationship between the amount of light absorbed and the concentration of analytes present in known standards can be used to determine unknown sample concentration by measuring the amount of light they absorb. The absorption of light is proportional to the concentration of free atoms in the flame. It is given by Lambert-beer law.

$$\text{Absorbance} = \log I_0/I_t = k.c.l$$

Where, I_0 = intensity of incident radiation emitted by the light source. It= intensity of transmitted radiation. c = concentration of sample (free atoms). k = constant l = path length

In order to determine the amount of zinc oxide present on fabric in the form of nanorods, the treated samples were dissolved in chlorhydric acid ($1M l^{-1}$), then the tests were carried out on PERKIN ELMER 1100 B with Zn Electrodeless Discharge Lamp (N3050691).

Before carrying out the experiments, calibration curves are prepared from solutions of known concentrations of ZnO (Figure 2-14). The concentration of the unknown is determined from the calibration curve. An average value of 5.6±0.6 percent Zn on the weight of fabric samples was calculated from.

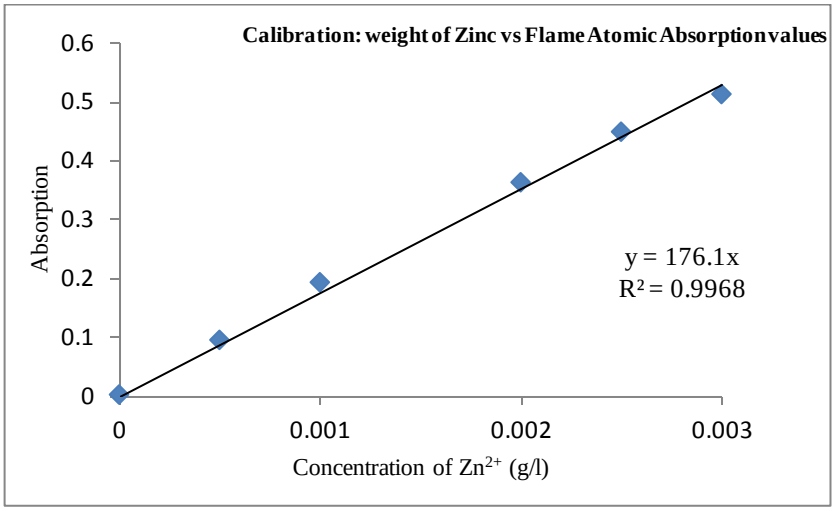

Figure 2-14: Calibration curve of Zn (g/l) versus absorption

I .2.3.3 X-ray photoelectron spectroscopy (XPS)

To determine the chemical composition of the surface at all stages of nanorods growth, X-ray photoelectron spectroscopy (XPS) was carried out. The analysis was performed on a SSX 100/206 photoelectron spectrometer from Surface Science Instruments (USA) equipped with a monochromatized micro focused Al X-ray source (powered at 20 mA and 10 kV). Pieces of about 5mm x 5mm were cut from each sample and fixed with a double sided adhesive tape on an insulating homemade ceramic carousel (Macor® Switzerland) instead of the aluminium one to avoid the distortion of peaks due to semi conductor nature character of samples. The pressure in the analysis chamber was about 10^{-7} Pa. The angle between the surface normal and the axis of the analyser lens was 55°.

The Table 1 presents the result of XPS analysis on each stage of nanorods growth. After plasma treatment, the percentage of oxygen is increased and that of carbon is decreased which shows the generation of polar group like carboxylic group. These carboxylic groups attach the nano seeds on the fabric on which nanorods grow. The seeded fabric has around 2.70% Zn on the surface which increases to 30.70% after the growth of nanorods.

Table 1 XPS analysis data

Binding energy / Sample	Na	Zn	-O-	C-(CH)-
	1071eV	1021eV	531eV	288eV
PET	0	0	29.32	70.68
Plasma treated PET	0	0	33.40	66.60
PET + seeds	1.72	2.66	30.26	65.36
PET + nanorods	0.89	30.64	40.22	28.25

The amount of Zn determined by atomic absorption spectroscopy is 5.60% whereas, with XPS analysis, it appeared to be more than 30%. This difference is due to the difference of measuring techniques. In atomic absorption spectroscopy, all the Zn is determined and is expressed in percentage with respect to the total weight of the fabric, but in XPS analysis, the amount present on the surface is calculated and is expressed in percentage with respect to the surface because the most of the surface is covered with ZnO, therefore, it appeared to be higher than the one measured with atomic absorption spectroscopy.

I .2.3.4 Atomic force microscopy (AFM)

To determine the roughness generated due to the growth of nanorods, atomic force microscope (AFM) was used. The vertical z-deflections of a micro tip scanning the fiber surface are measured when the sample is moved horizontally in the x and y directions. These allow the apparatus software to build-up a topographical image of the scanned fiber surface. The software also calculates the fiber surface roughness (R_a) *(Eq.0 1)* directly from AFM signals.

$$R_a = \frac{1}{L_x \cdot L_y} \int_{L_x} \int_{L_y} f(x,y).dx.dy \qquad \text{Eq 01}$$

Where,

$f(x,y)$ *: Average surface*

L_x *and* L_y *: Surface size chosen for the roughness calculation*

In our study, "Nanoscope III" from Digital Instrument was used in non contact mode to acquire the topographic images of the nanorods treated fabric. At least 3 three samples were prepared and on each sample, AFM topographs were obtained. The Figure 2-15 present the topograph of the sample on which nanorods were grown. It can be seen that the surface is uniformly nanostructured. This generates a roughness around 23±3.4nm.

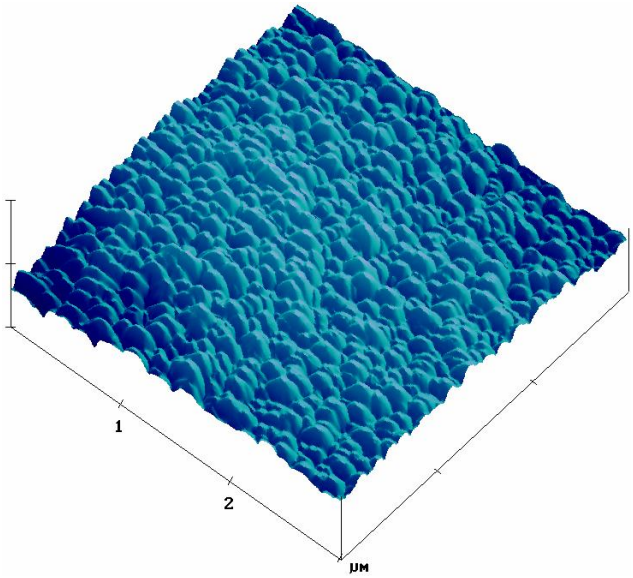

Figure2-15: Topograph of nanorods grown on micro fibers of polyester fabric

I .2.3.5 X-ray diffraction spectroscopy (XRD)

X-ray powder diffraction (XRD) is used for qualitative and quantitative analysis of crystalline compounds. The information obtained includes types and nature of crystalline phase present, structural make-up of phases, degree of crystallinity, the amount of amorphous content and orientation of crystallites. *PANalytical's X'Pert PRO* Materials Research Diffraction system operating at 45 KV and 40 mA was used to characterize crystal structures and their orientation at 2Θ. The wavelengths of tube Cu are; Kα1= 1.540593 Å, Kα2= 1.54442 Å, Kα3= 1.54187 Å.

The peaks obtained on untreated PET fabric and seeded PET fabric with XRD analysis at 2θ are same which shows that nano seeds deposited on fabric are either non crystalline or their amount is too low. The PET fabric treated with nanorods presented three main peaks at 32.01°, 34.649° and 36.417° which correspond to (100), (001) and (101) respectively (Figure 2-16). This is attributed to different orientations of the nanorods due to fiber curvature, as can be seen on powders.

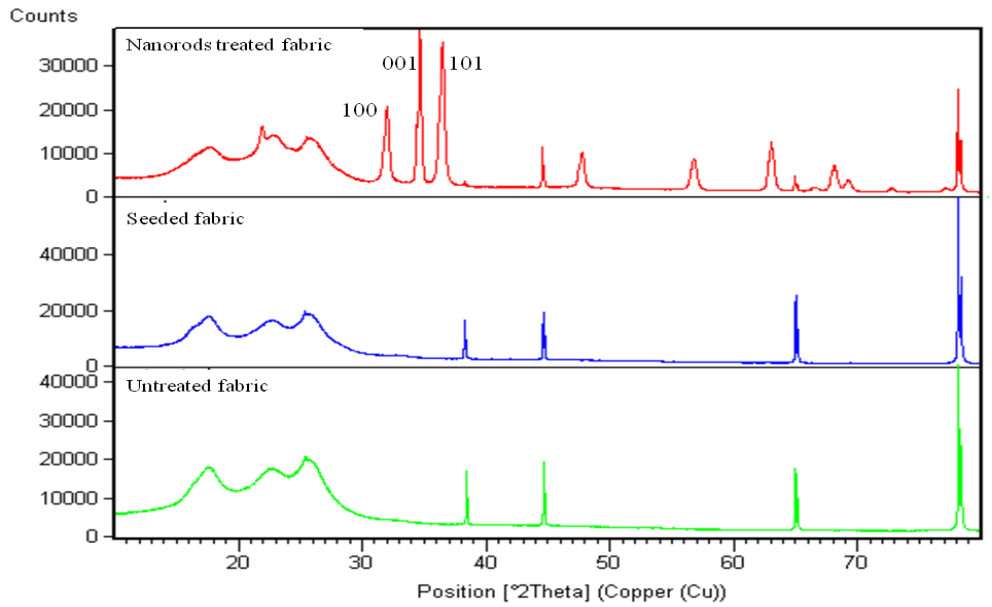

Figure 2-16: XRD analysis at 2θ on untreated seeded and nanorods grown sample.

I .2.3.6 Transmission electron microscopy (TEM)

To study the fine details of nanorods grown on PET fabric; morphology, crystal orientation and lattice structure, FEI Tecnai G2 20 transmission electron microscope (TEM) was used. The nanorods were scraped from the fabric surface and used for this study.

The TEM images are presented in Figure 2-17. The image A shows that nanorods grow in taper shapes, its diameter at the bottom is about around 100nm which reduces to 50nm at the top. As the nanorods grow along (001), the top of it tends to reduce surface area due to high surface free energy which leads to its growth in taper shape [4]. The crystal orientation is along (001) which shows that nanorods grow preferentially along (001) because this plane has maximum surface energy as compared to other planes which favors the growth along (001) [3]. The selected area electron diffraction SAED shows that the nanorods grow as mono whiskers and have wurtzite crystal structure.

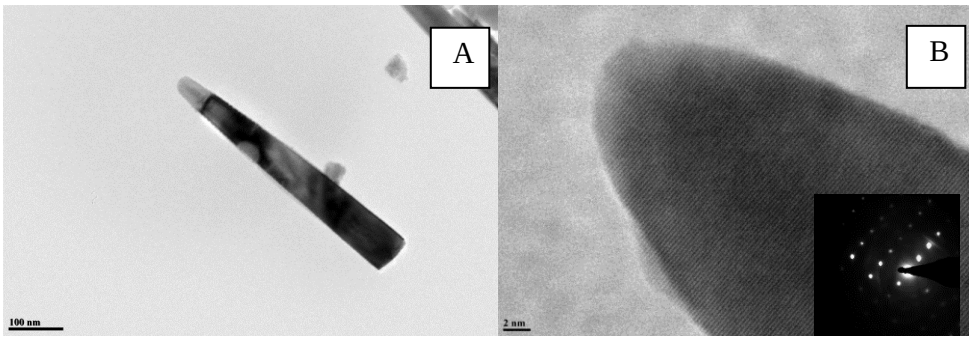

Figure 2-17: A. TEM images of nanorod showing its taper shape, B. High resolution TEM image and SAED in inset

I .2.4 Discussion

In the seeded method, the ZnO seeds act as nuclei for the growth of nanorods. As discussed in section III.4.2 of chapter 1, the energy barrier for heterogeneous nucleation on substrate is less than that of homogeneous nucleation in solution, the seeding of the surface further reduces it because the interfacial tension between solution species and a crystal nucleation site depends on the degree of structural fit, the same crystal type having the best fit and lowest energy barrier. Another important thing which favors the seeded growth is the presence of -OH groups on seeds which are similar to those present on (0001) face of ZnO crystals.

Another important thing is the hand feel of the fabric. Surprisingly, it does not change after the growth of nanorods. Rather, the nanorods functionalized fabric becomes little softer than the substrate. It is because, the nanorods attach on fabric surface but they are independent of each other. It can be said that they adhere well to fabric but do not cohere with each other as shown in Figure 2-18. The each nanorod grows on different seed and neither the seeds nor the nanorods are linked with each other. Otherwise, the fabric should become very stiff like after the crosslinking of gel as discussed in section I .1.1.1 of this chapter.

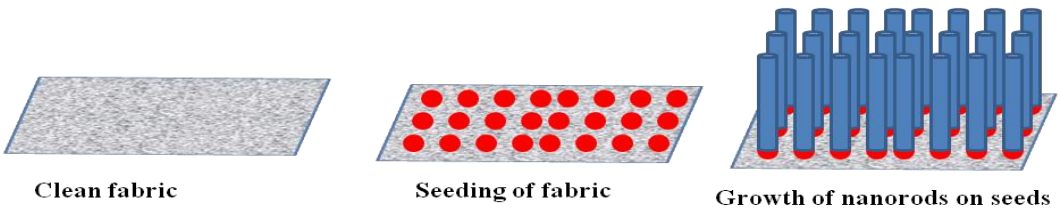

Figure 2-18: Different stages of nanorods growth in seeded method

The results obtained in the present study are similar with the previous works in which ZnO nanorods were grown on different surfaces by seeding method including nylon [5] Si wafer [6] and cotton fabric [7] under approximately similar process conditions.

I .2.5 Conclusion

The nanorods were successfully grown on micro fibers of polyester fabric by seeding method. The functionalized fabric contained around 5.60±0.6% ZnO in the form of nanorods. The plasma treatment played a vital role for the uniform growth. The XPS analysis showed that polar groups were generated during plasma treatment which attached the nano seeds on the surface on which the nanorods grew. The polyester fabric contained micro protrusions which were decorated with nanorods. This formation generated hierarchical

roughness structure. The analysis of nanorods with XRD spectroscopy and TEM showed that they were highly monocrystalline and grew preferentially along (001) direction in the form of mono rods.

II Effect of seed concentration on roughness

The hierarchical roughness structure like lotus leaf has been developed by growing the nanorods on micro fibers of polyester fabric by seeding method. Therefore, the seed concentration affects the growth of nanorods and nano-roughness.

II.1 Samples preparation

To study this effect, the concentrations of precursors used for seed preparation (zinc acetate dihydrate and sodium hydroxide) were varied according to Table 2, while keeping the other parameters constant (precursors; zinc nitrate hexahydrate and hexamethylenetetramine at 100 mM/l).

Table 2: Precursors concentrations for seeds

Sample Name	Zinc Acetate dihydrate (mM/l)	Sodium hydroxide (mM/l)
A	180	150
B	90	75
C	45	37.5
D	10	3.75
E	1	0.75

II.2 Morphological characterization

The morphologies of samples checked with SEM show that the ZnO crystals have grown as nanorods at the fibers surfaces (Figure 2-19). Apparently, all the samples except E look like uniformly covered with nanorods grown on different seed concentrations. Atomic force microscopy analysis reveals that each sample has different roughness and roughness patterns (Figure 2-20). As the seed concentration changes (sample A, B, C, D and E) the roughness patterns generated due to nanorods also change. The nanorods grow on scattered places on E because it has very low seed concentration; therefore, the AFM topographic images are very uneven.

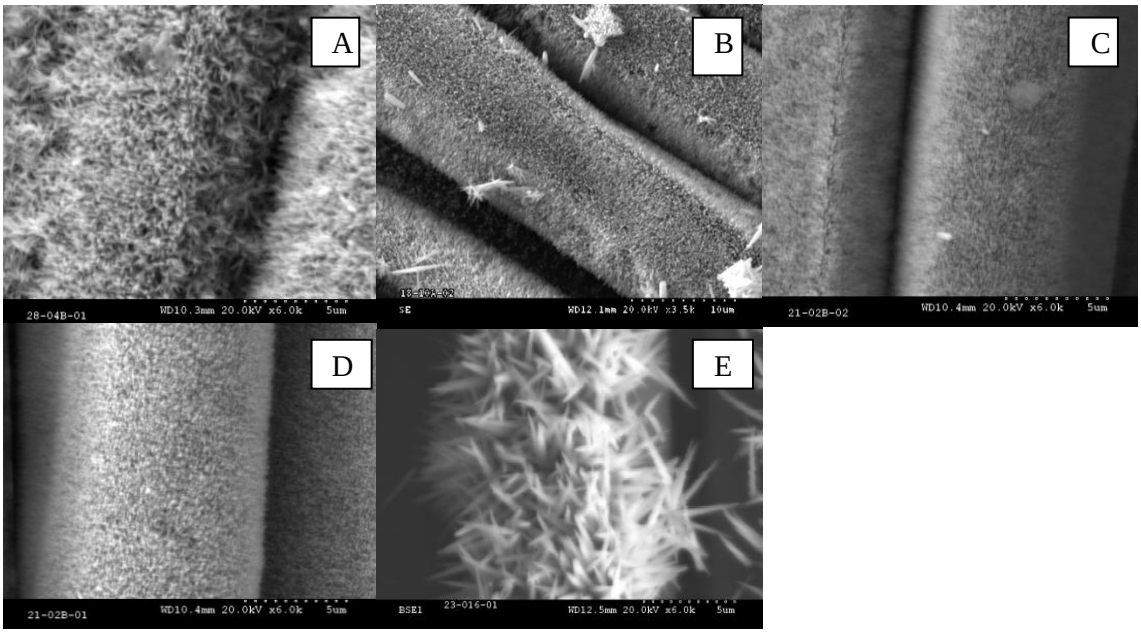

Figure 2-19: SEM images of A, B, C, D and E are samples with nanorods grown on different seed concentrations (see table 1)

As the nano seeds provide the site for nucleation which is pre-requisite for growth of nanorods, therefore, higher the seed concentration, higher is the nucleation on surface and denser will be array of nanorods grown on fabric.

Table 3 presents the average of roughness measured by AFM on 6 different places of each sample and its standard deviation which gives the uniformity of roughness generated on surface. The sample B has minimum roughness just 23nm as well as minimum roughness standard deviation that is 3.4. The sample A has roughness 30nm and its standard deviation is 7.3. The sample C and D have high roughness standard deviation. We can say that sample B has the less rough and most uniform surface structure.

Table 3: AFM analysis details of samples

Sample name	Roughness(nm)	Standard deviation
A	30	7.3
B	23	3.4
C	69	26
D	52	10
E	265	25

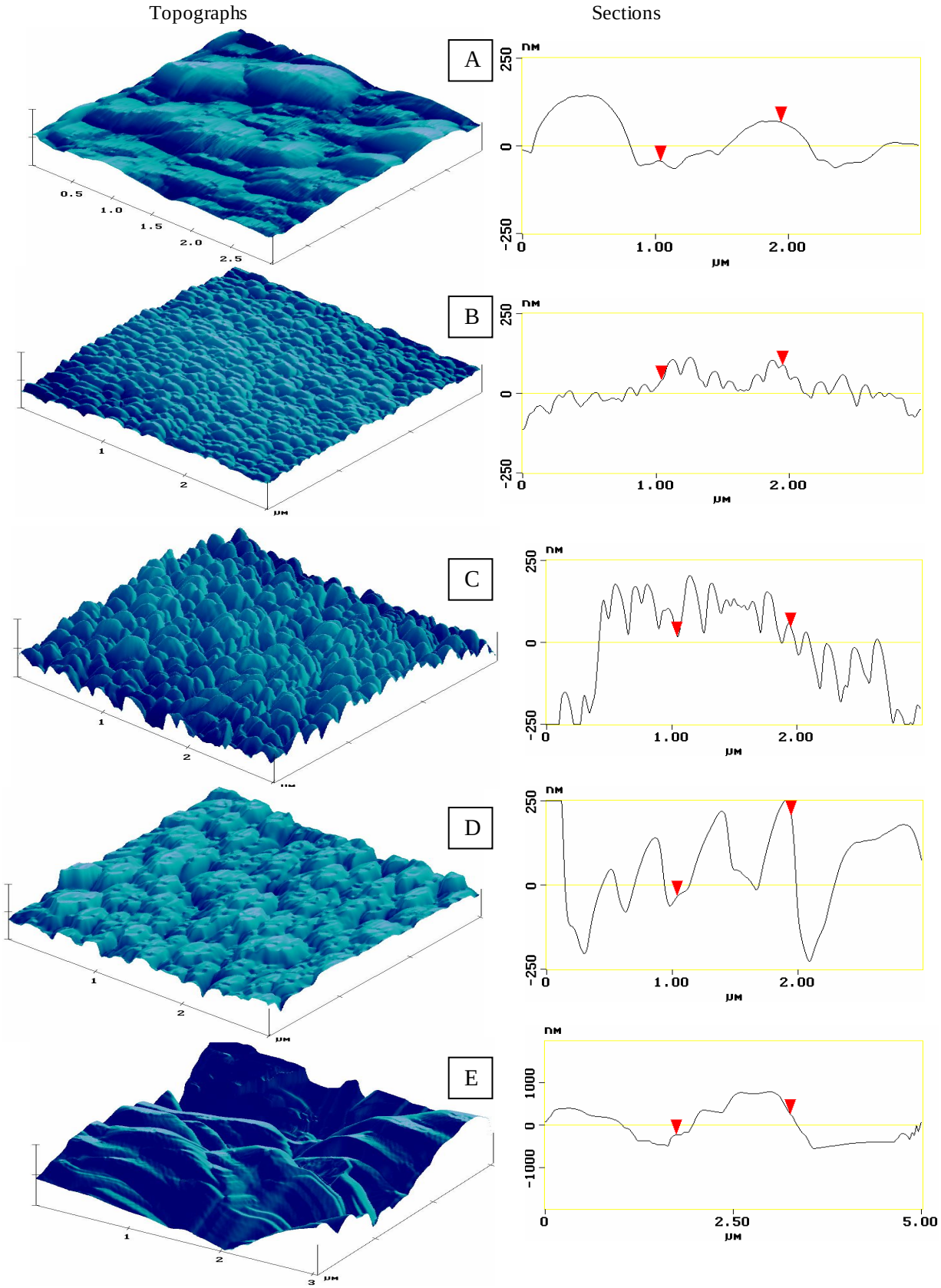

Figure 2-20: AFM topographs of samples A, B, C, D and E, and their section.

The SEM image of sample A shows the presence of nanorods while from AFM topograph (Figure2-19); it looks like the presence of very big particles on the surface. This is because of very high seed concentration due to which the growth of nanorods is very dense and from SEM image it looks like it has secondary growth due to which the tip of AFM cannot go between the nanorods and hence they appeared as big particles. In samples B and C, the AFM images show the presence of nanorods at a certain distance from each other which allow the movement of micro tip between the nanorods. But in case of sample C, the movement of tip is deep down the nanorods as compared to sample B. This is due to low concentration of nano seed on sample C (25% of A). The AFM image of sample D shows the presence of clusters of nanorods on surface. The possible reason for this is the low concentration of seed on sample D which is just 5% of sample A. It is assumed that nano seeds do not cover all the fibers. Therefore, nucleation takes place on scattered places and nanorods grow as clusters.

II.3 Conclusion

The concentration of nano seeds affects the growth of nanorods and the roughness as well as roughness pattern generated due to their growth. As the seed concentration decreases, the distance between the consecutive nanorods increases. When the concentration is very high, it seems that the secondary growth on nanorods take place due to which AFM topograph appears a big grains. When the concentration is very low, then nanorods grow on scattered places. It is worth mentioning that to the best of our knowledge, no study was conducted to study the effect of seed concentration on nanoroughness generated due to growth of ZnO nanorods.

References

1. C. Liu, Y. Masuda, Y. Wu and O. Takai, *A Simple Route for Growing Thin Films of Uniform ZnO Nanorod Arrays on Functionalized Si Surfaces*. Thin Solid Films, 2006. **503**(1-2): p. 110-114.

2. C. Liu, Y. Masuda, Z. Li, Q. Zhang and T. Li, *Site-Selective Growth of Highly Oriented ZnO Rod Arrays on Patterned Functionalized Si Substrates from Aqueous Solution*. Crystal Growth & Design, 2009. **9**(5): p. 2168-2172.

3. J.H. Park, P. Muralidharan, and D.K. Kim, *Solvothermally Grown ZnO Nanorod Arrays on (101) and (002) Single- And Poly-Crystalline Zn Metal Substrates*. Materials Letters, 2009. **63**(12): p. 1019-1022.

4. Y. Tong, Y. Liu, L. Dong, D. Zhao, J. Zhang, Y. Lu, D. Shen and X. Fan, *Growth of ZnO Nanostructures with Different Morphologies by Using Hydrothermal Technique*. The Journal of Physical Chemistry B, 2006. **110**(41): p. 20263-20267.

5. C.-H. Xue, R.-L. Wang, J. Zhang, S.-T. Jia and L.-Q. Tian, *Growth of ZnO Nanorod Forests and Characterization of Zno-Coated Nylon Fibers*. Materials Letters, 2010. **64**(3): p. 327-330.

6. G. Niarchos, E. Makarona, and C. Tsamis, *Growth of ZnO Nanorods on Patterned Templates for Efficient, Large-Area Energy Scavengers*. Microsystem Technologies,2010. **16**(5): p. 669-675.

7. B. Xu and Z. Cai, *Fabrication of a Superhydrophobic ZnO Nanorod Array Film on Cotton Fabrics Via a Wet Chemical Route and Hydrophobic Modification*. Applied Surface Science, 2008. **254**(18): p. 5899-5904.

CHAPTER 3

Functional Characteristics

Introduction

This chapter consists of four sections and each section is one functional characteristic of treated fabric. The first section is about superhydrophilicity of fabric due to hierarchical roughness structure. This section covers the methods of characterization for water contact angle (WCA), capillary rise and diffusion coefficient. The effect of seed concentrations on contact angle as well as diffusion coefficient and effect of UV pre - activation on diffusion coefficient are discussed. The second section is about lotus effect (physical self cleaning) of the nanorods functionalized fabric on treatment with octadecyltrimethoxysilane (ODS). The methods of characterization for WCA and water roll off angle (WRA), effect of nano seeds on physical self cleaning and effect of precursor concentrations are presented. In the third section, the chemical self-cleaning due to photocatalytic effect ZnO nanorods functionalized fabric is presented. The methods and kinetics of stain solution discoloration as well as stain degradation are discussed. The last section is about biological self-cleaning of treated fabric. The summary of functional characteristics studied is presented below.

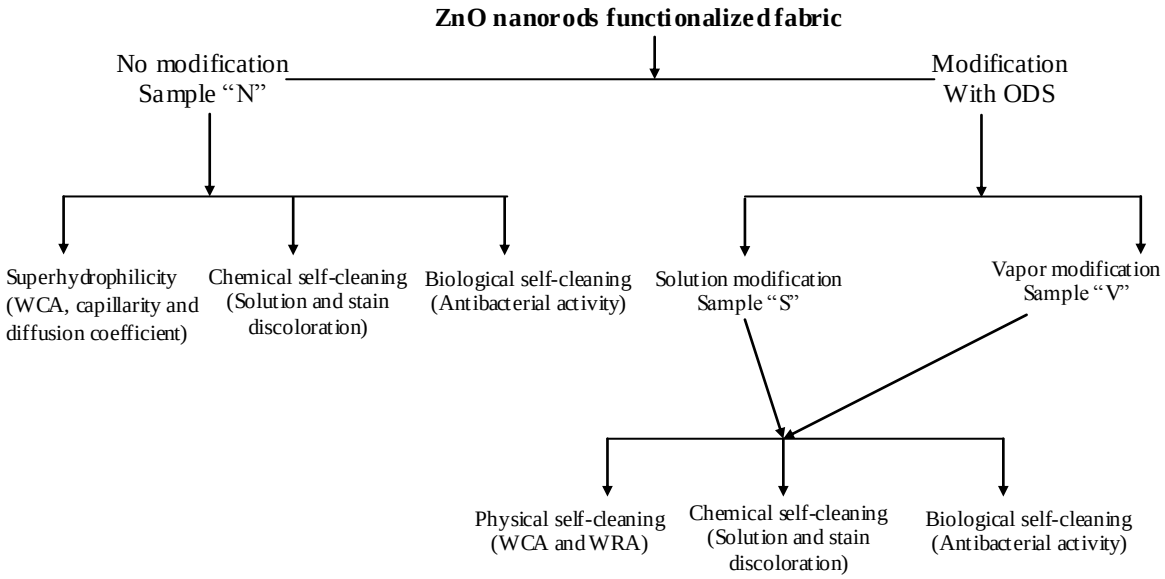

I Superhydrophilicity

If the water contact angle (WCA) on a surface is less than 90°, it is called hydrophilic, and if it is less than 10°, the surface is called superhydrophilic. The hydrophilicity of the surface depends on the chemistry and roughness of the surface. If the surface carries polar groups or roughness, the WCA will be low. According to Wenzel's law, if the roughness is generated on hydrophilic surface (Θ<90), it becomes superhydrophilic [1]. The WCA on polyester fabric was 88° without any treatment whereas that of on ZnO is 24°. ZnO has been used to generate roughness on polyester fabric which could lead to superhydrophilic behavior as mentioned in chapter 1. therefore, it will be interesting to know, what the surface properties are after this treatment. In this study, the concentration of nano seeds is the determining factor for the surface properties.

I.1 Characterization of Superhydrophilicity

The superhydrophilicity of samples was characterized by measuring the WCA, absorption of water by capillary rise and diffusion coefficient. For this purpose, GBX-3S balance was used in capillary mode. A rectangular-shaped fabric sample was connected to the tensiometer at the weighing position, and was then progressively brought into contact with the liquid placed in a container, which could move vertically up and down (Figure 3-1). As soon as the sample came in contact with the liquid surface, a sudden increase in the sample weight was detected by the balance, which then automatically stopped the movement of the liquid container remained in contact with sample for 2 minutes. The absorption of water by the sample as the function of time was recorded by the computer. After 2 minutes, the water container moved downward and as soon as the contact between water and sample was removed, the reading on the balance was recorded. This showed the amount of water absorbed due to capillary. The liquids used were water and decane. This test was carried out on three samples of each seed concentration

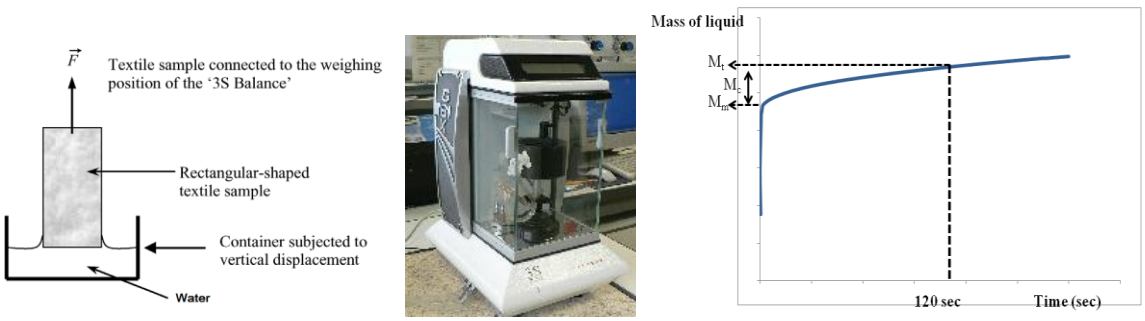

Figure 3-1: Arrangement for measuring water contact angle by tensiometeric method, picture of 3S balance and the graph of mass of liquid versus time

At the beginning of fabric contact with water, the mass increases rapidly as shown in Figure 3-1. This part of the curve corresponds to the meniscus M_m. Then the weight of fabric increases continuously but at slower rate. After 120 seconds, total weight of the liquid M_t was noted and the contact of fabric with liquid was broken, the instrument gave the capillary mass of the liquid. The contact angle between water and the fabric was determined from the meniscus weight M_m deduced from the liquid weight M_t in contact with the fabric.

Contact angle was obtained by the following relation:

$$M_m = \gamma_{LV}.p.\cos\Theta$$

Where p is the sample perimeter in contact with the liquid, which was determined by using decane ($\Theta = 0$, $\cos\Theta = 1$) in order to reduce the error in calculating the contact angle. ($P = (M_t.g - M_c.g) / \gamma_{LV}$). γ_{LV} : surface tension of the liquid (mN/m); g = 9.81 ms^{-2}; M_t : the total weight (mg); M_c : the capillary weight (mg). For each sample, 4 observations for hydrophilicity were made.

To determine the coefficient of diffusion of liquids, the graphs between weights of liquid absorbed by fabric due to capillarity as the function of "$t^{1/2}$" were drawn. The slope of this graph is the coefficient of diffusion which is expressed as $mg.s^{-1/2}$

I.2 Results and discussions

I.2.1 Effect of seed concentration on contact angles

The Table 1 represents the cosine of the water contact angles measured by tensiometeric method on samples described in chapter 2 - II. From sample E to A, the seed concentration increases, i.e. the concentration of precursor to prepare seeds expressed by concentration of zinc acetate dehydrate. The cosine of angles on samples A, B and C are approximately equal to 1 which means the contact angle on these samples is 0. The contact angle on sample D is 12° which in our opinion is also equal to zero because the $\cos\Theta$ is $0.97 \approx 1$ i.e. an error of 3% is possible. The sample E with very low seed concentration has 24° water contact angle because nanorods grow on scattered places and do not cover the surface completely. This means that as long as the nanorods cover the top of the fibers, the fabric is superhydrophilic.

The contact angles on untreated PET fabric and ZnO are 88° and 24° respectively which reduce to 0° on nanorods treated fabric. The improvement of water wettability may be attributed to 3 causes

i. The surface energy of ZnO is different from the PET one. The metal oxides have got high surface energy [2]. Thus on ZnO the spreading coefficient (according to section I.1.1.1 of chapter 1) should be higher compared to PET one and the contact angle decreases.

ii. This is due to the presence of polar hydroxyl groups because the nanostructures of ZnO always carry hydroxyl groups on their surfaces. The XPS analysis also reveals the presence of Zn in the form of Zn-OH as shown in Figure 3- 2. This shows that the nanorods are covered with hydroxyl groups and their number increases with the increase in seed concentration because, it leads to growth of more number of nanorods.

iii. Another reason for this superhydrophilicity is the generation of nano-roughness due to the growth of nanorods which also reduces the contact angle on any surface

Table 1: Superhydrophilicity; water contact angle and diffusion coefficients

Sample	cosΘ	Θ°	Coefficient of water diffusion ($mg.s^{-1/2}$)	Coefficient of decane diffusion ($mg.s^{-1/2}$)
A	1.01±0.024	0	12.51±2.55	8.47±0.30
B	0.99±0.008	0	10.01±0.48	8.38±0.02
C	0.99±0.004	0	9.11±0.88	8.75±0.77
D	0.97±0.17	12	7.32±1.85	9.50±0.90
E	0.91±0.05	24	6.46±1.20	10.25±0.25
Plasma treated PET	0.84±0.01	33	6.26±0.90	10.02±0.12
Untreated PET	0.035±0.005	88	5.13±0.60	9.36±0.45

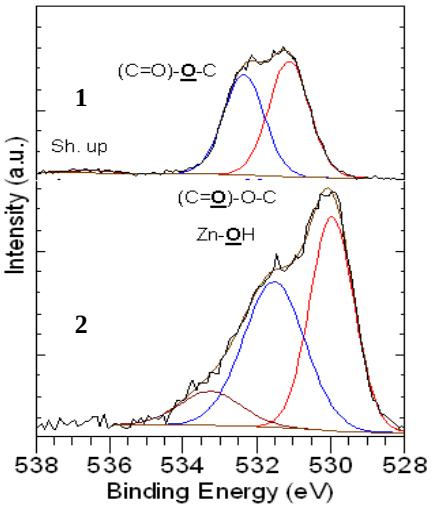

Figure 3-2: XPS analysis of 1. Untreated PET, 2. Nanorods treated PET

I.2.2 Effect of seed concentration on capillarity and diffusion coefficient

The Figure 3-3 presents the cosine of WCA and capillary rise of water as function of seed concentration. The weight of capillary rise of water increases with the increase in concentration of seeds. This means that the fibers surfaces inside the fabric are also covered by ZnO nanorods. As the seed concentration increases, the fibers inside the fabric become more and more hydrophilic, but the capillary weight does not attain a stable maximum value even at maximum concentration of seeds. The capillarity of water continue to increase with the increase in seed concentration whereas, the cosine of WCA reaches to 1 that means the contact angle is zero on fabric surface.

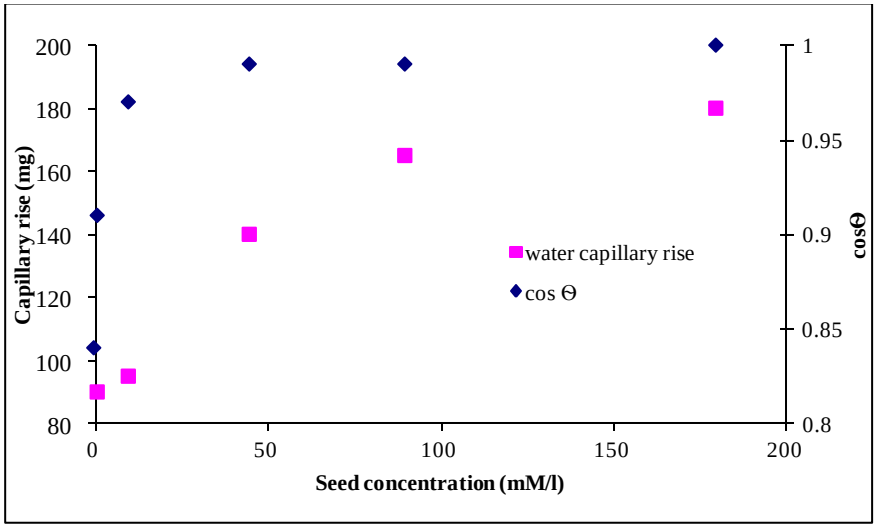

Figure 3-3: Contact angle and Capillary rise of water on samples with different seed concentrations

To quantify the fiber surface properties, the capillary kinetics has been studied with water and decane. Decane is supposed to wet completely the fibers due its very low surface tension. As shown in Figure 3-4, the weight of liquid absorbed by fabric due to capillarity is linear with square root of time according to the Lucas Washburn equation [2].The correlation coefficient R^2 is greater than 0.99 for all the experiments.

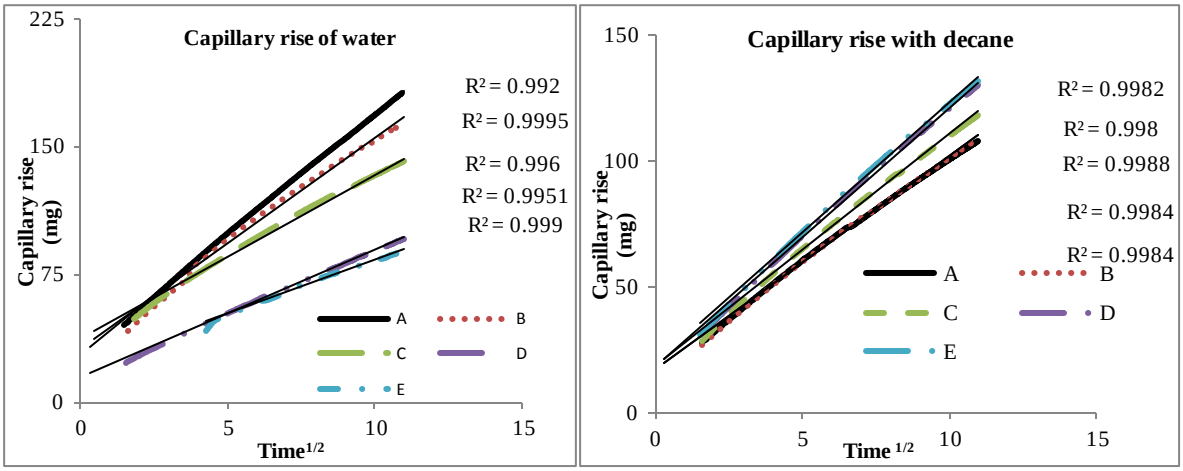

Figure 3-4: Effect of seed concentrations on capillary rise of water and decane as function of $t^{1/2}$

The diffusion coefficient D is the slope of capillary rise curve and is expressed as milligrams/$s^{1/2}$. With the increase in seed concentration, the coefficient of water diffusion increases while that of decane decreases (presented in table 1). Let R be the ratio between ZnO treated and untreated fabrics, $R=D_T/D°$. Depending on the seed concentrations, nanorods at fiber surfaces slow down the decane diffusion from 1 to 0.84, while the diffusion of water is multiplied by up to 2. There is a slight increase of the water capillary diffusion with sample E (1mM/l seeds concentration) and a continuous increase to 180mM/l. Contrary to the cosΘ variation, the diffusion D of water continues to increase with the increase in seed concentration.

In porous structures such as fabrics, the capillary diffusion coefficient D is related to [3, 4]

- The geometry of the porous structure, D=K(Rc), Rc being an equivalent capillary radius
- The physicochemical properties of the liquid P, $D=P(\gamma.\eta.\rho)$ where γ is the surface tension of liquid η the fluid viscosity, and ρ the density
- The cosine of contact angle between the liquid and the fibre surface,f(cosθ)

$$D = K(Rc),.P(\gamma.\eta.\rho).\ f(\cos\Theta) \qquad \text{eq 2}$$

As decane is a good wetting liquid, the contact angle is supposed to be zero, whatever the fabric treatment. When seed concentrations change, only the K factor varies. Higher seed concentrations cause the blockage of pores due to which decane diffuses slowly. The R_d ratio, for decane capillary coefficient, $R_d=D_{dT}/D_d°$ quantifies the decrease of the pores size geometry. The ratio of the water diffusion coefficients, $R_w=D_{wT}/D_w°$, increases

with seed concentration (Figure 3-5). The better water wettability due to growth of nanorods balances the reduction in pore size.

The nano-structuration by ZnO contributes to the change in the capillary diffusion. C. Ishino *et al* [5] have studied the diffusion in the 2D layer made by forest of micropillars. The capillary diffusion coefficient increases depending on the structure of the micropillars. These results have been applied by Cebeci *et al* to analyze their superhydrophilic results obtained by nanostructuration of film surfaces with silica nanoparticles [6].

As a conclusion, the superhydrophilic properties of the PET fabric nanorods treatment are clearly shown not only by cosϴ close to 1 at fabric surface, but also by the better capillary diffusion of water inside the treated fabric. When the fibers are covered with nanorods, the equivalent capillary radius of the pores fabric become smaller but the surface diffusion between the nanorods tends to improve the water capillary diffusion.

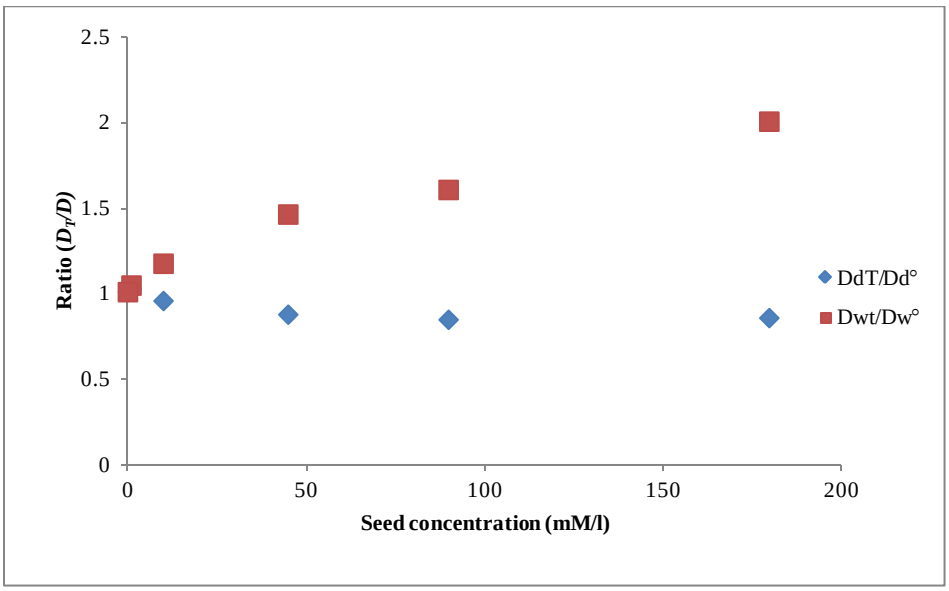

Figure 3-5: The effect of seed concentration on diffusion coefficient ratios of treated and untreated fabric for water (DwT/Dw°) and decane (DdT/Dd°)

I.2.3 Effect of UV activation on coefficient of diffusion

To study the effect of UV light activation of functionalized samples on diffusion coefficient of water, the sample B was chosen as model. Three samples of sizes 6cm × 2.8cm were used to measure the diffusion coefficient of water before UV activation. After that these samples were dried at room temperature and exposed to UV light for 24 hours; then again the diffusion coefficient was determined. The same process was repeated with same samples for next measurements. The Figure 3-6 represents the effect of UV activation on diffusion coefficient of

water by nanorods treated fabric. The coefficient of diffusion before exposure to UV light is 13.70mg.s$^{-1/2}$ which increases to 16.30mg.s$^{-1/2}$ on 24 hours exposure to UV light. After 48 hours exposure, it reaches to 20.64mg.s$^{-1/2}$. After this, the samples were put in complete darkness for 48 hours, then the coefficient of diffusion decreases to 17.80mgs$^{-1/2}$ which is slightly less than that of after 24 hours exposure. This means that the activated ZnO nanorods do not come back to the original position after same amount of time in dark.

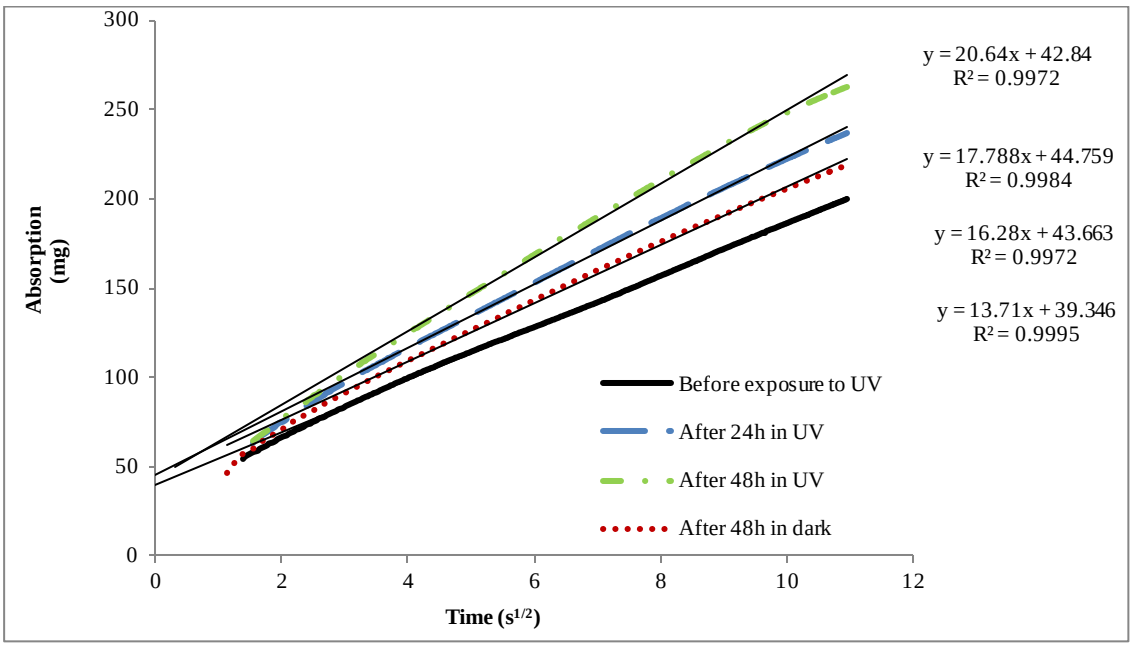

Figure 3-6: Effect of UV light exposure on diffusion coefficient of water

Under the effect of UV, the electrons in the valence band of ZnO jumps to the conduction band. Due to which, a positive hole is generated. Some of the holes react with lattice oxygen to form surface oxygen vacancies. Meanwhile, water and oxygen may compete to adsorb on them. The defective sites are kinetically more favorable for hydroxyl adsorption than oxygen adsorption. As a result, the surface hydrophilicity is improved [7]. It has been shown that the surface becomes energetically unstable after the hydroxyl adsorption, while the oxygen adsorption is thermodynamically favored, and it is more strongly bonded on the defect sites than the hydroxyl groups. Therefore, the hydroxyl groups adsorbed on the defective sites can be replaced gradually by oxygen atoms when the UV-irradiated films were placed in the dark. Subsequently, the surface evolves back to its original state (before UV irradiation) [8]. But the process of returning back to original position is relatively slow.

To the best of our knowledge, no study has ever been conducted on the superhydrophilicity (WCA and diffusion coefficient) of any textile functionalized with ZnO nanorods. Various studies have been conducted on

enhancement of hydrophilicity of ZnO after exposure to UV light, but none of these studies addressed the effect of this activation on diffusion coefficient of water.

I.3 Conclusion

In this section, the superhydrophilicity of the fabric on which hierarchical roughness structure was developed by growing the ZnO nanorod on micro fibers of polyester fabric, was studied. The seed concentration affects the nano-roughness. The effect of seed concentration on hydrophilicity was studied and it was found that the sample having seed concentration equal to or more than 10mM/l had 0° water contact angle. The capillarity of water increases with the increase in seed concentration but that of decane decreases. Similarly, the diffusion coefficient of water increases whereas that of decane decreases with increase in seed concentration.

The UV activation of ZnO nanorods has significant effect on diffusion coefficient of water. With the increase in UV exposure time, the diffusion coefficient also increases. On putting the same samples in dark, it decreases. But it does not return to the original value when the samples were put in dark for the same duration as it was exposed to UV.

II Physical self-cleaning (Lotus effect)

As it has been described in chapter 1, the lotus effect is due to the presence of hierarchical roughness structure; micro buds covered with nano needles made of hydrophobic wax crystals. The hierarchical roughness structure has been developed by growth of nanorods on micro fibers of polyester fabric; the next step is its modification by hydrophobic chemical.

II.1 Hydrophobization

PET fabric treated with nanorods was modified with octadecyltrimethoxysilane ODS (Sigma Aldrich Technical grade 90%). Two methods were used to apply ODS on the functionalized PET fabric by solution method and vapor deposition method. The details are available in annexe.

In solution method, 2% solution of ODS was prepared in absolute ethanol (Carlo Erba 99.7%). The sample was placed in this solution for 24 hours at 40°C. Then, it was cured at 150°C for 5 minutes. While in vapor deposition method, 200µl of ODS were placed in ceramic dish at the bottom of Teflon bottle in which nanorods treated PET samples were held vertically and the Teflon bottle was placed in oven at 150°C for 3 hours.

II.2 Characterization of Lotus effect

The lotus effect is the combination of two characteristics; superhydrophobicity and roll off angle, as described in section I.1.1 of chapter 1. In order to characterize a surface with lotus effect, the both aforementioned characteristics should be measured.

II.2.1 Superhydrophobicity

The superhydrophobicity was characterized by measuring the water contact angle on the surface. The water contact angle was measured by GBX digidrop which uses goniometric method to calculate the water contact angle on the surface. A droplet was the placed on the surface, the width of it touching the surface (L) and its height (H) was marked manually as shown in the Figure 3-7. From these two values, the software of the system calculated the water contact angle by using the equation 3. Three swatches were prepared for each sample and 6 measurements were made on each swatch and an average was calculated.

$$\theta = 2.Arctg\left(\frac{2H}{L}\right) \qquad \text{eq 3}$$

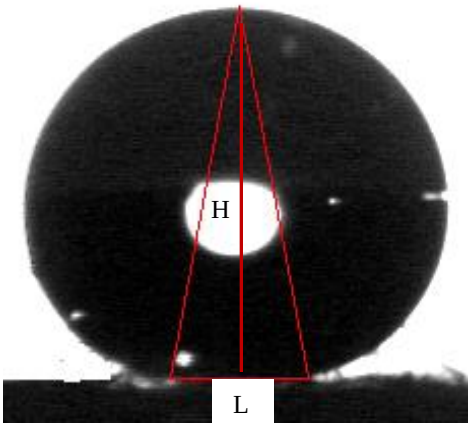

Figure 3-7: Measurement of water contact angle on a surface by sessile drop method

II.2.2 Water roll off angle

It is the angle at which when a surface is inclined, the falling droplet starts rolling. In order to measure the water roll off angles on treated samples, a device exclusively developed in our laboratory was used Figure 3-8. It consisted of a graduated scale marked with angles with an accuracy of one degree. The sample was adhered to glass slide with the help of scotch tape and was held in position shown in figure with the help of sample holder. The spirit level was used to balance this instrument on the table. Then the 5µL water droplet was dropped from 1 cm height. The angle of inclination was increased by one degree after each droplet fall until it started rolling off the sample. At this angle, three droplets were fallen one by one to confirm the water roll off angle of the sample.

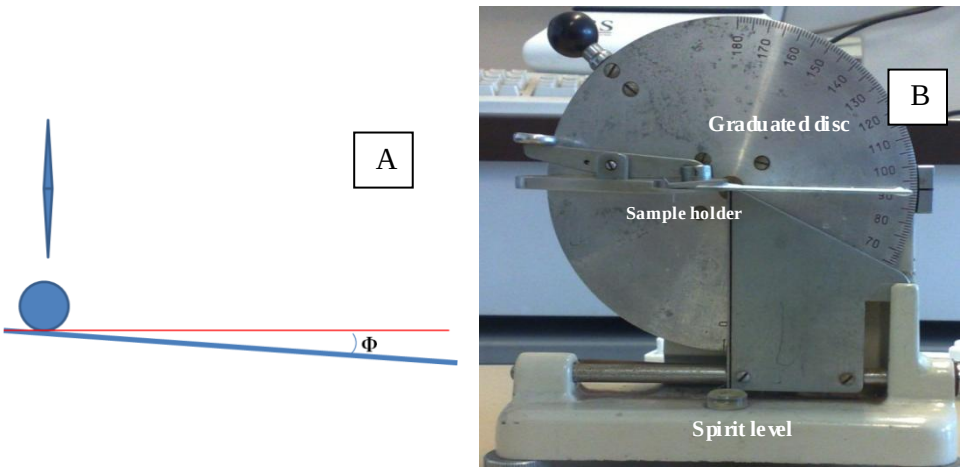

Figure 3-8: A. Schematic diagram of water roll off angle. B. Instrument used to measure to the roll off angle

II.3 Results and discussions

II.3.1 Effect of seed concentration on lotus effect

The Figure 3-9 represents the effect of seed concentration on WCA after modification with ODS. The WCA on untreated PET fabric modified with ODS by both methods is 125°. It increases to 147° when the seed concentration is 1mM/l when modified by vapor deposition. Similarly, the WCA increases to 134° in case of solution deposition method. It continues to increase and reaches it maximum value of 158° and 153° by vapor and solution modifications respectively when the seed concentration is 90mM/l. Then, its value once again decreases on further increase in seed concentration.

At very low seed concentrations, the standard deviation is very high but it decreases as the seed concentration increases. At low seed concentration, the nano-roughness is not uniform due to uneven growth of nanorods. But at high seed concentrations, the nanorods grow uniformly all over surface and hence the roughness is also uniform.

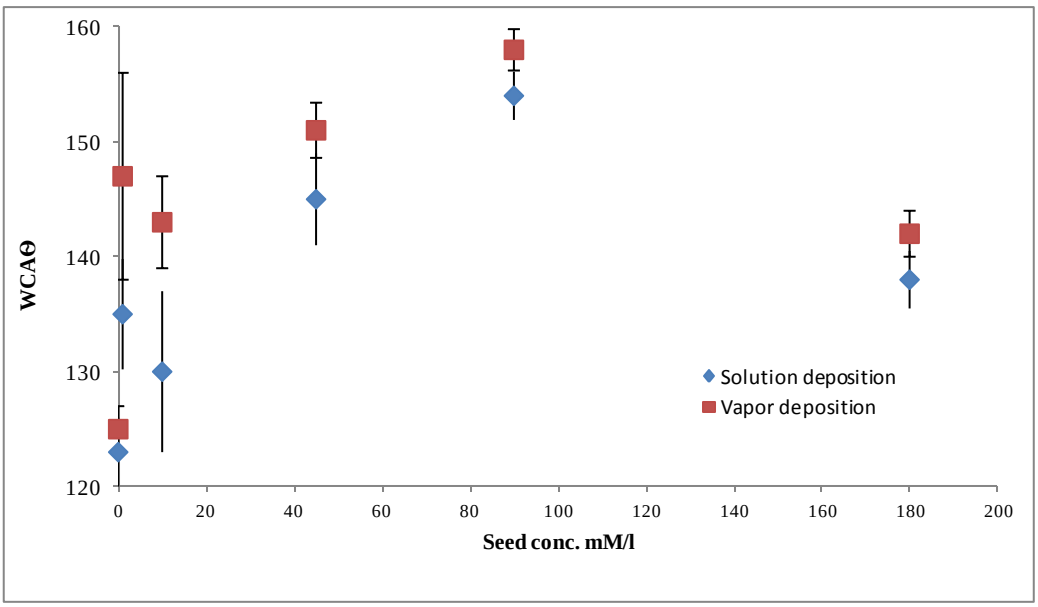

Figure 3-9: Effect of seed concentrations (zinc acetate dihydrate) on water contact angle

As discussed in section 1.2.2.3, the sections of AFM analysis reveal the distance between the nanorods or the distance of one group of nanorods from the other group and the roughness pattern on samples as function of seed concentration. It has been found that as the seed concentration increases, the distance between nanorods or group of nanorods decreases and the AFM sections become uniform. At very high concentration, the growth of nanorods is so dense that they appear as big particle on the surface when analyzed with AFM.

Whatever is the seed concentration, the samples treated with ODS by solution method have low water contact angle as compared to the ones modified by vapor deposition method. This is because, in solution method, high amount of ODS deposits on nanorods which masks the surface structure and changes the nano-roughness while in case of vapor deposition, only a mono layer of ODS is formed on the surface. The XPS analysis shows the presence of higher amount of carbon on solution deposition method treated samples as compared to one treated by vapor deposition method (Table 2).

The Figure 3-10 which are the SEM micrographs of the same sample treated with ODS by solution and vapor deposition methods confirms the masking of nano-roughness. The nanorods are quite visible in sample modified with vapor deposition (Figure 3-10A) but they appeared masked with solution deposition (Figure 3-10B). This confirms that in case of vapor deposition, very small of amount of ODS is deposited.

Table 2 XPS analysis carried out on sample B

Binding energy / Sample	Na	Zn	-O-	C-(CH)-	-Si-
	1071eV	1021eV	531eV	288eV	101eV
PET + nanorods + ODS by vapor method	1.67	27.31	32.99	36.41	1.62
PET + nanorods + ODS by solution method	0.66	17.37	29.18	51.28	1.51

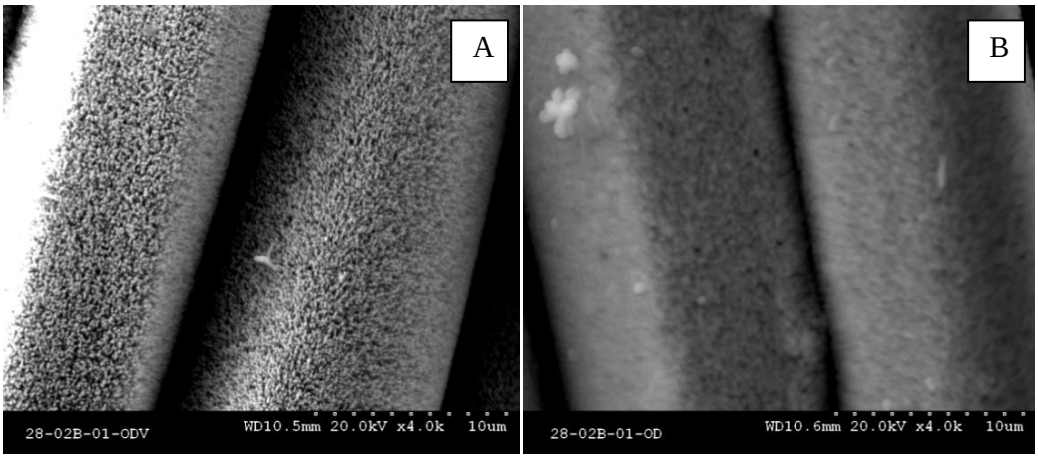

Figure 3-10: A. nanorods treated fabric modified by vapor deposition of ODS, B. the same sample modified by solution deposition

The Figure 3-11 represents the effect of seed concentration on water roll off angle. The water roll off is higher on the samples modified with solution deposition of ODS as compared the ones modified with vapor deposition. In general, it decreases with the increase in seed concentration and gains the minimum values in both ODS modification methods when the seed concentration is 90mM/l. After this, it increases once again on further increase in seed concentration.

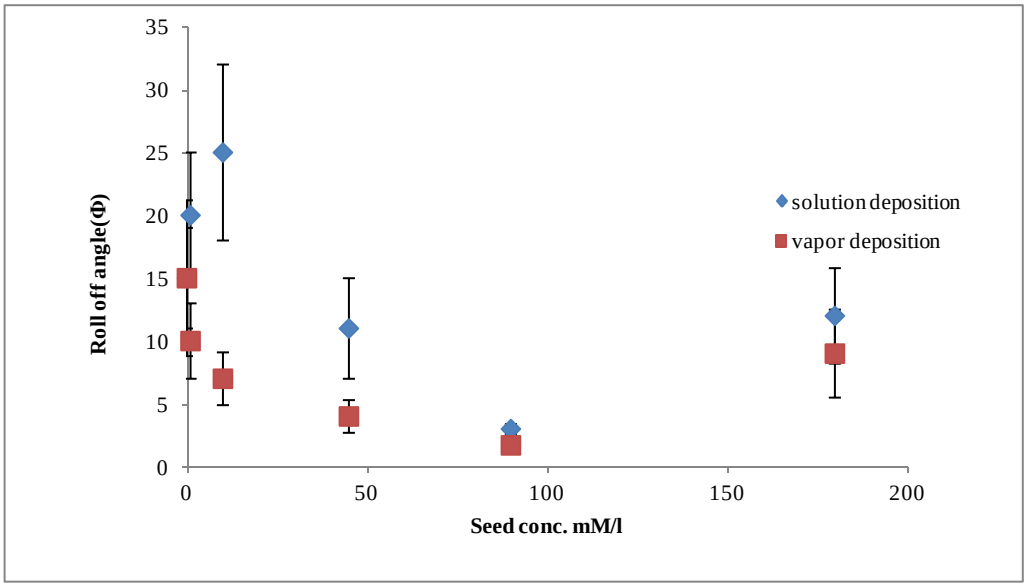

Figure 3-11: Effect of seed concentration on roll off angle

On a surface exhibiting lotus effect, a composite interface is formed between water droplet and solid surface, and water droplet and air. To understand the effect of seed concentration on water sliding, the surface fraction (interface between water droplet and solid surface) on each sample was calculated. As we measured the WCA on untreated (without nanorods but treated with ODS) and treated PET fabric (with nanorod modified with ODS), the surface fraction can be calculated by using the Cassie-Baxter equation;

$$\cos\Theta_c = f\cos\Theta_0 - (1-f)$$

where, "Θ_0" is the water contact angle on untreated sample, "Θ_c" is the composite contact angle formed between droplet, air and the fabric and "*f*" is the surface fraction.

The Figure 3-12 represents the effect of surface fraction on water sliding. With the increase in surface fraction, the water roll off angle also increases. This means that due to change in seed concentration, the number of nanorods grown also change which leads to change in surface fraction.

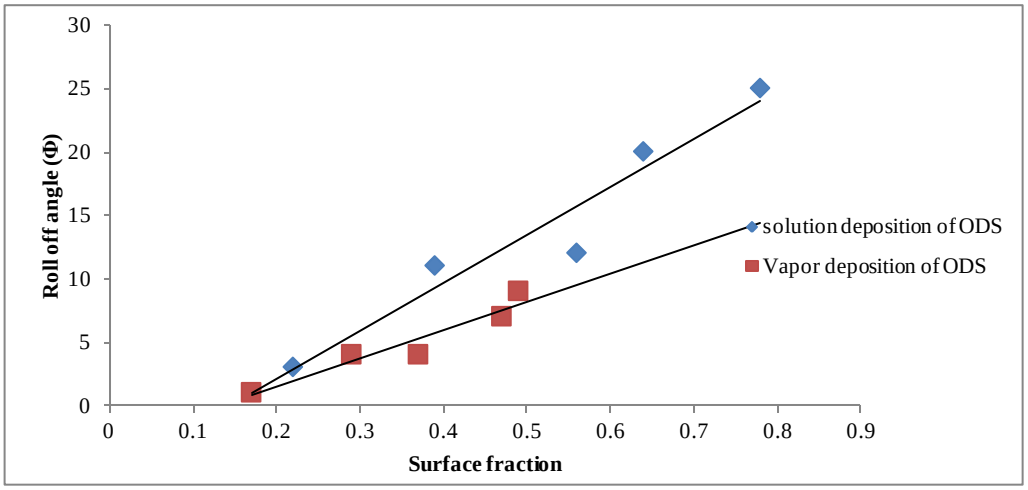

Figure 3-12: Effect of surface fraction on water roll off angle on samples modified by solution deposition and vapor deposition

Higher s0urface fraction means the more contact between water droplet and surface. Therefore, more will be coefficient of friction and the resistance to rolling off. Hence, the roll off angle will be high. The coefficient of friction and the resistance force on inclined surface can be calculated by using the following equations

$$\text{Coefficient of friction } (\mu) = \tan\Phi \qquad \text{eq02}$$

$$\text{Resistance force } (R) = \mu F = \mu mg \qquad \text{Eq03}$$

where, "Φ"and "m" are the roll off angle and the mass of water droplet. The volume of droplet used is 5µL, at room temperature the density of water is 1. Therefore, the mass of the water droplet is 5µkg. The coefficient of friction and resistance force on the sample which have just 1° water roll off angle are 0.017 and 8.48µN. These values in the previous study are 0.158 and 62.59µN [9].

The water roll off angle is directly linked with contact angle hysteresis. The low water roll off angle means that the water droplet rolls over the surface with ease and the surface has low contact angle hysteresis [10]. This implies that the sample (B) which has low roll off will also have low contact angle hysteresis.

II.3.2 Effect of ODS concentration on lotus effect

As the seed concentration for lotus effect has been optimized by keeping all other parameters constant. The sample B gave highest water contact angle and lowest roll off angle. Now the effect of octadecyltrimethoxysilane concentration was studied while keeping the seed concentration constant (sample B) and precursor concentration with 100mM/l of each; zinc nitrate hexahydrate and hexamethylenetetramine.

II.3.2.1 ODS deposition by solution method

The Figure 3-13 represents the effect of ODS concentration by solution method. The WCA increases with the increase in ODS concentration and it reaches its maximum value when the concentration of ODS solution is 2%. After this concentration of ODS, the WCA starts decreasing.

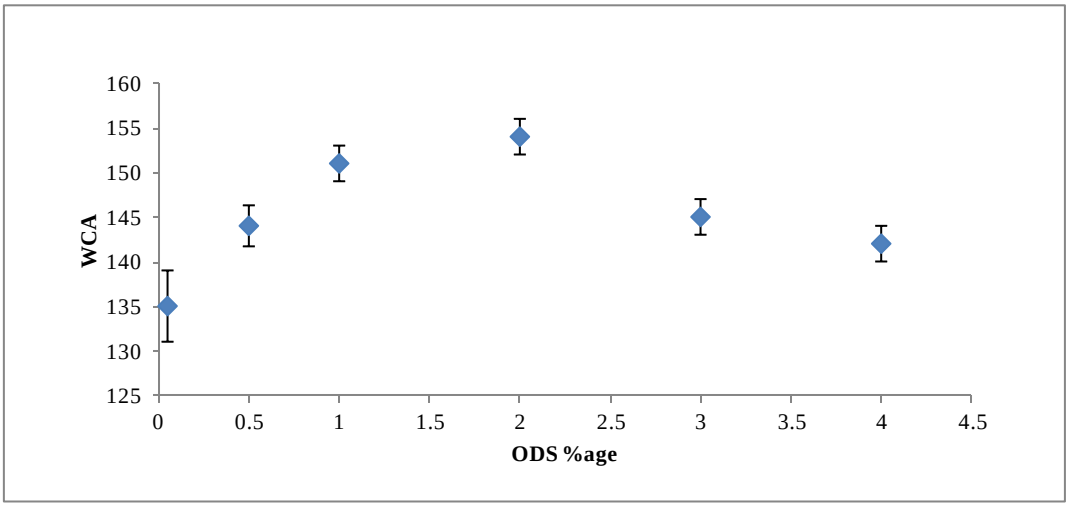

Figure 3-13: Effect of ODS concentration in absolute ethanol on WCA by solution deposition method

As the ODS concentration increases, the more and more molecules deposit on the surface and make it hydrophobic. But after 2%, the deposition of ODS molecules is so high that it starts masking the nano-roughness generated due to the growth of nanorods. The SEM images of the samples treated with 2% and 3% of ODS are shown in Figure 3-14. It is quite visible that the nanorods can be seen on sample modified with 2% whereas, all the nanorods are completely masked when ODs concentration is 3%. Due to this masking, the roughness changes and, the interface between water droplet and the surface become homogeneous which decreases the WCA.

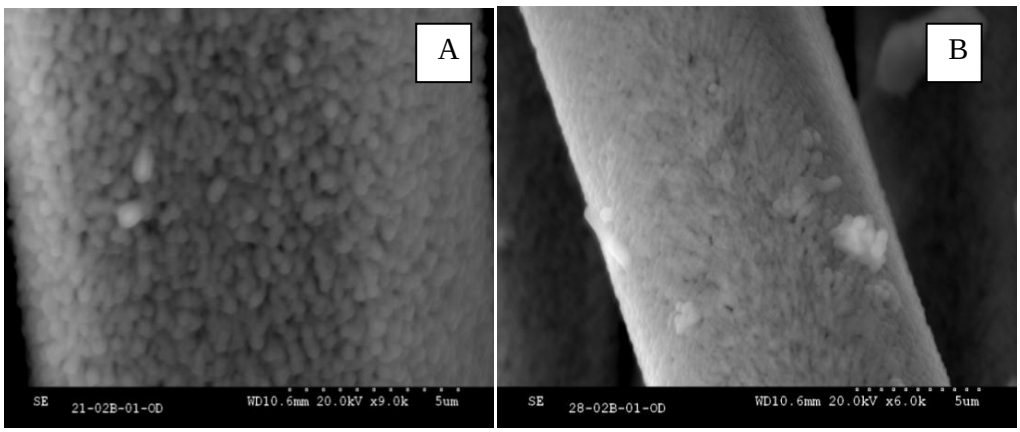

Figure 3-14: Nanorods treated sample modified with A.2% ODS, B. 3% ODS by solution method

The Figure 3-15 shows the effect of ODS by solution method on water roll off angle. The water roll off angle (WRA) decreases as the ODS concentration increases and gains its minimum value at ODS concentration at which it has maximum WCA i.e 2%. Then, it slightly increases due to masking of nano-roughness.

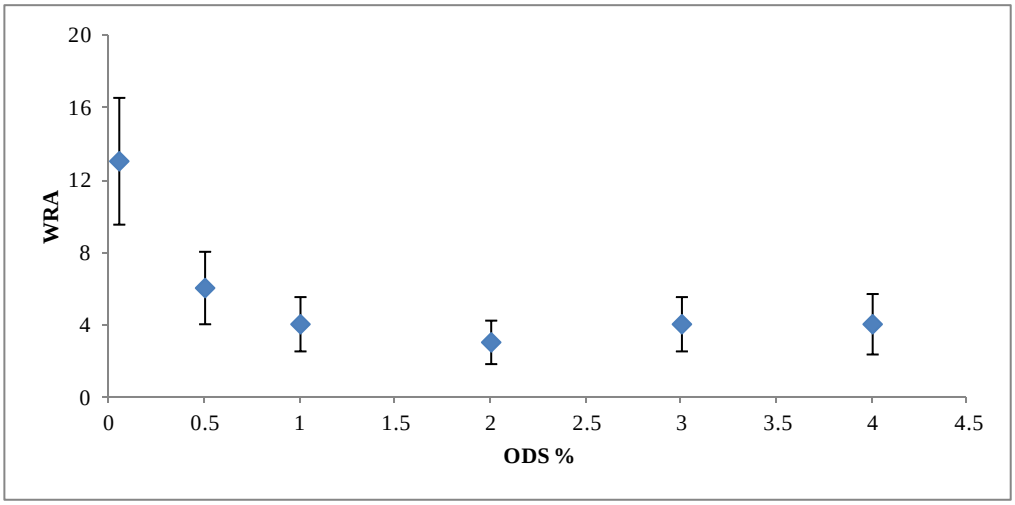

Figure 3-15: Effect of ODS concentration by solution method on water roll off angle

II.3.2.2 ODS deposition by vapor deposition

The Figure 3-16 represents the effect of the time of ODS vapor deposition. As the time of deposition increases, the WCA also increases and reaches at its maximum value of 158° when the deposition time was 3 hours. Then, it stays constant but the color of fabric after 3 hours deposition changes slightly to yellow due to excessive heating possibly because of degradation of chemical.

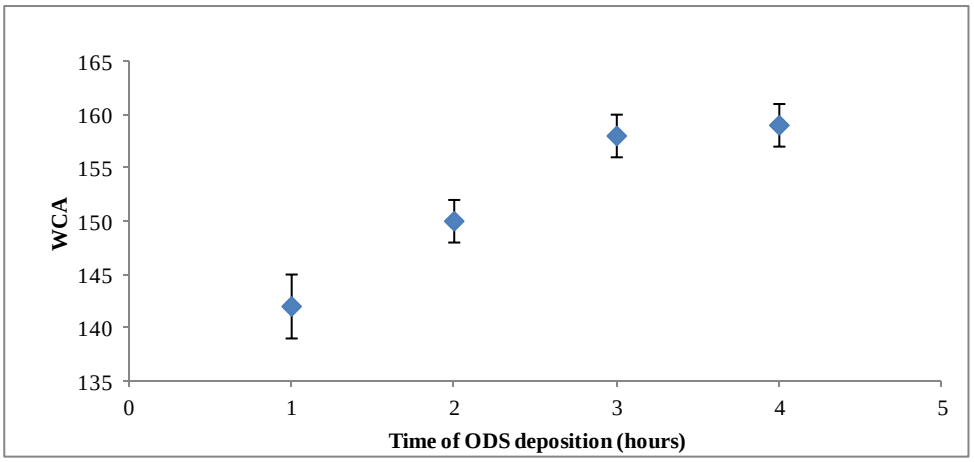

Figure 3-16: Effect of time of ODS deposition by vapor deposition method on WCA

When the deposition times is low, ODS does not completely cover the top of nanorods. Therefore, the contact angle is also low but it increases with increase in deposition time. The Figure 3-17 represents the effect of ODS deposition time on water roll off angle. As the deposition time increases, the roll off angle decreases and reaches its minimum value of 1 degree when deposition time is 3 hours.

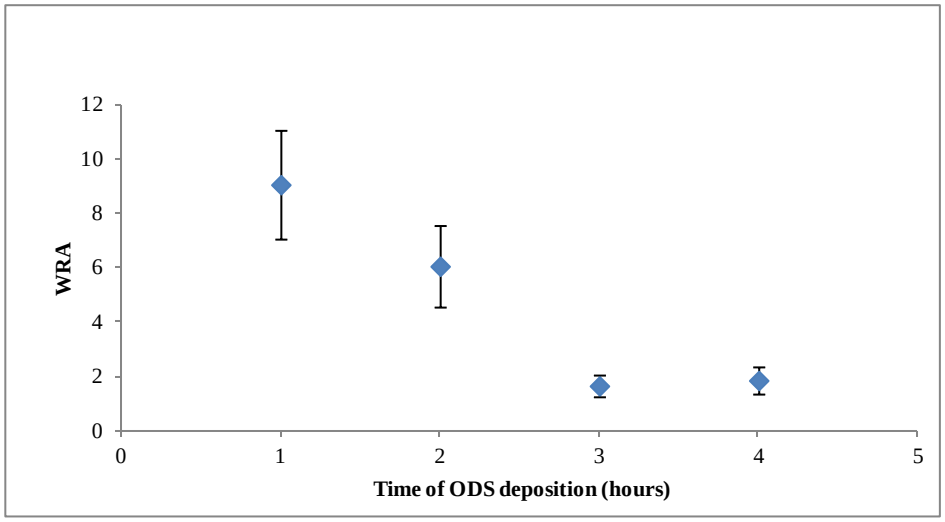

Figure 3-17: Effect of time of ODS deposition by vapor deposition method on water roll off angle

II.3.3 Effect of precursor concentration on lotus effect

To study the effect of precursor concentration (zinc nitrate hexahydrate and hexamethylenetetramine) on lotus effect, the seeded sample B was chosen. After the growth of nanorods, the samples were modified with ODS by vapor deposition method for 3 hours.

The Figure 3-18 represents the effect of precursor concentration on WCA. It is apparent that it does not have any significant effect on WCA. From this, it can be assumed that due to change in precursor concentration, only the heights of nanorods change and it does not change the distance between the nanorods. Therefore, it does not affect the WCA.

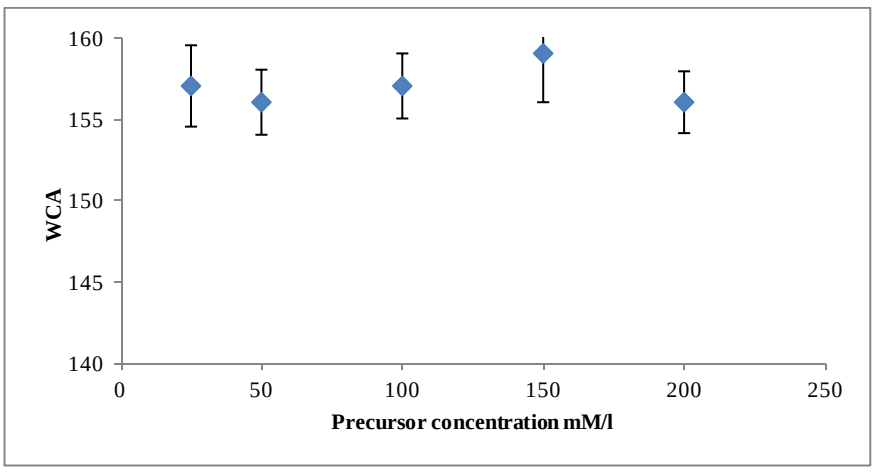

Figure 3-18: Effect of precursor concentration on WCA

The Figure 3-19 represents the effect of precursor concentration on water roll off angle. It is quite visible that the precursor has no significant effect on water roll off angle.

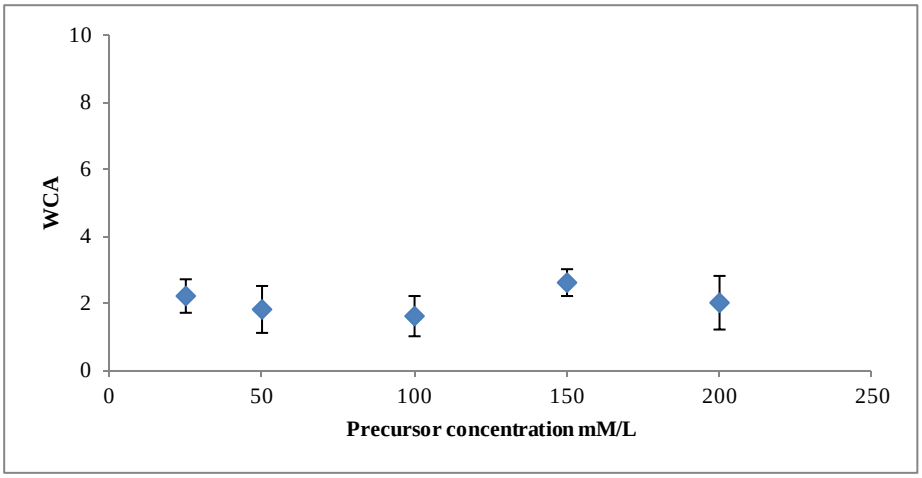

Figure 3-19: Effect of precursor concentration on water roll off angle

Due to the change in precursor concentrations, only the height of nanorods changes but the lotus effect depends on the distance between the nanorods which is governed by seed concentrations. Therefore, the change in precursor concentration does not have any significant effect on lotus effect.

II.4 Conclusion

On modification with ODS, the samples with hierarchical roughness exhibit lotus effect. The seed concentration affects the lotus effect because it changes the roughness and roughness pattern on fabric. The samples which have high water contact angles also have low water roll off angles. Therefore, the roll off angle is directly linked with contact angle. The method of hydrophobization also affects the WCA and roll off angle. Generally, the samples modified by vapor deposition have higher WCA and lower roll off angle as compared to the ones modified by solution deposition. The highest WCA obtained is 158±1.8° on a sample which has just 1.7±0.2° roll off angle. This means that this sample has lotus effect with excellent self-cleaning characteristics.

The concentration of ODS affects the lotus effect. In solution method, the self-cleaning characteristics (WCA and roll off angle) increase till 2% ODS concentration then start decreasing. The time of ODS deposition by vapor method also affects the self-cleaning of fabric. The precursor concentration does not have any significant effect on self-cleaning.

III Chemical self-cleaning

The chemical self-cleaning refers to the degradation of color stains deposited on fabric or discoloration of color solutions with which it comes in contact under the effect of UV light due to the photocatalytic effect of ZnO. To study it, the sample with seed formulation B was chosen. For instance, the seeding was done on plasma treated fabric by using 90mM.l^{-1} zinc acetate dihydrate and 75mM.l^{-1} sodium hydroxide. 100mM.l^{-1} zinc nitrate hexahydrate and 100mM.l^{-1} hexamethylenetetramine solutions were used to grow nanorods. The chemical self-cleaning was studied by using three different colors, C.I. acid blue 9 (triphenylemethylene; molar mass = 792), C.I. reactive orange 13 (azo; molar mass = 762) and C.I. reactive violet 5 (azo; molar mass = 735) were used. Their structures are shown in Figure 3-20.

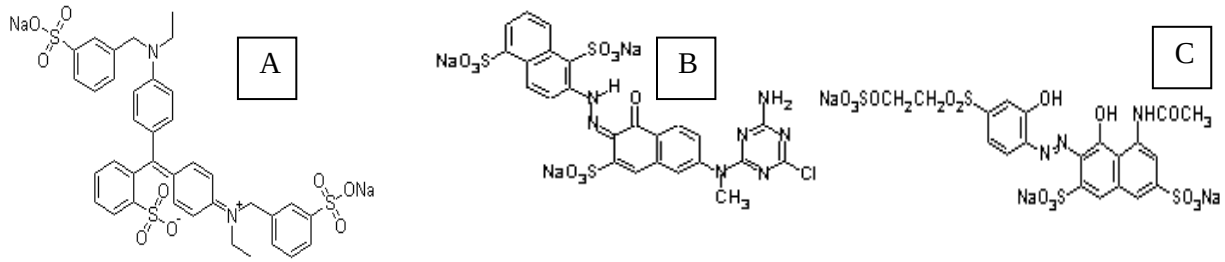

Figure 3-20: Structures of colors, A. acid blue 9, B. reactive orange 13, C. reactive violet 5

III.1 Solution discoloration

The solution discoloration by treated fabric was studied first on nanorods treated fabric without lotus effect, as they have no further treatment they are called sample N). Then, the chemical self-cleaning was carried out on nanorods functionalized samples modified with ODS, that means samples with physical self-cleaning. The sample which was modified with ODS by solution method was called S whereas, the one modified by vapour deposition method was called V.

III.1.1 Characterization

To study the ability of ZnO functionalized fabric to degrade dyes in solution, 6ml of aforementioned dye solutions with different concentrations were taken in beakers (100ml) and a circular piece with diameter 2.8cm of ZnO nanorods treated PET fabric was immersed in each beaker. These beakers were placed in light box (VeriVide CAC60) at 18cm from 20W UV source which emits the UV between 300nm to 400nm with maximum emission at 368nm. To measure the concentration of color in a solution, transmittance

spectrophotometer is used. A typical transmittance spectrophotometer consists of a spectrometer which produces the light of desire wavelength and a photometer meter which measures the intensity of the reaching to it. The liquid in a cuvette is placed between spectrometer and photometer. The light of each wavelength with specific intensity is made to pass through the solution and photometer detects its intensity and translates it into a voltage signal. This signal is displayed on the screen as the percentage of light absorbed as shown in Figure 3-21.

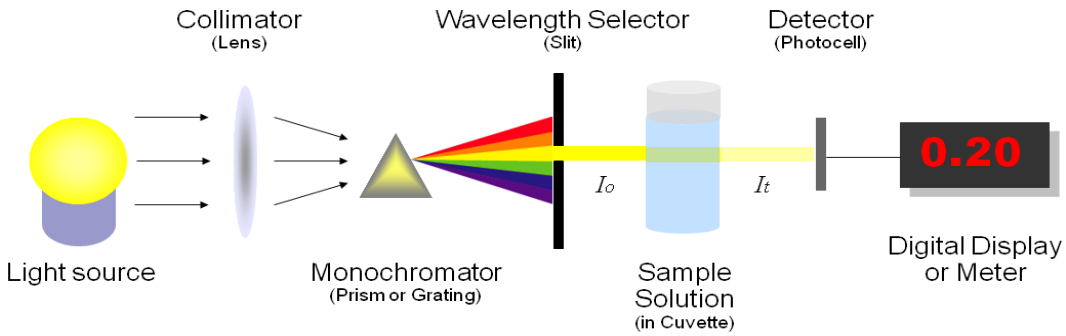

Figure 3-21: Schematic diagram of transmittance spectrophotometer

According to Lambert-Beer law, the absorption of light by a solution is directly proportional to concentration of solution(C) and its path length (*l*).

$$A \alpha lC$$

$$A = \varepsilon lC$$

Where "ε" is the molar absorptivity.

In this study, JASCO UV/VIS spectrophotometer V-530 was used to characterize the discoloration of solutions, the small amount of solutions were removed and their absorbance were checked after each hour and then poured back.

III.1.2 Results and discussions

III.1.2.1 Discoloration by nanorods treated sample (N)

To study the discoloration of solution by nanorods treated fabric without lotus effect, all three dyes presented in figure 20 were used. The solutions of these dyes with different concentrations were prepared and were exposed to UV light with treated sample placed in them. To evaluate the rate of reaction and to understand the mechanism, the kinetics of discoloration were studied.

III.1.2.1.1 Kinetics of solution discoloration

Before carrying out the kinetics study, an attempt was made to get adsorption isotherm of dyes. The size of the functionalized sample in contact with 6ml of each dye solution was so small that the decrease in absorption of solution due to adsorption of dye by the sample could not be detected with the spectrophotometer. Therefore, to model the kinetics, the modified form of the Langmuir-Hinshelwood equation adopted by M.A. Behnajady *et al.* [11] to study the kinetics of UV/ZnO process, was used. This equation also covers the adsorption properties of dyes on the photocatalyst surface. We proposed to transpose this law adapted to powder of ZnO to our ZnO/PET system (method A) by making the same assumptions which were made by M.A. Behnajdy *et al* that at t=0, C $=C_0$

$$k_{ads} C + \sum k_i C_i = k^A_{ads}(C)_0$$

Where, k_i and C_i are the adsorption equilibrium constant and concentration for intermediates,

$$R^A = -\frac{d(C)}{dt} = \frac{k^A_{L-H} k^A_{ads}(C)}{1 + k^A_{ads}(C)_0} = k^A_{ap}(C) \quad eq.1$$

Where R^A is the reaction rate (mg l^{-1} min^{-1}), k^A_{ap} the apparent reaction constant rate, k^A_{L-H} the reaction rate constant (mg l^{-1} min^{-1}), k^A_{ads} the adsorption coefficient of dye on the catalysis (mg^{-1} l), and (C) the concentration of dye (mg l^{-1}). Eq. (1) shows a pseudo first order reaction with respect to the concentration of dye (C).

The concentration of color (C) present in solution at any time during UV irradiation was calculated from absorbance by using the calibration curves (Figure 3-22). Initial concentration of aqueous solution of dye $(C)_0$ correspond to the beginning of UV irradiation (t=0).

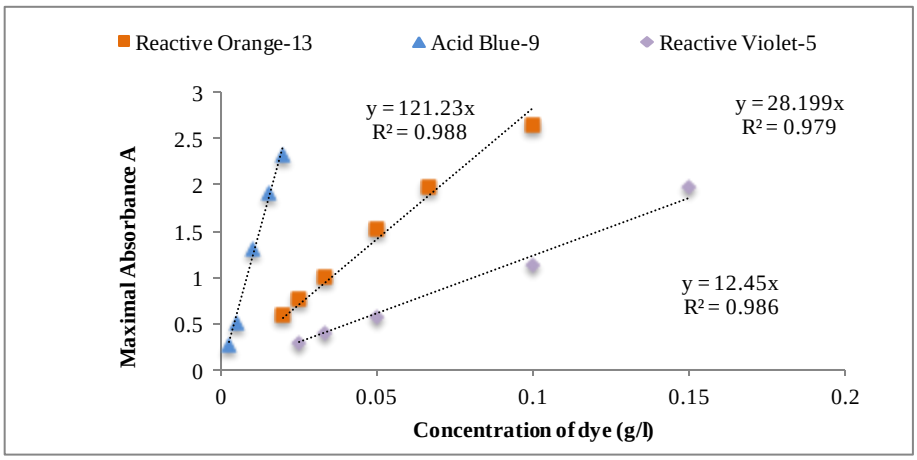

Figure 3-22: Calibration curves: Absorbance A vs. concentration of aqueous solution of dye

The apparent reaction rate constants (k^A_{ap}) were calculated from experimental data (Figure 3-23) using a linear regression, the graphical representation of $ln(C/C_0)$ as function of time of irradiation t and it gives good coefficients R^2 (0.96-0.99). It shows that the discoloration of solution by treated fabric follow pseudo first kinetics.

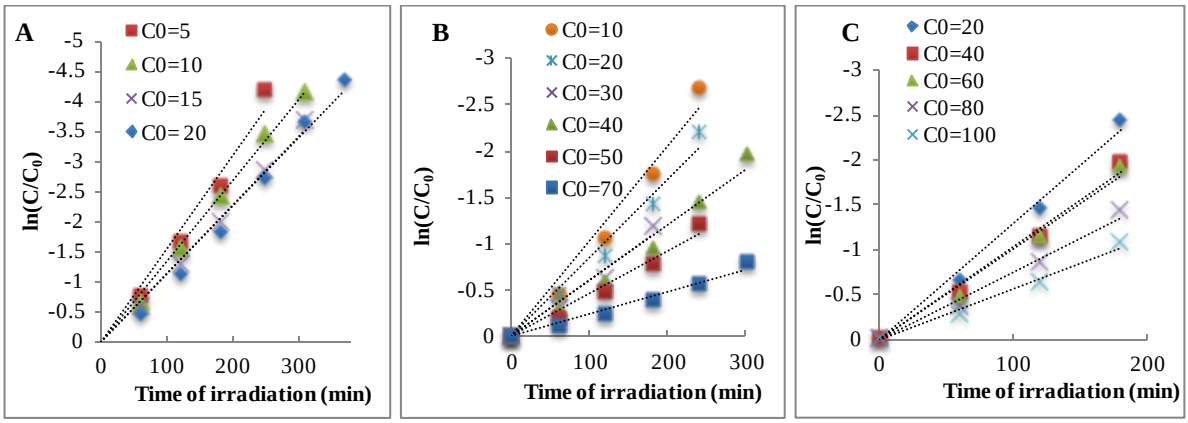

Figure 3-23: UV/ZnO-PET process. Derivation of the apparent reaction rate constants k^A_{ap} of various initial concentration (C_0) of dye (mg/l) by linear regression: A. C.I. acid blue 9 B. C.I. reactive orange 13 C. C.I. reactive violet 5. Each colorant were tested by using various initial concentration (noted C_0) of dye (mg/l).

The eq. 2 is deducted from equation 1 and was used in the form of equation 3 to calculate each constants k^A_{L-H} and k^A_{ads} in L–H model thanks to experimental values of k^A_{ap} and corresponding initial concentration $(C)_0$.

$$k^A_{ap} = \frac{k^A_{L-H} k^A_{ads}}{1 + k^A_{ads}(C)_0} \quad eq.2 \quad ; \quad \frac{1}{k^A_{ap}(C)_0} = \frac{1}{k^A_{L-H} k^A_{ads}} \cdot \frac{1}{(C)_0} + \frac{1}{k^A_{L-H}} \quad eq.3$$

The Graphic $1/(k^A_{ap}C_0)$ vs. C_0 presented in Figure 3-24 show that equation 3 is valid for our experimental data with R^2=0.98-0.99. This equation has also been used by De Heredia, J.B., *et al.*,[12] and our results are in good accordance with it

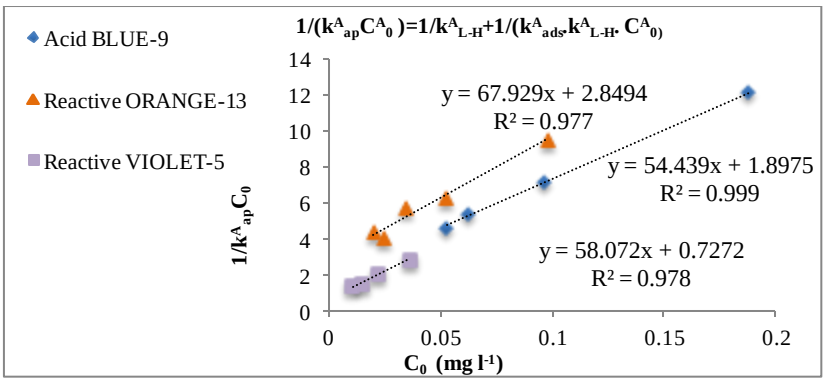

Figure 3-24: Determination of the reaction rate constant k^A_{L-H} (mg l-1 min-1) and the adsorption coefficient of dye on the ZnO/PET system Kads (mg-1 l) by using experimental apparent rate constant $\mathbf{k^A_{ap}}$.

The evolution of k_{ap}^{A} as function of initial dye concentration is presented in Figure 3-25.

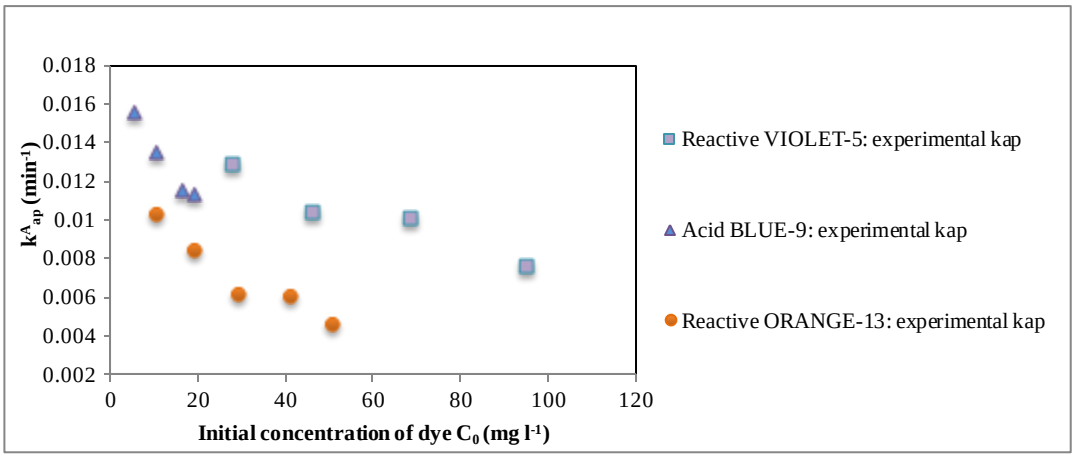

Figure 3-25: Evolution of experimental apparent constants k_{ap}^{A} vs. initial concentration of dye C_0.

As the initial concentrations of dyes increase, the k_{ap}^{A} decreases and this is valid for all three dyes. This result is in accordance with the previous works [12, 13]. This decrease can be due to different reasons. The maximum emission wavelength is 368nm and at this wavelength, all three dyes absorb some light shown in Figure 3-26. This absorption will increase as the concentration of dye in solution increases. At low concentrations, the UV light can easily reach to zinc oxide to activate it but with the increase in initial concentration, the shielding effect of dye is also increased and less UV light can reach to zinc oxide which slows down the degradation rate. Another presumed reason is that at high dye concentrations the generation of ·OH radicals on the surface of catalyst is reduced since the active sites are covered by dye molecules [14].

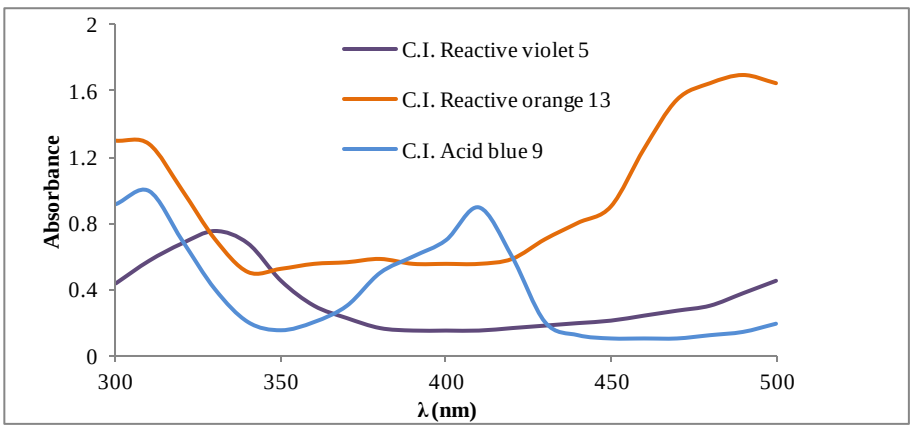

Figure 3-26: UV absorbance of colors

It can be concluded that the discoloration of solutions by treated fabric validate the Langmuir–Hinshelwood equation and the reaction takes in 3 steps: i) the molecules adsorb on the surface of photocatalyst, ii) the reaction

takes place, iii) the product desorbs and the site of photocatalyst is ready for next reaction. Therefore, it follows unimolecular kinetics.

III.1.2.1.2 Robustness of treated fabric

To check the ability of treated fabric to degrade dyes for more than once, successive discolorations of solution for 5 times without intermediate washing were carried out. For this purpose, reactive violet 5 was used with initial concentration of 80mg.l^{-1}. The Figure 3-27 presents the values of k_{ap}^{A} for each discoloration. After every discoloration, the apparent rate constant decreases. This is possibly because of the deposition of degraded products on nanorods which block some of the sites. Even after 5 times discoloration, the fabric retains good activity to degrade the dyes.

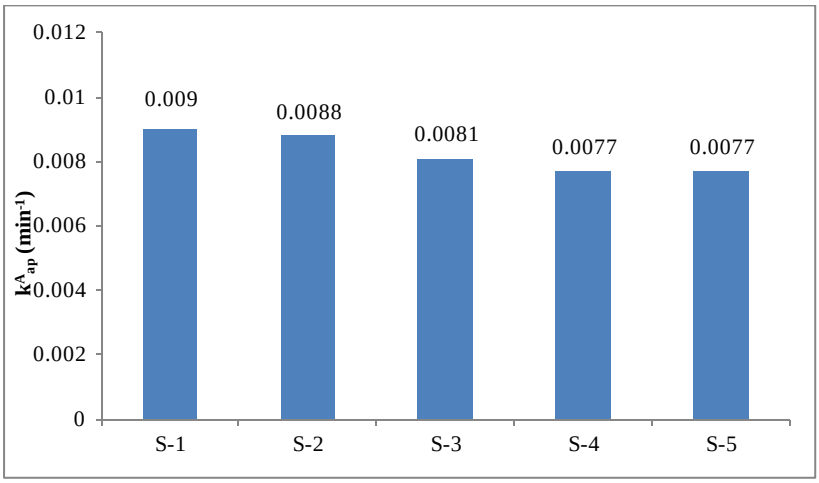

Figure 3-27: k^{A}_{ap} of 5 successive solution discolorations (S-1= first discoloration, S-2 = second discoloration and so on)

In the previous study, it was shown that the cotton fabric functionalized with nanoparticles of TiO_2 decolorized the methyl orange solution three times successively [15].

III.1.2.1.3 Effect of ZnO concentration on solution discoloration

As equimolar concentrations of zinc nitrate hexahydrate and hexamethylenetetramine were used to grow nanorods on fabric. The effect of precursor concentration on the amount of ZnO deposited on fabric in the form of nanorods and its effect on degradation of dye was also studied. The Figure 3-28A shows that with the increase in precursor concentration, the amount of ZnO deposited on fabric increases linearly. The Figure 3-28B represents the effect of amount of deposited ZnO on apparent degradation rate constant. Generally, as the amount of ZnO increases, the k^{A}_{ap} also increases but when the amount of ZnO is fabric is around 6 %, the rate of discoloration is the highest.

This might be because of change in surface area. At low precursor concentrations, the surface area of nanorods is very low because their thickness and heights are low. With the increase in precursor concentration, their surface area increases and reaches its maximum value when the precursor concentration is 100mM.l^{-1}. On further increase in concentration, the nanorods start touching each other due to increase in their thickness which reduces the surface area. At surface area, the number of active sites will be high.

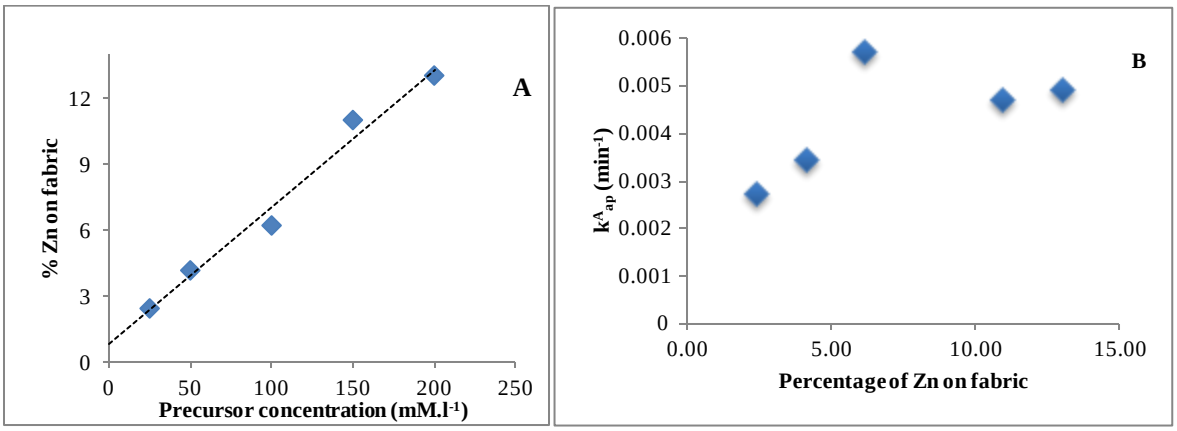

Figure 3-28: A. Effect of precursor concentration on amount of Zn deposited on fabric, B. Effect of amount of ZnO deposited on fabric on apparent degradation rate constant k^{A}_{ap}

III.1.2.2 Discoloration with lotus effect (samples S and V)

To study the solution discoloration by the fabric which has lotus effect (physical self-cleaning), the nanorods treated fabric (sample B) was modified with octdecyltrimethoxysilane (ODS) by solution "S" and vapor deposition methods "V" as described in section II.1 of this chapter.

The ODS modified samples (S and V) were superhydrophobic and it was not possible to submerge them in color solution. To overcome this problem, the samples were first dipped in acetone and immediately submerged in color solution of acid blue 9 prepared with 20mg/l and exposed to UV light. The absorbance of solutions was measured with spectrophotometer. There was no change in absorbance of solution in which the sample S was submerged whereas, the absorbance of the solution containing fabric V decreased with the passage of time.

The Figure 3-29 presents the apparent degradation rate constant k^{A}_{ap} of solution discoloration by fabric without (N) and with lotus effect by vapor deposition (V). It shows that the degradation by fabric treated with ODS is very slow as compared to that of without treatment.

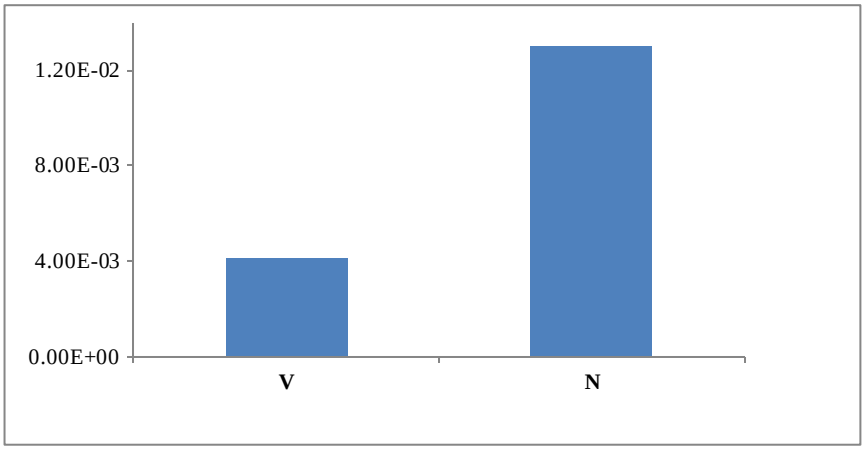

Figure 3-29: Comparison of apparent degradation rate constant k_{ap}^{A} of fabric N (without lotus effect) and V (with lotus effect by vapor method)

This is due to the deposition of ODS which blocks the most of reactive site of ZnO. This happened because the nanorods were completely masked with ODS deposited by solution method "S" as shown in Figure 3-30. Due to this masking, the solution cannot come in direct contact with nanorods which is the pre-requisite for discoloration. Whereas, it is believed that only a monolayer is formed on the top of the nanorods in case of vapor deposition method "V". Therefore, the discoloration of solution takes place. The unmodified nanorods functionalized fabric "N" has very quick degradation as compared sample "V".

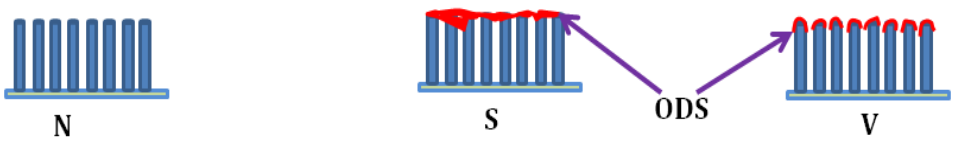

Figure 3-30: Graphical representation of nanorods functionalized fabric "N", functionalized fabric modified with ODS solution method "S" and functionalized fabric modified with ODS by vapor deposition method

III.2 Stain degradation

The stain degradation of treated fabric was studied by using the same three colors used for solution discoloration. It was studied on both types of fabrics; the nanorods treated fabric without lotus effect (without physical self-cleaning) and nanorods treated fabric with lotus effect (physical self-cleaning).

III.2.1 Characterization of stain degradation

To characterize the stain degradation, K/S values were measured with the help of spectrophotometer at different times during the exposure of stained samples to UV light. It measures the intensity of the reflected light at a series of discrete visible spectrum, usually spaced from 5nm to 20nm.

According to Kubelka-Munk equation; $K/S = (1–R)^2/2R$. Where, K= absorption coefficient, S= scattering coefficient, R= reflectance. During degradation, the K/S values decrease that shows the stain is disappearing. The K/S values are directly proportional to the amount of color present on a surface. The stained samples were exposed to UV light in the same way as solutions were exposed. The K/S values were measured at different time intervals with the help of DATA COLOR spectrophotometer SPECTRA FLASH SF 600 PLUS.

Here, it is worth mentioning that the usage of K/S to measure the concentration of color on textiles has been criticized by several researchers. Because it measures the color strength just on the top surface but in textiles, the color is also present in the interior of fibers which cannot be measured by this method. In this study, the objective was not to measure the color in absolute but in relative terms. The K/S values measured before UV irradiation of stained samples were used as reference values.

III.2.2 Results and discussions

III.2.2.1 Stain degradation with nanorods treated sample (N)

In the first step, the stain degradation was studied on fabric treated with just nanorods without modification with ODS for lotus effect. The same three colors were used for this study which was used for solution discoloration. The Figure 3-31 presents the stains of all three colors on treated fabric before UV irradiation, after 300 minutes and after 24 hours, it is quite visible that about 90% of stains of three colors are degraded within 300 minutes and after 24 hours, it disappears completely.

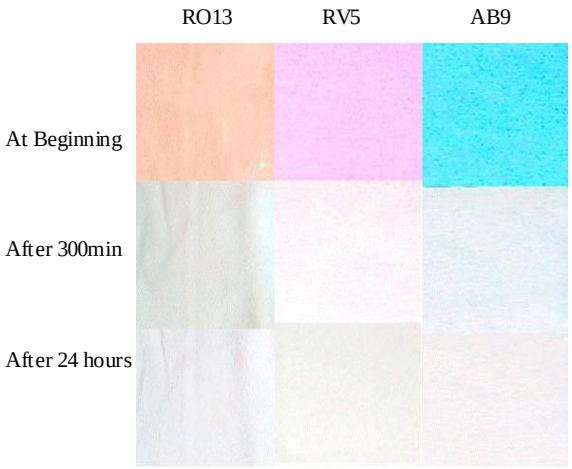

Figure 3-31: Stain of C.I. reactive orange 13, C.I. reactive violet 5 and C.I. acid blue 9 before exposure, after 300 minutes and 24 hours of exposure to UV light

The blank experiments were also carried out to check the UV sensitivity of colors. For this purpose, Untreated PET was stained with color solutions, dried and exposed to UV light. The Figure 3-32 shows that the degradation of stains on untreated fabric. There is only nominal reduction in K/S values of all three colors after 24 hours. The K/S values decrease by 10 percent. This means that there is no significant degradation of stains and the colors have very good UV fastness.

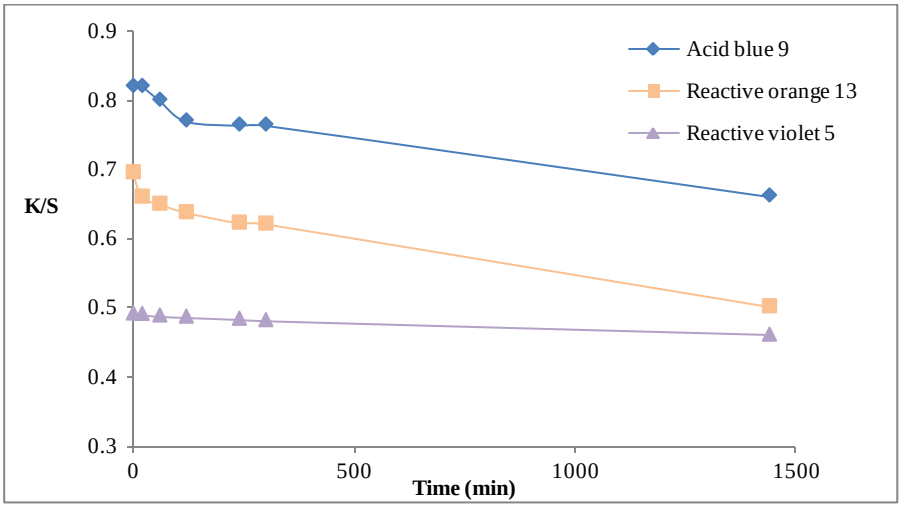

Figure 3-32: Blank experiment; stains degradation on untreated fabric

The Figure 3-33 shows the decrease in K/S values of stained samples as function of time under UV light. The reduction is K/S values is very quick at the beginning of UV irradiation which slows down with the passage of time.

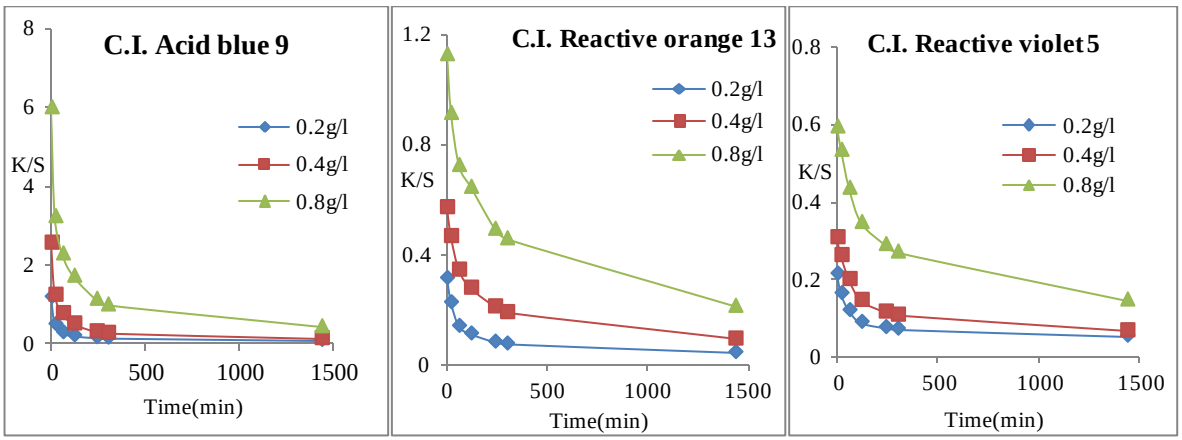

Figure 3-33: Decrease in K/S values of stains as function of time during UV irradiation

The degradation of stains is very quick at the beginning but it decreases with the passage of time. As the dye stain is deposited on nanorods, the part of stain which is on top of nanorods degrades quickly because it is completely exposed to UV whereas; the dye deposited on the sides of nanorods takes more time to degrade.

III.2.2.2 Robustness of treated fabric

a. Successive stain degradation

To check the ability of fabric to degrade color stains more than once, the successive stain degradation was carried by using C.I. acid blue 9. The fabric was stained with color solution, dried and exposed to UV light for degradation. After 24 hours exposure, it was re-stained with the same solution on the same place, dried and exposed to UV light. This process was repeated 5 times. K/S values were measured (Figure 3-34).

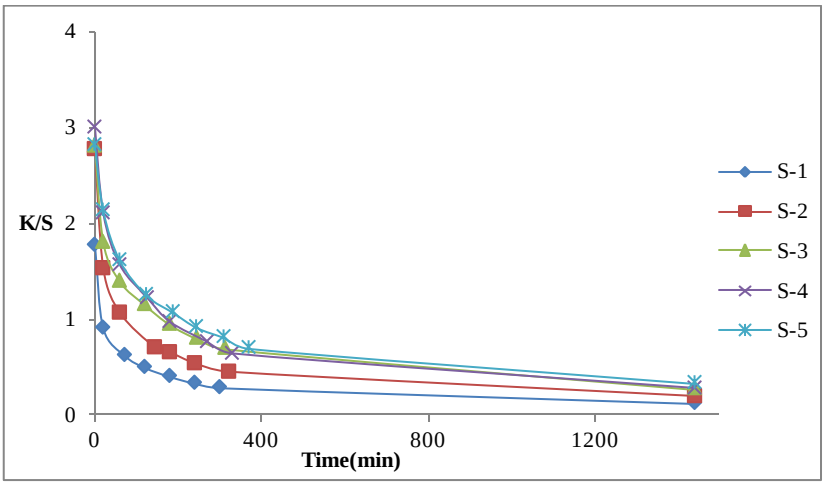

Figure 3-34: Successive stain degradations (S-1= first stain degraded, S-2 = second stain degraded and so on)

Apparently, the ability to degrade stains decreases with successive degradation. In reality, the fabric absorbs more color due to UV activation of ZnO during first stain degradation as explained in section I.2.2 of this chapter. Therefore, the depth of stain is higher than the previous one which prevents the UV light from reaching to ZnO rods (shielding effect). Therefore, apparent degradation rate constant of S-2 is less than the R-1. In the three successive degradations, the depth of color stain is approximately same but the rate constant decreases after each stain degradation. This is possibly due to the presence of the degraded products of previous stains on the nanorods. These products mask the nanorods and reduce their photocatalytic activity.

b. Water durability

To check the water fastness, the nanorods treated fabric was agitated in water at 40°C and 60°C for 30 minutes on WASHTEC (washing machine). After rinsing in water, the samples were stained with acid blue 9 solution, dried and exposed to UV light for degradation. The Figure 3-35 presents the comparison of apparent degradation rate constants of sample before rinsing, after rinsing at 40°C and after rinsing at 60°C. It shows that nano treated sample retain excellent ability to degrade the color stains after rinsing 40°C and 60°C rinsing.

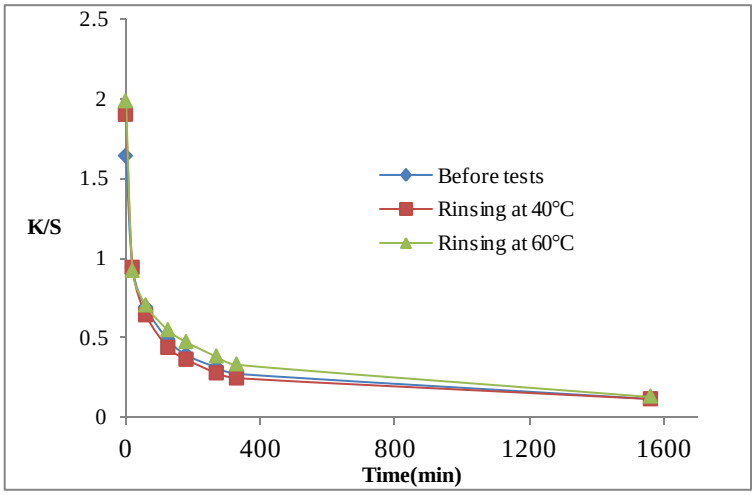

Figure 3-35: Stain degradation carried out on samples before and after rinsing test conducted at 40°C and 60°C for 30 minutes

c. Rubbing Durability

In order to evaluate the ability of nano treated fabric to withstand friction, rubbing test was carried out. For this, the samples were rubbed against cotton abradents at low pressures and in continuously changing directions for 100 cycles and 500 cycles using Martindale m235. The stain degradation was studied before and after these tests. The samples were stained with acid blue 9. The Figure 3-36 presents the results before test, after 100 cycles and after 500 cycles. It shows that the stain degradability of fabric is considerably reduces with the increase in number of cycles. This means that nanorods are removed from fibers leading which reduces the stain degradability.

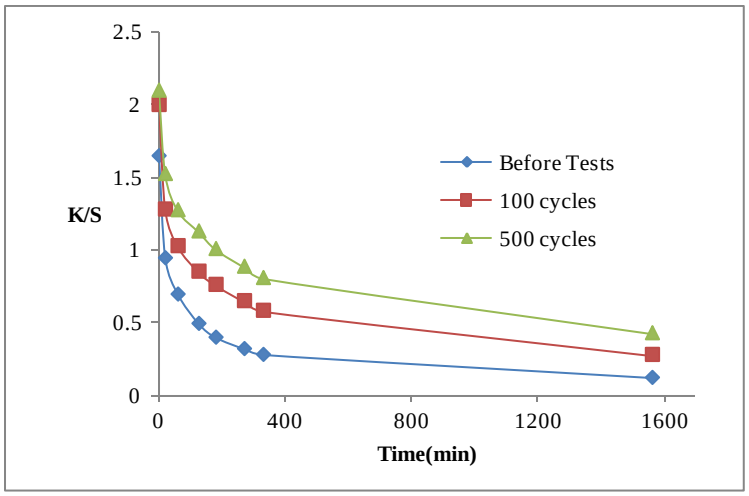

Figure 3-36: Stain degradation carried out on samples before and after Martindale rubbing test at 100 cycles and 500 cycles

III.2.2.3 Effect of ZnO concentration on stain degradation

The Figure 3-37 presents the effect of ZnO concentration (in the form of nanorods) on stain degradation. Apparently, the amount of ZnO does not have any significant effect on stain degradation. As the stain is

deposited on the top of the nanorods and is in dried state, it does not matter how much ZnO is present on the fabric surface. Therefore, rate of stain degradation does not change with the change in precursor concentration.

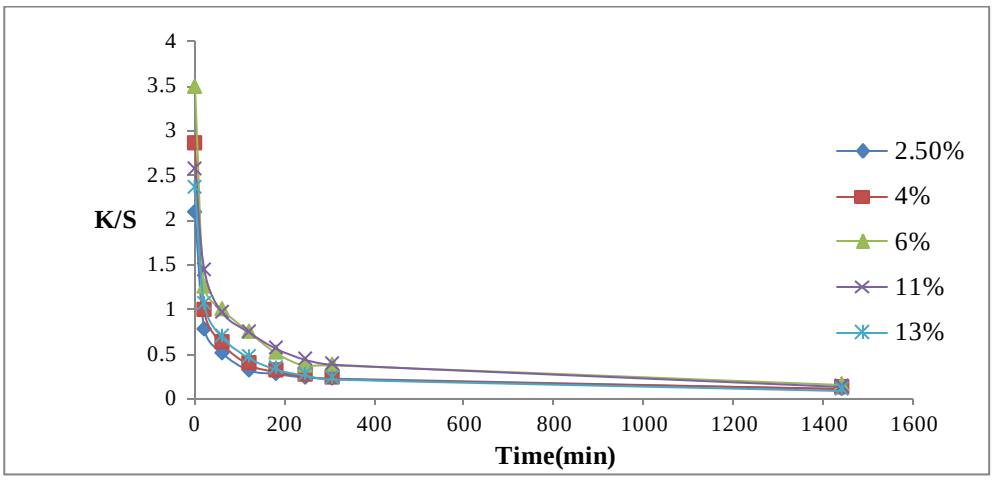

Figure 3-37: Effect of ZnO on stain degradation

III.2.2.4 Stain degradation with lotus effect (samples S and V)

To study the stain degradation by the fabric which has lotus effect (physical self-cleaning), the nanorods treated fabric (sample B) was modified with octadecyltrimethoxysilane (ODS) by solution and vapor deposition methods under the same process conditions described in section II.1 of this chapter. To stain the samples, the solution of acid blue 9 was used.

The ODS modified samples were superhydrophobic, therefore, it was not possible to stain them with the color dissolved in water. Even the color dissolved in methanol and ethanol could not stain them. Therefore, a very low surface energy solvent acetone was used to prepare the color solution for staining. The samples were immersed in the solutions for several second to make sure that they are completely stained. The sample V was stained completely whereas, the sample S was stained partially. The dried samples were exposed to UV for stain degradation and K/S values were measured at regular intervals with spectrophotometer.

It was found that that there was no change in K/S of stained sample S whereas, in case of V, the K/S values decreased with the passage of time (Figure 3-38). This means that the stain was not degraded on sample S, while it was degraded on sample modified by sample V. In case of V, only a monolayer of ODS is formed, due to which some active sites of ZnO are available to degrade the stains but for solution deposition, all the nanorods are completely masked as shown in Figure 3-10

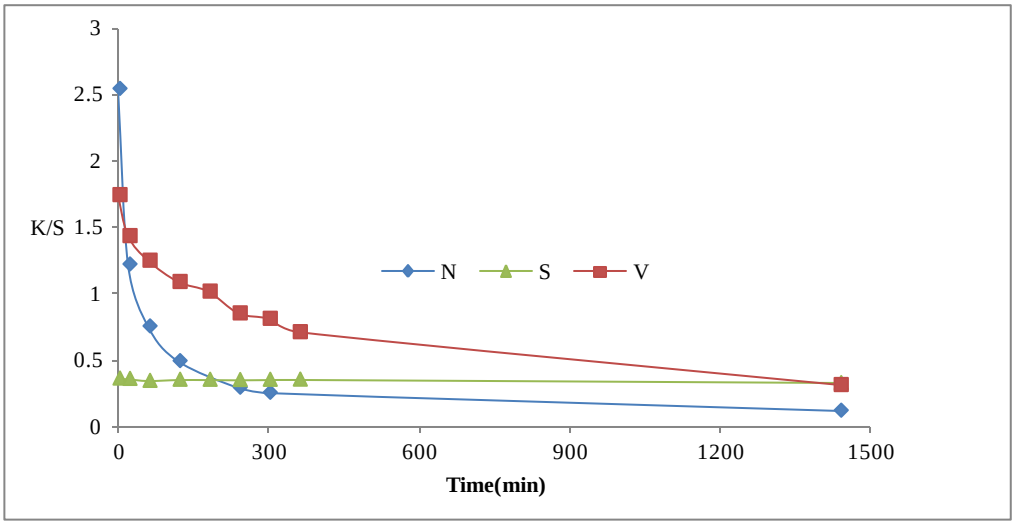

Figure 3-38: Comparison of stain degradation by fabric N (nanorods functionalized fabric), samples with physical self cleaning; S= ODS by solution method and V = ODS by vapor deposition method.

A relative efficacy of stain degradation of sample with lotus effect by vapor and solution depositions of ODS with respect to the one without lotus effect is shown in Figure 3-37. Although the fabric with lotus effect (vapor deposition of ODS) degrades the stain but at relatively slower rate. The sample modified by solution method did does not degrade the stain (as explained in section III.1.2.2 of this chapter).

III.3 Conclusion

The nanorods treated fabric has ability to degrade the color stains and decolorize the color solutions with which it comes in contact due to photocatalytic effect of ZnO under UV irradiation. The kinetics of solution discoloration was studied and it was found that it followed pseudo first order kinetics. An equation to predict the apparent degradation rate constant was derived by using Langmuir–Hinshelwood equation. With the increase in the amount of ZnO present on the fabric in the form of nanorods, the apparent discoloration constant also increased. The fabric had ability to decolorize color solution more than once. But after each discoloration, the apparent degradation rate constant decreased due to the deposition of degraded products.

On modification with ODS (sample S and V), the ability to decolorize solutions depends on the method of modification. The sample S completely lost its ability to decolorize solution but V retained its ability but the rate of discoloration was very low as compared to the sample N.

The treated fabric also showed self-cleaning in terms of stain degradation under the effect of UV light. The fabric had ability to degrade color stains successively several times but its degradation rate also decreased due to

deposition of degraded products. The fabric had excellent water durability whereas, it had poor abrasion durability.

The fabric with lotus effect also degraded the color stains but only in vapor deposition method modified samples (V). The sample S did not degrade the stains. The relative efficacy of stain degradation showed that the rate of stain degradation on sample with lotus effect was very low as compared to without lotus effect.

IV Biological self-cleaning

The biological self-cleaning refers to antibacterial activity of fabric. To study biological self-cleaning, the same sample was chosen used for study chemical self-cleaning study.

The antibacterial activity (A) was assessed on nanorods treated samples (N), the samples modified by vapor deposition of ODS (V) and the ones modified by solution deposition of ODS (S).

IV.1 Evaluation of antibacterial activity

IV.1.1 Bacterial material

Three bacteria were used in this study two Gram negative bacteria*:* *Escherichia coli* ATCC 8739 and *Pseudomonas aeruginosa* ATCC 27853, and a Gram positive bacterium: *Staphylococcus aureus* ATCC 6538. Pre-cultures were performed at 37°C for 24 h by the inoculation of Muller Hinton (MH) broth (5 ml) (Biocar Diagnostic, Beauvais, France) with a colony of the desired bacterium. A culture was then realized by injecting 0.1 ml of bacterial suspension into 5 ml of MH broth. The overnight cultures performed at 37°C were used to prepare cell suspensions of (1-3) x 10^6 Colony-Forming Units.ml^{-1} (CFU.ml^{-1}) into a fresh MH broth. These cell suspensions were used for qualitative or quantitative antibacterial experiments to study the antibacterial effect of the functionalized polyester fabric by growing zinc oxide nanorods.

Before carrying out the antibacterial activity evaluation, the bacterial contamination of samples was tested and the presence of bacteria was 1 to 10^2 CFU/cm^2. It is negligible as compared to bacterial culture used for tests (10^6 CFU/ml). Therefore, decontamination of samples was not carried out. For details, see Annexe.

IV.1.2 Qualitative Antibacterial Assessment

The qualitative method was the primary approach to assess the behavior of the bacterial culture. The Muller Hinton (Biocar Diagnostic, Beauvais, France) agar plates were inoculated with 1 ml of the dilution described above. Afterward, a swatch of the test sample (1.2 cm in diameter) was placed on the agar surface and incubated at 37 °C for 24 h before observation. At least 3 repetitions of each fabric were performed

IV.1.3 Quantitative Antibacterial Assessment

Reduction of bacterial growth on the finished samples was estimated for the Gram negative bacteria *Escherichia coli* (ATCC 8739) and the Gram positive bacteria *Staphyloccocus aureus* (ATCC 6538) using the NF ISO 20743:2009 Transfer Method.

The agar plates were inoculated with 1 ml of a Muller Hinton (Biocar Diagnostic, Beauvais, France) nutrient broth culture containing (1-3) x 10^6 CFU.ml^{-1}. Afterward, a swatch of the test sample (3.8 cm in diameter) was placed on the agar surface and pressed down with a 200 g cylindrical weight for 60 ± 5 s. For every fabric sample, six samples were performed: three of them were removed from the agar surface and immediately analyzed for counting; the three other test samples were then removed from the agar surface, placed in a container with the transferred surface face up, and incubated at 37 °C for 24 h in a humidity chamber. For each fabric, 20 ml of neutralizing solution was poured on the test sample in a sterile bag and shaken vigorously using a stomacher shaker for 1 min on each side of the bag.

Serial dilutions were performed with sterilized in physiological saline (0.85% NaCl) with tryptone (0.1%) (Biocar Diagnostic, Beauvais, France), and the appropriate dilutions were plated onto agar medium as requested by the ISO 20743:2007(F) standard and incubated at 37 °C for 24 h. The details of the test are available in annexe.

The antibacterial activity (A) of the functionalized polyester fabric by zinc oxide nanorods was calculated as follows:

$$A = (\log C_t - \log C_0) - (\log T_t - \log T_0)$$

Where

- A is the antibacterial activity value
- log C_0 and log C_t are the decimal logarithm average corresponding to the number of bacteria obtained from the three untreated samples immediately after inoculation and after an incubating period of 24h respectively.
- log T_0 and log T_t is the decimal logarithm average corresponding to the number of bacteria obtained from the three treated samples immediately after inoculation and after an incubating period of 24h.

IV.2 Results and Discussions

IV.2.1 Qualitative Assessment

The qualitative evaluation of A of treated fabric was carried out with two Gram negative; *E. coli* and *P. aeruginosa*, and one Gram positive; *S. aureus* bacteria. The untreated sample C (without nanorods) and treated samples with nanorods (N) as well as samples modified by vapor deposition (V) and solution deposition of ODS (S) were placed on agar plates containing bacterial cultures. After 24 hours of incubation in dark, it was observed that the bacteria grew below, above and in the immediate proximities of sample C. The sample S inhibited the growth of bacteria above and below but the growth was observed in their vicinities. The samples V and N inhibited the growth of bacteria on, below as well as in the immediate proximities. The zone of inhibition was bigger in case of sample N than sample V. The antibacterial activity of was remarkable for *S. aureus* but it decreased for *E. coli* and it further reduced for *P. aeruginosa*.

The growth inhibition of bacteria can be due to chemical as well as physical reasons. If the size of ZnO is very small like in our case, the tip of the nanorods is around 50nm, it can penetrate the cell membrane leading to its disintegration and malfunctioning of the permeability barrier [16], which causes the death of bacteria. The second important reason for bacterial growth inhibition by ZnO is the production and penetration of reactive oxygen species (ROS). The ROS includes $^{\cdot}OH$, H_2O_2 and O_2^{2-}. As the bacteria carry negative charge on the surface, therefore, the penetration of O_2^{2-} seems impossible but the hydroxyl radical and hydrogen peroxide can penetrate into the cell membrane which leads to the death of bacteria. It has been reported that these are the main reasons of bactericide even the tests are carried out in dark [17]. Another reason for bacterial growth inhibition can be the release of Zn^{++} ions in the bacterial culture. As the bacteria have negative on their surface, the Zn^{++} ions adhere on them and modify the membrane structure.

To understand why the samples inhibit the growth of bacteria in their vicinities and why the inhibition zone is bigger for sample “N” than “V” and no zone for sample “S”, the atomic absorption spectroscopy (AAS) was carried out on the bacterial cultures after the removal of samples. The Table 3 presents the amount of Zn measured in bacterial culture by AAS.

Table 3: The amount of Zn measured in bacterial culture

Sample	Average [Zn] (g/l)	Zone of inhibition
N	0.0473 ± 0.0042	++
V	0.0357 ± 0.0006	+
S	undetectable	---

It can be inferred that in bacterial culture, ZnO dissolves and generate Zn^{++} ions which attach on the bacterial surface and prevent the growth of bacteria in the vicinities of the treated samples. Without ODS modification, the amount of Zn^{++} is higher due to which the zone of inhibition is also higher. The amount of Zn reduces on treatment with ODS by vapor deposition method. Therefore, the zone of inhibition was relatively smaller. For solution treated sample S, there was no zone of inhibition because there was no release of Zn.

IV.2.2 Quantitative assessment under laboratory conditions

To evaluate the antibacterial activity of the treated fabric quantitatively, one Gram positive; *Staphyloccocus aureus (S.aureus)* and one Gram negative; *E.coli*, bacteria were chosen. The Figure 3-39 shows the counting of *S. aureus* population and *E.coli* (in decimal logarithm average per milliliter) directly on the samples after inoculation (t=0) and after an incubation period of 24h (t=24h) in dark.

The cell enumeration of *S. aureus* from the contaminated samples N, S and V show a decrease of the initial cell count from 3.5, 3.5 and 3.75 $CFU.ml^{-1}$ respectively to up *ca* 0 $CFU.ml^{-1}$ after 24h of incubation, under dark conditions, However, *S. aureus* enumeration realized on the control fabric (C) shows an increase of the cell count of *ca* 1 log $CFU.ml^{-1}$ after 24h of incubation under same conditions. The results obtained for *E. coli* show a decrease of the initial cell count from 4.5 log $CFU.ml^{-1}$ to 2 log $CFU.ml^{-1}$ for sample N, 4.1 log $CFU.ml^{-1}$ to 2 log $CFU.ml^{-1}$ for sample S and 3.75 log $CFU.ml^{-1}$ to 0.1 log $CFU.ml^{-1}$ for sample V after 24h of incubation, under dark conditions. The cell count performed on control fabric shows an increase of *E. coli* cell count from 4.7 log $CFU.ml^{-1}$ to 5.3 log $CFU.ml^{-1}$.

The calculation of the antibacterial activity of the functionalized PET fabric by zinc oxide nanorods on the basis of the NF ISO 20743:2009 are presented in Table 4. It shows that the antibacterial activities of all the samples are much higher on *S. aureus* as compared to *E. coli*.

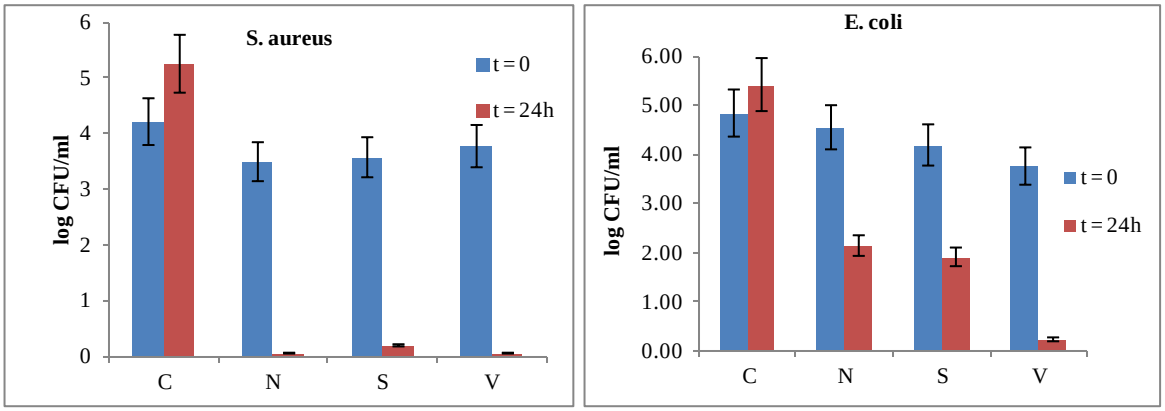

Figure 3-39: Counting of *S. aureus* and *E. coli* population directly after inoculation (t=0) and after an incubating period of 24h (t=24h) on control sample C, nanorods treated sample N, nanorods treated sample modified with ODS by solution method S and nan rods treated sample modified with ODS by vapor deposition method.

Table 4: Antibacterial activity of different samples

Bacteria	N	S	V
S. aureus	4.47	4.42	4.75
E. coli	2.99	2.85	4.10

The percentage mortality of the bacteria was calculated by using the following formula and is presented in Table 5;

$$\text{Percentage mortality} = (\log T_t - \log C_t) \times 100/\log T_t$$

Table 5: Percentage mortality of bacteria

Bacteria	N	V	S
S.aureus	99.08	99.16	96.64
E.coli	53.2	95.1	58.1

It is quite clear that the treated samples are more effective against *S. aureus* than *E. coli*. This difference in antibacterial activity of treated fabric is due to the difference in cell membranes of both bacteria. The killing and inhibition of bacteria take place due to both physical and chemical mechanisms. There are certain components in the cell membrane of Gram negative bacteria which are not found in Gram positive bacteria. For instance, Gram negative bacteria contain the extra outer membranes and the pathogen-associated molecular patterns which include lipopolysaccharide (consisting of lipid A, core polysaccharide and O antigen), porins and particular fragments of peptidoglycan. This structure prevents the attachment of ZnO on the surface [18]. The complex structure of Gram negative bacteria mentioned above also acts as permeability barrier to ROS and prevents their

penetration into the membrane [19]. *S. aureus* is charged less negatively as compared to *E. coli* [20]. This will lead to penetration of negatively charged reactive oxygen species like peroxide ions, hydroxyl radicals and superoxide into *S.aureus* membrane which cannot penetrate into *E.coli* which has higher negative charge. This penetration causes the death of *S.aureus*.

Another important point is the higher antibacterial activity of samples V and S as compared to N. To understand this difference, it is important to recall the formation of biofilm on a surface which takes place in five steps [21]; (i) Reversible attachment of bacteria on surface, (ii) Transition from reversible to irreversible attachment by production of extracellular polymers by the bacteria, (iii) Early development of biofilm architecture, (iv) Development of micro colonies into a mature biofilm, (v) Dispersion of cells from the biofilm into the surrounding environment. It shows that bacterial will grow only when the transition between their reversible and irreversible attachment take place. On nanostructured superhydrophobic surfaces, the rod like bacteria cannot attach themselves properly [22]. *E.coli* having rod like morphology find it difficult to attach on nanostructured superhydrophobic samples V and S. The antibacterial bacterial activity of V is far better than S due to synergistic effect of superhydrophibicity and generation of ROS because only a monolayer of ODS is formed on the top of the nanorods therefore, active site are available to produce ROS whereas, in case of solution deposition, the nanorods are completely masked.

IV.2.3 Quantitative assessment under controlled laboratory conditions

To quantify the effect of UV pre-activation on antibacterial activity of treated fabric, *S. aureus* was chosen for this study because of its higher antibacterial sensitivity. The one piece of sample was put in complete dark, second and third was put under UV light at a distance of 18cm for 24 hours and 48 hours respectively. The results of antibacterial tests are presented in Figure 3-40. The antibacterial activity on the sample which was put in complete dark before test was 4.29 which increased to 4.45 and 4.67 after 24 hours and 48 hours UV pre-activation respectively. The percentage cell death increased from 96% to 99% after 24 hours of UV activation. Due to UV illumination, the electron present in the valence band jumps to the conduction band which causes generation of positive hole and electron pair. Some of the positive holes react with the lattice oxygen leading to the formation of surface oxygen vacancies. Similarly, the electrons generated react with surface metal (Zn) to reduce it from Zn^{++} to Zn^{+} to form defective sites [8]. The water and oxygen may compete to adsorb on them. The defective sites are kinetically more favorable for hydroxyl adsorption than oxygen adsorption [7]. After UV

illumination, the surface of ZnO will be rich in hydroxyl which is one of the reactive oxygen species and has ability to kill bacteria.

The antibacterial activity on *S. aureus* presented in Figure 3-39 is higher (AA=4.50) than the one presented in Figure 3-40 for the sample (AA=4.30) put in complete dark. Although the samples used were same but the one used to study the UV effect was first put in complete dark before carrying out the test whereas, the other was used as prepared without putting it in dark. It must have been activated by the sun light and the normal tube light because both contain some amount of UV light.

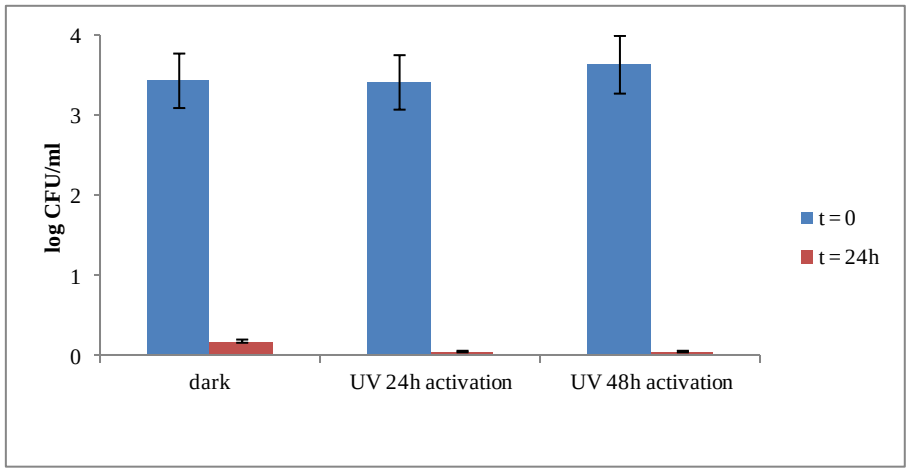

Figure 3-40: Counting of S. aureus atcc 6538 population (in decimal logarithm average per milliliter) directly after inoculation (t=0) or after an incubating period of 24h (t=24h) on nanorods treated fabrics conserved in dark, after 24h of uv activation, and after 48h of uv activation

IV.3 Conclusion

It can be concluded that the functionalized fabric has biological self-cleaning. The treated fabric not only prevents the growth of bacteria but also kills the ones which attach on it. The sample N and V prevent the growth of bacteria in their immediate vicinities due to release of Zn. The inhibition zone is bigger for sample N than V. The sample S has no zone of inhibition around it because the nanorods are completely masked with ODS and do not release Zn as shown by atomic absorption spectroscopy analysis of bacterial culture after incubation.

The treated samples (N, S and V) showed higher antibacterial activity against *S. aureus* than *E. coli*. The antibacterial activity of sample V against *E. coli* is much higher than the samples N and S due to the synergistic effect of both physical self-cleaning and release of reactive oxygen species. This effect is completely new in

textiles because it brought the two characteristic to fabric; prevention of bacteria from attachment due to superhydrophobicity and the killing of them of if they attach. This is attributed to hierarchical structure and antibacterial property of ZnO.

The UV light pre-activation of sample N has positive effect on its antibacterial activity. The antibacterial activity was increased 4.30 to 4.70 after 48 hours UV activation.

References

1. R. Wenzel, *Resistance Of Solid Surfaces To Wetting By Water*. Industrial & Engineering Chemistry, 1936. **28**(8): p. 988-994.

2. E.W. Washburn., *The Dynamics of Capillary Flow*. Physical Review, 1921. **17**(3): p. 273-283.

3. B.V. Zhmud, F. Tiberg, and K. Hallstensson, *Dynamics of Capillary Rise*. Journal of Colloid and Interface Science, 2000. **228**(2): p. 263-269.

4. L. Zhu, A. Perwuelz, M. Lewandowski and C. Campagne, *Static and Dynamic Aspects of Liquid Capillary Flow in Thermally Bonded Polyester Nonwoven Fabrics*. Journal of Adhesion Science and Technology, 2008. **22**(7): p. 745-760.

5. C. Ishino, M. Reyssat, E. Reyssat, K. Okumura and D. Quéré, *Wicking Within Forests Of Micropillars*. EPL (Europhysics Letters), 2007. **79**(5): p. 56005.

6. F. Ã. Cebeci, Z. Wu, L. Zhai, R. E. Cohen and M. F. Rubner, *Nanoporosity-Driven Superhydrophilicity: A Means to Create Multifunctional Antifogging Coatings*. Langmuir, 2006. **22**(6): p. 2856-2862.

7. X. Feng, L. Feng, M. Jin, J. Zhai, L. Jiang and D. Zhu, *Reversible Super-hydrophobicity to Super-hydrophilicity Transition of Aligned ZnO Nanorod Films*. Journal of the American Chemical Society, 2003. **126**(1): p. 62-63.

8. R.-D. Sun, A. Nakajima, A. Fujishima, T. Watanabe and K. Hashimoto, *Photoinduced Surface Wettability Conversion of ZnO and TiO2 Thin Films*. The Journal of Physical Chemistry B, 2001. **105**(10): p. 1984-1990.

9. B. Xu and Z. Cai, *Fabrication of a Superhydrophobic ZnO Nanorod Array Film on Cotton Fabrics Via A Wet Chemical Route And Hydrophobic Modification*. Applied Surface Science, 2008. **254**(18): p. 5899-5904.

10. N. Yoshida, Y. Abe, H. Shigeta, K. Takami, H. Osaki, T. Watanabe, K. Hashimoto and A. Nakajima, *Preparation and Water Droplet Sliding Properties of Transparent Hydrophobic Polymer Coating by Molecular Design for Self-Organization*. Journal of Sol-Gel Science and Technology, 2004. **31**(1): p. 195-199.

11. M.A.Behnajady, N. Modirshahla, and R. Hamzavi, *Kinetic Study on Photocatalytic Degradation of C.I. Acid Yellow 23 By Zno Photocatalyst*. Journal of Hazardous Materials, 2006. **133**(1-3): p. 226-232.

12. J. B. De Heredia, J. Torregrosa, J. R. Dominguez and J. A. Peres, *Oxidation of P-Hydroxybenzoic Acid by UV Radiation And By TiO2/UV Radiation: Comparison And Modelling Of Reaction Kinetic*. Journal of Hazardous Materials, 2001. **83**(3): p. 255-264.

13. C. M. So, M. Y. Cheng, J. C. Yu and P. K. Wong, *Degradation of Azo Dye Procion Red MX-5B by Photocatalytic Oxidation*. Chemosphere, 2002. **46**(6): p. 905-912.

14. I.K. Konstantinou and T.A. Albanis, *TiO2-Assisted Photocatalytic Degradation of Azo Dyes in Aqueous Solution: Kinetic And Mechanistic Investigations: A review*. Applied Catalysis B: Environmental, 2004. **49**(1): p. 1-14.

15. D. Wu, M. Long, J. Zhou, W. Cai, X. Zhu, C. Chen and Y. Wu, *Synthesis and characterization of self-cleaning cotton fabrics modified by TiO2 through a facile approach*. Surface and Coatings Technology, 2009. **203**(24): p. 3728-3733.

16. G. Applerot, A. Lipovsky, R. Dror, N. Perkas, Y. Nitzan, R. Lubart and A. Gedanken, *Enhanced Antibacterial Activity of Nanocrystalline ZnO Due to Increased ROS-Mediated Cell Injury*. Advanced Functional Materials, 2009. **19**(6): p. 842-852.

17. J. Sawai, S. Shoji, H. Igarashi, A. Hashimoto, T. Kokugan, M. Shimizu and H. Kojima, *Hydrogen Peroxide as an Antibacterial Factor in Zinc Oxide Powder Slurry*. Journal of Fermentation and Bioengineering, 1998. **86**(5): p. 521-522.

18. A. A. Tayel, W. F. El-Tras, S. Moussa, A. F. El-Baz, H. Mahrous, M. F. Salem and L. Brimer, *Antibacterial Action of Zinc Oxide Nanoparticles Against Foodborne Pathogens*. Journal of Food Safety, 2011. **31**(2): p. 211-218.

19. P. Espitia, N. d. t. Soares, J. l. d. Coimbra, N. l. Andrade, R. Cruz and E. Medeiros, *Zinc Oxide Nanoparticles: Synthesis, Antimicrobial Activity and Food Packaging Applications*. Food and Bioprocess Technology, 2012. **5**(5): p. 1447-1464.

20. R. Sonohara, N. Muramatsu, H. Ohshima and T. Kondo, *Difference in Surface Properties Between Escherichia Coli and Staphylococcus Aureus as Revealed by Electrophoretic Mobility Measurements*. Biophysical Chemistry, 1995. **55**(3): p. 273-277.

21. R. Van Houdt and C.W. Michiels, *Role of Bacterial Cell Surface Structures in Escherichia Coli Biofilm Formation*. Research in Microbiology, 2005. **156**(5-6): p. 626-633.

22. E. Fadeeva, V. K. Truong, M. Stiesch, B. N. Chichkov, R. J. Crawford, J. Wang and E. P. Ivanova, *Bacterial Retention on Superhydrophobic Titanium Surfaces Fabricated by Femtosecond Laser Ablation*. Langmuir, 2011. **27**(6): p. 3012-3019.

23. A.A. Hebeish, M.M. Abdelhady, and A.M. Youssef, *TiO2 Nanowire and TiO2 Nanowire Doped Ag-PVP Nanocomposite for Antimicrobial and Self-cleaning Cotton Textile*. Carbohydrate Polymers, 2013. **91**(2): p. 549-559.

24. B. A. Çakır, L. Budama, Ö. Topel and N. Hoda, *Synthesis of ZnO nanoparticles using PS-b-PAA reverse micelle cores for UV protective, self-cleaning and antibacterial textile applications*. Colloids and Surfaces A: Physicochemical and Engineering Aspects, 2012. **414**(0): p. 132-139.

25. R. Dastjerdi and M. Montazer, *Nano-colloidal functionalization of textiles based on polysiloxane as a novel photo-catalyst assistant: Processing design*. Colloids and Surfaces B: Biointerfaces,2011. **88**(1): p. 381-388.

4 General Conclusion

This work was aimed to grow ZnO nanorods on poly (ethylene terephtalate) fabric to obtain multi-functional textile. In this research work, the nanorods were grown by two processes: seedless and seeded methods. Their growth by seedless method was carried on both cotton and polyester substrates which were modified with different hydrophobic chemicals to obtain the optimized nucleation and growth. But this method met with limited success, as nanorods were grown either in the form of flower like structures or on scattered places.

The seeded method was tested only on poly (ethylene terephtalate) fabric without pre-activation of fabric surface and it was observed that the nanorods grew but once again, on scattered places. This happened due to the hydrophobic surface of polyester, the nano seeds of ZnO could not attach to polyester fabric due to the absence of any polar groups. To overcome this problem, an air atmospheric-plasma treatment was carried out to generate polar groups so that nano seeds could have good affinity with polyester fabric. The presence of ZnO seeds at the surface of polyester fabric is crucial for the uniform growth of nanorods. Due to plasma treatment and equimolar concentration of precursors, the nanorods grew uniformly all over the micro fibers of polyester fabric. The amount of Zn present on fabric in the form of nanorods was 5.60±0.6 percent with respect to weight of fabric, and 30% with respect to surface of fabric. The nanorods were highly crystalline and mono whiskers, and they grew along (001) direction. The hand feel of fabric did not change after functionalization with nanorods which showed that they did not attach with each other.

The micro roughness of the polyester fabric was characterized by profilometery. It showed that the fabric had micro protrusions which looked like micro-roughness of lotus leaf. As the nano seeds provided the site for growth of nanorods, the effect of seed concentration on nano-roughness was studied. The AFM topographs obtained showed that the nano-roughness changed with the change in seed concentration. When the seed concentration was high, the distance between the consecutive nanorods was low and vice versa. Not only we succeeded to nano-structurize the fiber surface but also we were able to control the nanoroughness by varying the seed concentration

First functional property of nanorods functionalized fabric (N) studied was superhydrophilicity. The water contact angle was around 0° and its diffusion coefficient was very high (8.38±0.02mg/s$^{1/2}$). The roughness generated due to growth of nanorods as well as presence of hydroxyl groups on them reduced the water contact angle and increased its diffusion coefficient with respect to plasma treated and untreated PET fabric. The high

water diffusion coefficient also showed that the interior of fabric had been functionalized with nanorods. The diffusion coefficient of water was increased whereas, that of decane decreased with the increase in seed concentration because water is polar whereas, decane is apolar with low surface energy. With the increase in seed concentration, the pores of fabric were blocked due to growth of higher number of nanorods which decreased the diffusion of decane. However, the better wettability linked to nanorods growth enhanced the diffusion of water

The UV pre-activation of treated fabric showed enhanced superhydrophilicity. The diffusion coefficient of water increased with the increase in duration of treated samples' exposure to UV light. The diffusion coefficient reduced when the sample was put in dark for same period of time due to de-activation of ZnO but it did not gain the same values which it had before UV activation.

As the hierarchical roughness structures have been developed by growth of nanorods on microfibers of PET fabric, the next step was to do the hydrophobization for the physical self-cleaning. The functionalized samples were modified with hydrophobic chemical ODS (octadecyltrimethoxysilane) by two methods; solution deposition (S) and vapor deposition (V). The vapor deposition method appeared to impart better self-cleaning characteristics than solution deposition. This is because of the formation of very thin layer of ODS by vapor deposition without changing roughness. The highest water contact angle obtained was 158±1.8° and the lowest roll off angle was 1.7±0.2°. As the concentration of ODS was increased in solution deposition method, the functionalized fabric exhibited better physical self-cleaning characteristic until 2% then it started decreasing. By vapor deposition of ODS, it increased with the increase in deposition time and gave the best results when it was 3 hours after that it did not change.

The seed concentration affected the lotus effect because it changed the roughness. The concentrations of precursors (zinc nitrate hexahydrate and hexamethylenetetramine) to grow nanorods did not have any significant effect on physical self-cleaning characteristics. The superhydrophobicity and roll off angle depends on the distance between the consecutive nanorods not on the height of nanorods. The water roll off angle was directly linked to surface fraction (percentage of surface touching the water droplet). It increased with the increase in surface fraction.

The third functional property envisaged was the chemical self-cleaning which was studied by two ways; stain degradation and solution discoloration. These both characteristics were studied on fabric with and without physical self-cleaning (N, S and V). The sample N decolorized the solutions and degraded stains due to

photocatalytic effect of ZnO under the effect of UV light. The kinetics study of solution discoloration showed that it followed first order kinetics and was modeled by using Langmuir Hinshelwood equation. The apparent discoloration rate constant increased with the increase in precursor concentrations to grow nanorods but it did not have any impact on stain degradation. With the increase in precursor concentration, the amount of ZnO deposited on fabric was increased due to higher number of active sites were available for discoloration of solution. In stain discoloration, the stain was deposited on the top of the nanorods and in the dry state; therefore, the increase in ZnO did not have any impact on it. The treated fabric had excellent water durability but poor rubbing durability. Contrary to literature, the treated fabric had ability to decolorize the color solution and stains several times without any significant loss of photocatalytic activity.

As the samples S and V were superhydrophobic due to deposition of ODS, neither they got stained by dye solutions in water, methanol and ethanol nor submerged in them. Only dye solution in acetone could stain them. Similarly, they submerged in dye solution, only once they were soaked in acetone. Although, the sample V was more hydrophobic as well as more repellent than S but it decolorized the stains and solutions whereas, the sample S did not. This was due to the deposition of higher amount of ODS in solution method (sample S) which completely masked the nanorods leading to loss of photocatalytic effect. Whereas, very small amount was deposited in vapor deposition (V) therefore, the nanorods were not completely masked and some of active sites were available for photocatalytic effect. To the best of our knowledge, this is the first study on the discoloration of stains and solutions by the fabric which also has physical self-cleaning.

The last functional characteristic studied was biological self-cleaning (antibacterial activity) of treated fabric. It was also studied on both samples functionalized with ZnO nanorods with and without physical self-cleaning (N, S and V). The qualitative assessment of antibacterial activity showed that all the samples inhibited the growth of Gram positive and Gram negative bacteria above and below. However, the zones of inhibition around them were different. The sample N had biggest zone of inhibition. The zone around sample V was relatively smaller, whereas, the sample S did not have any zone for all bacteria tested. This difference was due to release of Zn in the bacterial culture by the treated sample as detected by atomic absorption spectroscopy.

The quantitative assessment showed that all the samples had excellent biological self-cleaning against *S. aureus* with bacterial mortality more than 95%. The sample V also showed excellent antibacterial activity against *E. coli* with bacteria mortality of 95% contrary to S and N which had bacterial mortality around 55%. The higher

antibacterial activity of V is attributed to synergistic effect of superhydrophobicity and nanorods (mechanical penetration, release of Zn^{++} and generation of reactive oxygen species).

The originality of this work is the functionalization of PET fabric which exhibits multi self cleaning characteristics. This is due to the choice of ZnO and the development of hierarchical roughness structure due to the growth of nanorods.

The combination of all the results of this work shows that each sample has multifunctional characteristics. Superhydrophilicity, chemical and biological self-cleanings have been demonstrated by sample N. The sample S has physical and biological self-cleanings. All three self-cleanings; physical, chemical and biological have been integrated into sample V.

Perspective

The process to grow nanorods on polyester fabric has been successfully optimized. This technique needs to be applied to other substrates (fibers of different chemistry and different textile structures) as well. Other functional characteristics like fireproofing, gas detection (due to change in surface conductivity), and remediation of water etc needs to be studied.

Future work

1. The seedless growth of nanorods is very sensitive to process conditions. To grow the nanorods by this method, it is important to optimize the process conditions.
2. Further investigations are needed to understand the effect of UV pre-activation on hydrophilicity and diffusion coefficients.
3. The sample with physical self-cleaning modified by solution deposition of ODS neither degraded the stain nor decolorized the solutions however, it showed excellent antibacterial activity against *S. aureus* and fairly good activity against *E. coli*. It showed the mechanism of antibacterial activity of ZnO, and stain degradation as well as solution discoloration are not same. It needs further work to investigate it.
4. More work is needed to investigate how to enhance the rubbing durability of nanorods treated fabric because it has low rubbing fastness.

Annexes

I. Materials

I.1 Methyltrimethoxysilane (MTMS)

It is a colorless liquid with molecular weight 136.22g/mole and linear structure $CH_3Si(OCH_3)_3$ (Sigma Aldrich). It was used without any further purification. The molecular structure of MTMS is reperesented in Figure 1

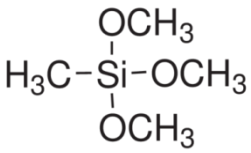

Figure 1: Molecular structure of Methyltriethoxysilane

I.2 Isobutyl(trimethoxy)silane (IBTMOS)

It is a colorless liquid with molecular weight 178.3 g/mol and linear structure $(CH_3)_2CHCH_2Si(OCH_3)_3$ (Sigma Aldrich). The molecular structure of IBTMOS is represented in Figure 2

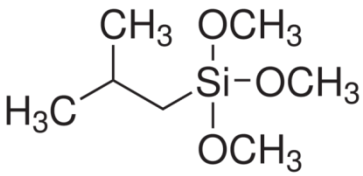

Figure 2: Molecular structure of Isobutyl(trimethoxy)silane

I.3 Oleophobol CO

It is a white dispersion of fluorinated polymer with specific gravity of 1.07–1.09 g/ml at 20°C. It is a commercial textile finishing product supplied by Huntsman.

I.4 Octadecyltrimethoxysilane(ODS)

Octadecyltrimethoxysilane is colorless liquid with molecular weight 374.67g/mole. It is hydrophobic chemical used for preparation of self assembly monolayers. Its linear formula is $CH_3(CH_2)_{17}Si(OCH_3)_3$. The technical grade octdecyltrimethoxysilane with assay 90% used as it was bought from Sigma Aldrich without further purification. Its molecular structure is shown in Figure 3.

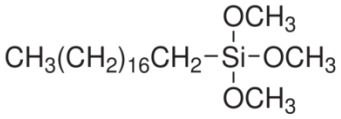

Figure 3: Molecular structure of octadecyltrimethoxysilane

I.5 Zinc acetate dihydrate

Zinc acetate dihydrate is a white powder with formula weight 219.51g/mole. American Chemical Society (ACS) reagent grade zinc acetate dihydrate with assay ≥ 98% used as it was bought from Sigma Aldrich without further purification. Its molecular structure is shown in Figure 4.

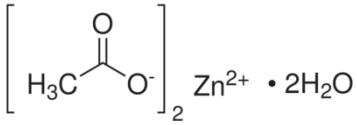

Figure 4: Molecular structure of zinc acetate dihydrate

I.6 Zinc nitrate hexahydrate

Zinc nitrate hexahydrate is a colorless powder with temperature of fusion 45°C and has molecular eight 297.49g/mole. ACS reagent grade zinc nitrate hexahydrate with assay 98% used as it was bought from Sigma Aldrich without further purification. Its linear formula is $Zn(NO_3)_2 \cdot 6H_2O$.

I.7 Hexamethylenetetramine

Hexamethylenetetramine exists as colorless crystals with fish like odour. Its molecular weight is 140.19g/mole and point of fusion is 280°C. The density of hexamethylenetetramine is 1.331 g/cm^3. ACS reagent grade hexamethylenetetramine with assay ≥99.0% used as it was bought from Sigma Aldrich without further purification. Its liner formula is $C_6H_{12}N_4$ and structural formula is shown in Figure 5.

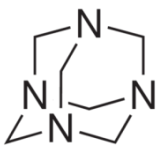

Figure 5: Molecular structure of hexamethylenetetramine

I.8 Sodium hydroxide

Sodium hydroxide is also known as lye or caustic soda, exists as white pellets, flakes and granules. Its molecular weight is 40g/mole and linear formula is NaOH. ACS reagent pellets (Sigma Aldrich) of sodium hydroxide with assay ≥97.0%, were used without further purification.

I.9 Ethanol

Analytical reagent grade 99.7% Ethanol (Carlo Erba, France) was used in this study without any further purification.

I.10 Methanol

Pure methanol 99.6% (Carlo Erba, France) was used in this study without any further purification

I.11 Nitric acid

Nitric acid 65% (Puriss.p.a grade, Sigma Aldrich) with density 1.37-1.41g/ml at 20°C was used

I.12 Water

The distilled water was used in this study. The surface tension and conductivity of water measured at room temperature were 72.4±1.5dyens/cm and 0.68±0.06µS/cm, respectively.

I.13 Fabrics

I.13.1 Cotton

1/1 plain woven cotton fabric having grammage 123±2g/m^2 was used in this study. Bleached fabric was bought from market without any finish (no application of chemical to modify the surface). The freshly picked cotton fibers are perfectly circular because the inner most part of cotton fibers called lumen are filled with liquid which dries with the passage o0f time. This drying causes twists and convolution of the fibers. In order to remove them, a process called mercerization was carried out.

In this process, the fabric was treated with concentrated caustic soda solution (400g/l) for 10 minutes at room temperature. Then it was rinsed 10 times in water and subsequently in water containing 5ml/l of 0.1 mole acetic acid to neutralize it. To confirm, the fabric did not have any caustic soda on it, a 2cm×2 cm fabric was immersed

in 100ml water for 10 minutes and pH was checked before and after which was remained same at 6.2. This treatment swells the fibers and makes them very uniform.

I.13.2 Poly(ethylene terephthalate) PET

A 1/1 plain woven polyester fabric made up of micro fibers (9-10µm) with grammage 82.6±0.8g/$m^2$was used in this study. In order to remove the spinning oil and other organic impurities, Soxhlet process was carried out. In this process, the fabric to be cleaned is loaded into the main chamber of the Soxhlet extractor. The Soxhlet extractor is placed onto a flask containing the extraction solvent (petro ether). The Soxhlet is then equipped with a condenser.

The solvent is heated to reflux and its vapors travel up in distillation arm, and floods into the chamber housing the fabric. The condenser ensures that solvent vapors cool, and drips back down into the chamber. The chamber containing the solid material slowly fills with warm solvent. Some of the desired compound will then dissolve in the warm solvent. When the Soxhlet chamber is almost full, the chamber is automatically emptied by a siphon side arm, with the solvent running back down to the distillation flask [1]. Soxhlet process was carried out for 4 hours to clean the fabric.

Then the fabric was dried at room temperature. The cleanliness of fabric was checked by tensiometeric method. For instance, a small piece of cleaned fabric was dipped in distilled water for 5 minutes and the surface tension of this water was checked before and after dipping. There was no significant change in surface tension; before dipping= 73.5mN/m, after dipping= 72.4mN/m. This shows that the fabric is clean and there is no organic impurity present on it. If organic impurity was present on it, it could go into water which caused the significant change in surface tension.

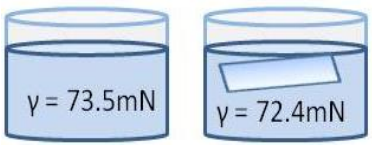

Figure 6: verification of impurities on fabric after cleaning by Soxhlet process.

II. Processes

II.1 Padding

This process is used to apply various chemicals on textile surfaces. For this, the fabric is passed through the trough carrying the solution of the chemical that is to be applied on it, and then squeezed between two rolls at nip pressure of 2 bar called padding rolls to remove the excess of solution from fabric surface and to force the solution to penetrate into the interior of the fabric Figure 7. The fabric is dried in dryer. The amount of solution present on fabric after squeezing is called percentage expression and is calculated by using the following equation

$$\text{Percentage expression} = \frac{m - m_0}{m_0} \times 100$$

m_0 = mass of fabric before application of solution

m = mass of fabric after application of solution and squeezing

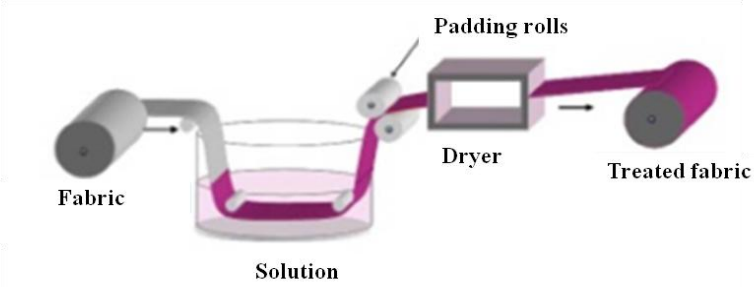

Figure 7: Schematic diagram of padding process

II.2 Solution deposition of ODS

ODS solutions were prepared by pouring it in ethanol at room temperature. The fabric samples(7cm×5cm) were placed in the Teflon bottle containing 100ml of solutions for 24 hours at 40°C without agitation as shown in Figure 8-A. Then, it was dried and cured at 150°C for 5 minutes.

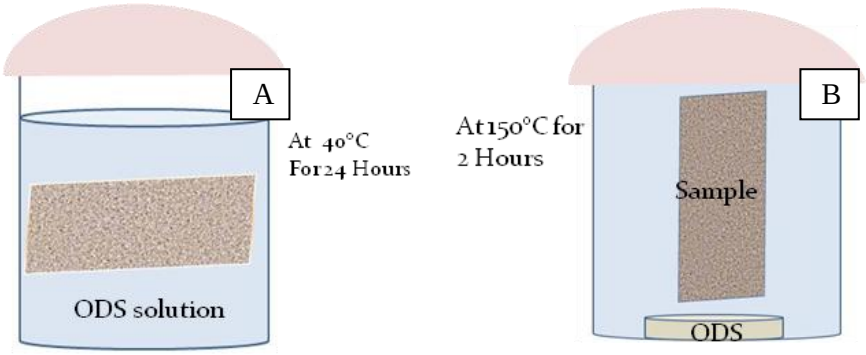

Figure 8: A. modification of fabric with ODS by solution method, B. modification of fabric with ODS by vapor deposition method

II.3 Vapor deposition of ODS

In this method, 200µl of pure ODS were placed in ceramic dish at the bottom of Teflon bottle in which fabric (7cm×5cm) was held vertically as shown in Figure 8-B and the Teflon bottle was placed in oven at 150°C. The time of vapor deposition was varied from 0.5 hour to 4 hours.

II.4 Growth of nanorods

The nanorods were grown by using the hydrothermal process for both seedless and seeded methods described in section II.6 of chapter 1. For this, equimolar solutions of zinc nitrate hexahydrate and hexamethylenetetramine in distilled water were used. Transparent solutions were obtained as both the reagents are readily soluble in water at room temperature. The fabric sample (10cm×8cm) was held vertically in 500ml Teflon bottle (Figure 9) with 250ml solution of each reagent at room temperature. The bottle was closed tightly to avoid the evaporation of water and placed in oil bath already heated at 90°C with continuous stirring for 4 hours, and then the sample was washed in distilled water and dried at 120°C for 5 minutes. The vertical position to hold the textile in Teflon bottle was adopted to avoid the deposition of those nanorods which grow in solution and deposit on fabric.

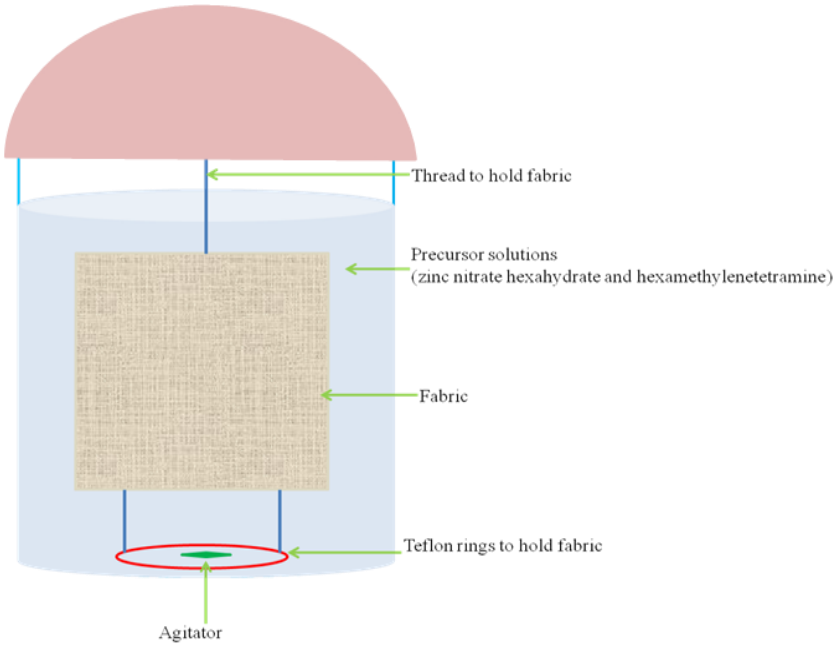

Figure 9: Schematic diagram of fabric held vertically in Teflon containing precursor solutions to grow the nanorods

III. Characterization of surface

III.1 Profilometery (for microroughness)

The surface structure of fabric was characterized by using profilometer AltiSurf® 500. The AltiSurf® 500 is a multi-sensor system created to read accurately component surfaces. It measures several profiles, which, automatically put together, allow rebuilding the morphology of the sample. Then post-treatment software enables to apply analysis parameters such as roughness, tribology, forms and dimensions as well as topographic phenomenon. It was used to characterize the surface morphology of PET fabric.

The white light spot (S) scans the surface through a lens with an axial chromatic aberration (deformation). Instead of focusing on a single point, the lens acts as a prism and separates the wave lengths which all match with a point of the measuring range. The perfect focus of a wave length (the one with the most light intensity after spatial filtering) gives the maximal peak, which, converted by a CCD spectrometer (charge coupled device), determines the height of a point, here called M (Figure 12).

On PET fabric, the profilometery test was carried out on three different places and average roughness was calculated.

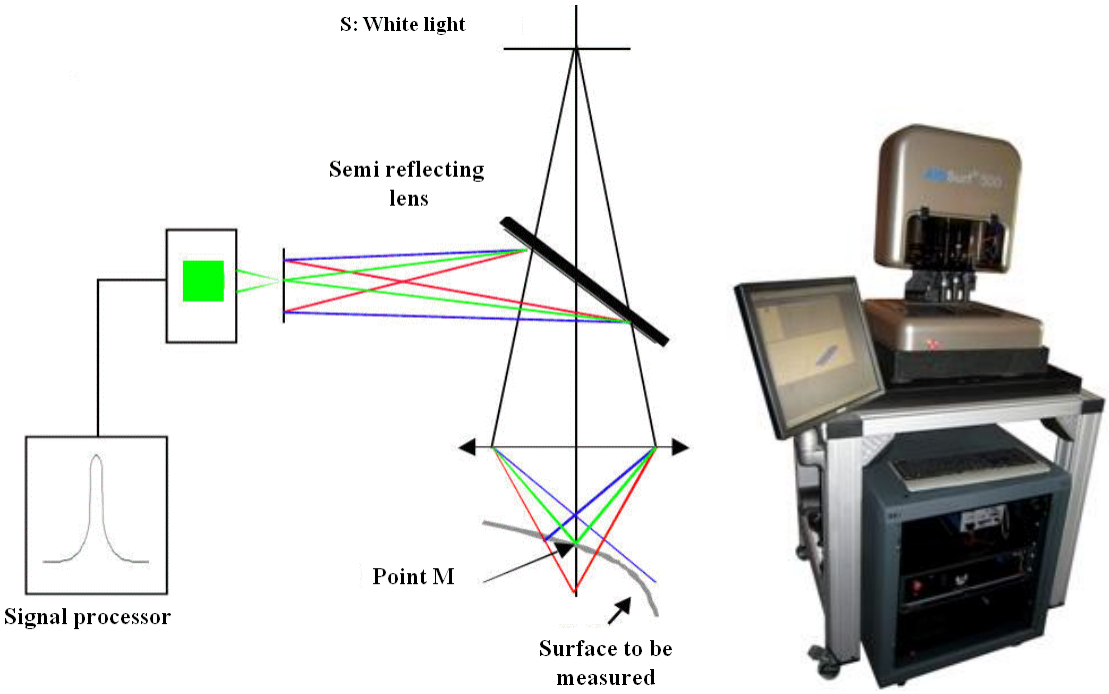

Figure 12: Working principle of Altisurf 500 and machine itself

III.2 Atomic force microscopy (AFM)

To determine the roughness generated due to the growth of nanorods, atomic force microscope (AFM) was used. A typical AFM system consists of a microcantilever probe with a sharp tip mounted to a piezoelectric actuator with a position sensitive photo detector receiving a laser beam reflected off the end-point of the beam to provide cantilever deflection feedback (Figure 13)

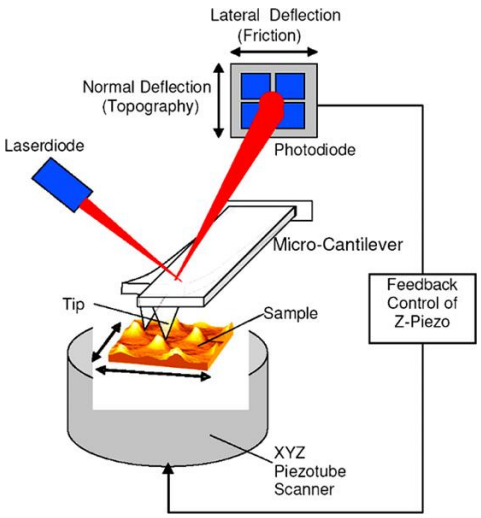

Figure 13: Schematic depicting basic AFM operation and sub-components

The vertical z-deflections of a micro tip scanning the fiber surface are measured when the sample is moved horizontally in the x and y directions. These allow the apparatus software to build-up a topographical image of

the scanned fiber surface. The software also calculates the fiber surface roughness (R_a) *directly* from AFM signals.

$$R_a = \frac{1}{L_x \cdot L_y} \int_{L_x} \int_{L_y} f(x,y).dx.dy$$

Where,

$f(x,y)$ *: Average surface*

L_x *and* L_y *: Surface size chosen for the roughness calculation*

In our study, "Nanoscope III" from Digital Instrument was used in non contact mode to acquire the topographic images of the nano rods treated samples. On each sample, at least three topographic images were obtained and surface roughness was calculated.

III.3 X-Ray photoelectron spectrometry (XPS)

To determine the chemical composition of the surface at all stages of nanorods growth, X-ray photoelectron spectrometry (XPS) was carried out. In (XPS) analysis, a sample introduced in an ultra high vacuum chamber, is irradiated with an X-ray beam. The kinetic energy (in electron volt, eV) of electrons of all elements (except H and He) present at the surface is measured with a precision of about 0.2 eV. The probed depth is between 1 and 10 nm. Shape and position of recorded peaks depend on the chemical state (the so-called "chemical shift" effect). Peaks areas normalised with respect to acquisition parameters and corrected with elemental sensitivity factors allow calculating mole fractions. The detection limit is less than 1 %. A detailed analysis of well-resolved peaks allows quantifying chemical functions

The analyses were performed on a SSX 100/206 photoelectron spectrometer from Surface Science Instruments (USA) equipped with a monochromatized micro focused Al X-ray source (powered at 20 mA and 10 kV),. Pieces of about 5mm x 5mm were cut from each sample and fixed with a double sided adhesive tape on an aluminium conductive carousel. A differential charging effect was detected on some samples, due to their semi-conductor character. This provoked broadening, distortion, or even splitting of peaks which can be confused with a chemical shift effect. The differential charging effect was avoided by mounting these samples on an insulating homemade ceramic carousel (Macor® Switzerland) instead of the aluminium one, with the nickel grid mentioned below, still grounded to the carousel support. The pressure in the analysis chamber was about 10^{-7} Pa. The angle between the surface normal and the axis of the analyser lens was 55°. The analysed area was

approximately 1.4 mm^2 and the pass energy was set at 150 eV for the survey scan and 50 eV for narrow scans. In the latter conditions, the full width at half maximum (FWHM) of the Au $4f_{7/2}$ peak of a clean gold standard sample was about 1.1 eV. A flood gun set at 8 eV and a Ni grid placed 3 mm above the sample surface were used for charge stabilisation. The following sequence of spectra was recorded: survey spectrum, C 1s, O 1s, Zn 2p, Zn $L_3M_{45}M_{45}$ (Auger peak) Na 1s, Cl 2p, N 1s, Si 2p and C 1s again to check for charge stability as a function of time and the absence of sample degradation. The **C**-(C,H) component of the C1s peak of carbon was fixed to 284.8 eV to set the binding energy scale. Data treatment was performed with the Casa XPS program (Casa Software Ltd, UK), some spectra were decomposed with the least squares fitting routine provided by the software with a Gaussian/Lorentzian (85/15) product function and after subtraction of a non linear baseline. Molar fractions were calculated using peak areas normalised on the basis of acquisition parameters and sensitivity factors provided by the manufacturer [mean free path varying according to the 0.7^{th} power of the photoelectron kinetic energy; Scofield cross sections; transmission function assumed to be constant

IV Characterization of functional characteristics

IV.1 Chemical Self-cleaning

IV.1.1 Solution discoloration

To carry out the solution discoloration, 6ml of each solution were taken in 100ml Duran® beaker and 2.8cm nanorods functionalized fabric was placed in it. This beaker was placed in light box (VeriVide CAC60) carrying 20W UV light (300nm-400nm with maximum emission wavalenth at 368nm) at a distance of 18cm for UV irradiation as shown in Figure 14. The light box was placed in room under standard conditions 65% relative humidity and 25°C in such a way that no sunlight and tube light could reach inside the box.

To study the successive solution discolorations, the functionalized sample with diameter 2.8cm was placed in 6ml of reactive violet 5 with 80mg.l^{-1} initial concentration. After discoloration, the same sample without intermediate washing was once again put in 6ml of same solution and exposed to UV light. This process was repeated 5 times.

For the samples with physical self-cleaning (after modification with ODS by solution and vapor deposition methods), the fabric was first soaked in acetone for few seconds before dipping in dye solution because the fabric was superhydrophobic and it was not possible to immerse it in solution.

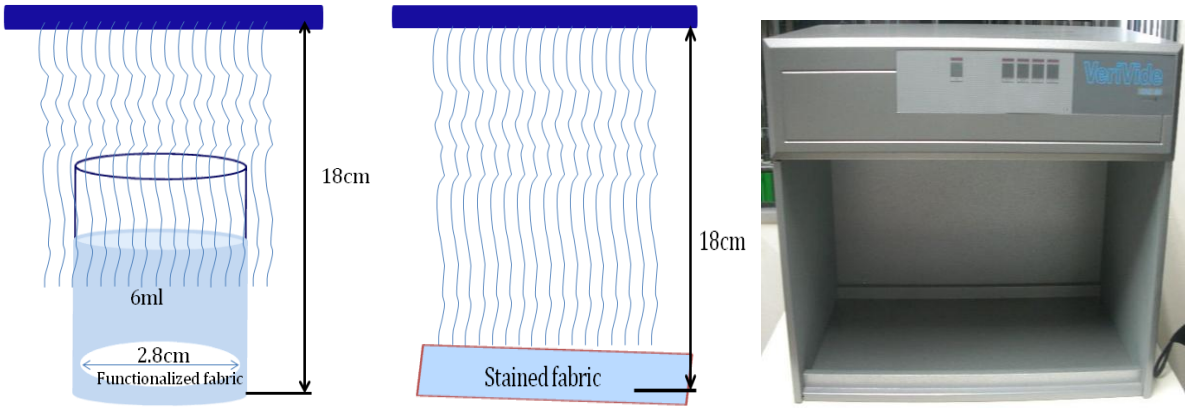

Figure 14: Arrangement for solution and stain discolorations by functionalized fabric under UV light, and VeriVide CAC60 light box carrying the UV light in which samples were exposed to UV light.

IV.1.2 Stain discoloration

For stain discoloration, the functionalized samples (5cm × 2cm) was dipped in dye solutions with different concentrations for 5 seconds, it was dried at 120°C for 5 minutes and then exposed to UV light at distance of 18cm as shown in Figure 14 in light box.

For successive stain discolorations, the fabric was stained with acid blue 9 solution (0.4g/l), dried and exposed to UV light. After 24 hours, the fabric was re-stained with the same solution at the same place. It was dried and once again exposed to UV light. This process was repeated 5 times without intermediate washings. The K/S values of each degradation cycles were measured by using spectrophotometer and a comparison was made for 5 successive discolorations.

For the staining of samples with physical self-cleaning, the acid blue 9 (0.4g/l) solution was prepared in acetone and the samples S and V were stained by dipping in solution. They were dried at 120°C for 5 minutes and exposed to UV light

IV.1.3 Durability of functionalized fabric

IV.1.3.1 Water durability

The water durability test was carried out on WASHTEC-P (Figure 15). The samples were placed in washpot containing distilled water with sample to water ratio of 1:50. Then the samples in washpot were agitated at 40°C and 60°C for 30 minutes. After drying at 120°C for 5 minutes, the stain degradation was studied by using C.I. acid blue 9 solutions in water and comparison was made with the stain degradation results of sample before this test.

Figure 15: Washtech-P machine used for water durability test and washpot

IV.1.3.2 Rubbing durability

To determine the abrasion resistance, the samples (equal to template size) were rubbed against cotton abradents at low pressures (9kPa) and in continuously changing directions for 100 and 500 cycles using M235 Martindale Abrasion Tester Figure 16. The stain degradation was studied by using 0.4g/l C.I. acid blue 9 solution as described in section IV.1.2 and comparison was made with the stain degradation results of sample before this test.

Figure 16: M235 Martindale Abrasion Tester used for rubbing durability test

IV.2 Antibacterial activity test

To meet the objectives of the study, bacterial models chosen are:

- *Staphylococcus aureus ATCC 6538*
- *Escherichia coli ATCC 8739*
- *Pseudomonas aeruginosa*

These are the bacteria which are listed in analysis standard as well as the main microorganism involved in nosocomial infections and food (more than 70% of MN just for S. aureus). These organisms are classified as pathogens and need to be handled in a confined laboratory class P2.

IV.2.1 Material preparation

For the experiments, liquid cultures were prepared by inoculation of an aliquot of cryopreserved cells into test tubes containing 5 ml of BHI (Brain Heart Infusion) broth (Biokar diagnostic, Beauvais, France) and maintained at 37°C overnight.

A subculture was then prepared by injecting 0.1 ml of bacterial suspension into 5 ml of Muller Hinton broth (Biokar diagnostic, Beauvais France), and this was grown at the same temperatures as those described above. Cells were harvested after 18 to 24 hours growth period. One milliliters of this previous suspension were inoculated on agar plates of Muller Hinton broth supplemented with 15g/l of agar in order to test the purity of the culture. After 18 to 24 hours at 37 ° C, the bacterial culture ready to use was obtained. Their concentration was too high; we performed a dilution of this culture by placing 0.1 ml of culture in 50 ml of new MH to obtain a cell concentration of about 1-3 x 10^6 CFU / ml. This inoculum was immediately used for experiments.

IV.2.2 Contamination test

In order to check the contamination of samples with bacteria before carrying out the antibacterial test, fabrics were put in 20 ml of neutralizer broth. Samples were then shacked using a LSE vortex mixer (Corning, NY) 5 x 5s in room tube light. The solution was then used for cell counting. Bacterial amount ranged from 1 to 10^2 CFU/cm². This bacterial population can be considered as negligible in comparison with the bacterial concentration (10^6 CFU/ml) used in experiments. Therefore, the decontamination of fabric before carrying out

the antibacterial tests was not carried out. The cell counting was carried out in the same way described in quantitative assessment.

IV.2.3 Qualitative assessment

Qualitative method is the first step in the analysis of the antibacterial effect. The Muller Hinton (Biocar Diagnostic, Beauvais, France) agar plates were inoculated with 1 ml of the dilution described above. Afterward, a swatch of the test sample with diameter 1.2cm (neither it was put in dark nor in UV light before carrying out the test: used as it was prepared) was placed on the agar surface and incubated at 37 °C for 24 h before observation. This test was repeated 3 times for each sample.

IV.2.4 Quantitaive assessment

This method helps to quantify the antibacterial activity of the functionalized samples. It is based on NF ISO 20743 Transfer method which is carried out in 6 steps.

1. Preparation of the petri dish for transfer.

One milliliters of the previous suspension were inoculated on agar plates composed with O.75g/l tryptone, enzymatic digest from casein, 0.25g/l of peptone from casein soya bean digest, 5g/l of sodium chloride and supplemented with 15g/l of agar. Petri dishes were inclined in several directions in order to inundate the entire surface of the plate before removing the excess of liquid. A released time of 300+/6 30 s was performed before the experiments. Twelve petri dishes were inoculated.

2. Transfer to samples

Six samples of PET used as control and six samples of functionalized fabrics were cut with a diameter of 3.8 cm using a size template. These samples were put on the agar plate under a shot of 200g during 60 ± 5s as shown in Figure 17. Three samples were used immediately for counting; the 3 others were put in petri dishes face up and incubated 24 hours at 37°C in a hydric-controlled chamber in dark.

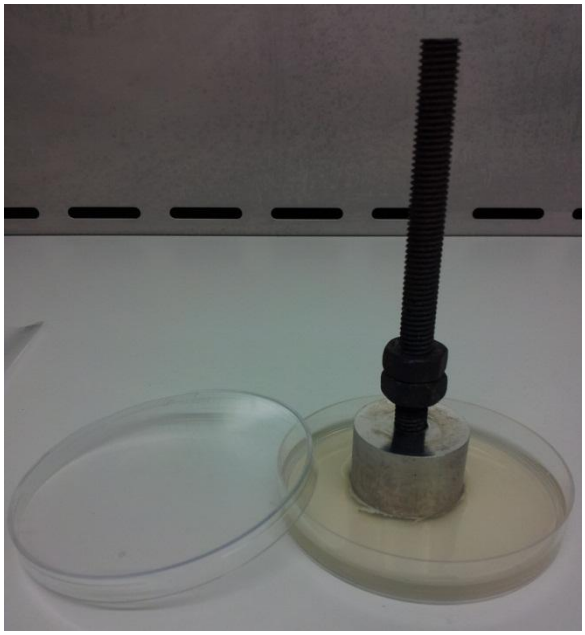

Figure 17: Photograph illustration Transfer step

3. Extraction after transfer

Immediately after transfer, samples were put in sterile bag with 20ml of neutralizer broth composed of 30g/l of mono-oleic polyethoxylated sorbitan, 3g/l of lecithin from egg yolk, 1g/l of histidine hydrochloride, 1g/l peptone from meat digested, 4.3g/l of sodium chloride, 3.6g/l of monopotassium phosphate, and 7.3g/l of disodium phosphate dihydrate.

The neutralizer broth is composed with both tensioactive and emulsifier in order to promote desorption of microorganisms from the fabrics. If the neutralizer broth is not enough effective, the quantity of sorbitan or lecithin can be adjusted or a new neutralizer can be added.

Microorganisms were detached from fabrics with mechanical process using a stomacher apparatus (shown in Figure 18) whose speed could be adjusted from 6 hit per second to 8 hit per second on each side of the bag.

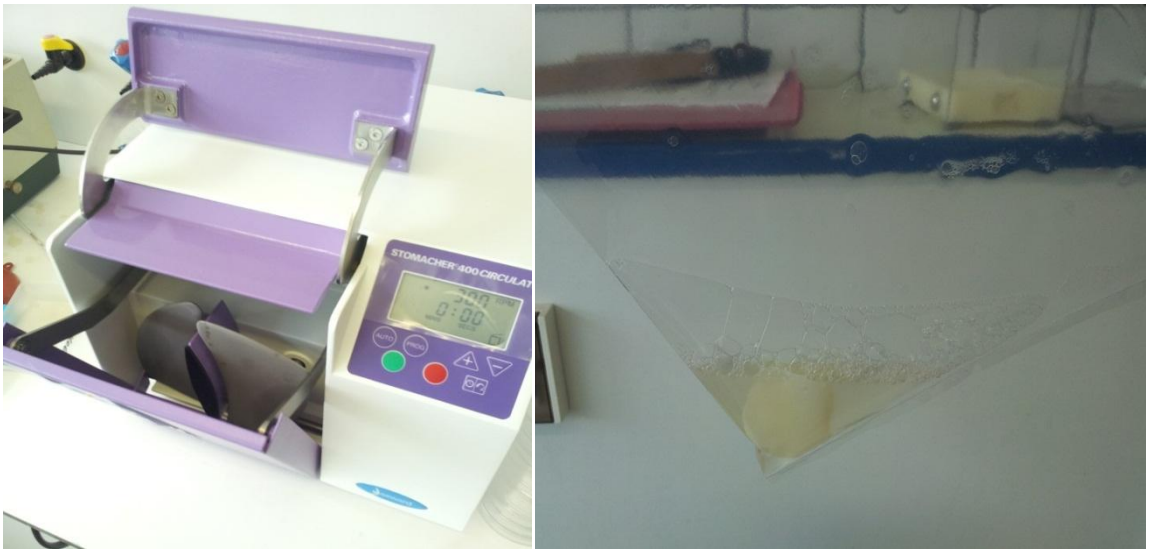

Figure 18: Stomacher and the bag containing the textile sample in neutralizing solution

4. Extraction after incubation

After 24 hours incubation at 37°C samples were put in sterile bag with 20ml of neutralizer broth and shacked with a stomacher 1 minute on each side of the bag.

5. Cell counting

After extraction, one milliliter of the neutralizing broth was added to a test tube containing 9ml of peptone water broth. After shaking, with a new pipette one milliliters of the previous solution were introduced in a new test tube containing 9ml of sterile peptone water broth. One milliliters of each dilution were dropped in two petri dishes and recovered with 15ml of liquid agar - MH broth (temperature close to 45°C). Petri dishes were properly moved and maintained at room-temperature until being solidified and incubated 24-h at 37°C. After incubation, the number of colony on each plate is counted. Only plates where the amount of colonies was spread from 30 to 300 CFU were registered. In order to have the sufficient dilution to obtain agar plate with this countable number of colonies, the operation of dilution previously described was repeated 7 times.

The concentration of bacteria in the solution can be calculated by using the following formula:

$$CB = Z \times R$$

Where CB is the concentration of bacteria colony forming units per milliliter (CFU / ml), Z is the average value in the two Petri dishes in colony forming units (CFU), R is the rate of dilution.

The antibacterial activity (A) of the functionalized polyester fabric by zinc oxide nanorods was calculated as follows:

$$A = (\log C_t - \log C_0) - (\log T_t - \log T_0)$$

Where

- A is the antibacterial activity value
- $\log C_0$ and $\log C_t$ are the decimal logarithm average corresponding to the number of bacteria obtained from the three untreated samples immediately after inoculation and after an incubating period of 24h respectively.
- $\log T_0$ and $\log T_t$ is the decimal logarithm average corresponding to the number of bacteria obtained from the three treated samples immediately after inoculation and after an incubating period of 24h.